Calibration of oxygen isotope fractionation and calcite-corundum thermometry in emery at Naxos, Greece

Short running title: Calcite-corundum oxygen isotope fractionation

Rachelle B. Turnier[1], Yaron Katzir[2], Kouki Kitajima[1], Ian J. Orland[1], Michael J. Spicuzza[1], John W. Valley[1]

[1]Department of Geoscience, University of Wisconsin, Madison, WI 53706, USA
[2]Department of Geological and Environmental Sciences, Ben Gurion University of the Negev, Be'er Sheva 84105, Israel

Returned to editor, Sept. 17, 2019

Final publication:
Turnier RB, Katzir Y, Kitajima K, Orland IJ, Spicuzza MJ, Valley JW (2019) Calibration of oxygen isotope fractionation and calcite-corundum thermometry in emery at Naxos, Greece. J Meta Geol. 00: 1-18. https ://doi.org/10.1111/jmg.12512

Correspondence
Rachelle B. Turnier, Department of Geoscience, University of Wisconsin-Madison, Madison, WI 53706
Email: turnier@wisc.edu
Declarations of interest: none

ABSTRACT

Corundum (Crn), including sapphire, occurs in emery pods surrounded by marble on the island of Naxos, Greece. The emery formed from bauxite deposited in karst that was metamorphosed to 400 to 700 ^{o}C at 20-15 Ma. Many of these rocks initially appeared well suited for refractory accessory mineral (RAM) thermometry, which uses oxygen isotope fractionation between a refractory accessory mineral, corundum, and a modally dominant phase with faster diffusion of oxygen, calcite (Cc), to determine peak metamorphic temperatures. However, previous attempts at oxygen isotope thermometry were confounded by highly variable fractionations ($\Delta_{18}O$) measured at mm-scale and the uncertain calibration of $\Delta_{18}O$(Cc-Crn) versus temperature.

Secondary Ion Mass Spectrometry (SIMS) permits *in situ* analysis of $\delta_{18}O$ in corundum and calcite at the 10-μm scale in adjacent grains where textures suggest peak-metamorphic equilibrium was attained. SIMS analyses of adjacent mineral pairs in eight rocks yield values of Δ(Cc-Crn) that systematically decrease from 7.2 to 2.9‰ at higher metamorphic grade. Pairing these data with independent temperature estimates from mineral isograds yields an empirical calibration of $1000\ln\alpha(\text{Cc-Crn}) = 2.72 \pm 0.3 \times 10^6/T^2$ (T in K). The new fractionations are significantly smaller than those calculated from the modified increment method (Zheng, 1991, 1994) (2.7 vs. 6.5‰ at 1000 K), which yield unreasonably high temperatures of 630 to 1140 °C when applied to the new Naxos data.

The new calibration of Δ(Cc-Crn) can be combined with published fractionations to calculate A-factors for corundum versus a range of 14 other minerals. These new fractionation factors can be used for thermometry or to constrain the genesis of corundum. A compilation of

gem corundum $\delta^{18}O$ values shows that many igneous sapphires, including important deposits of basalt-associated sapphire, are mildly elevated in $\delta^{18}O$ relative to the calculated range in equilibrium with mantle values (4.4 to 5.7‰) and formed from evolved magmas.

Keywords: SIMS, corundum, calcite, oxygen isotope fractionation, thermometry

1 INTRODUCTION

Mineral-corundum fractionation factors have many applications, one of which is investigating sapphire genesis. Most gem sapphire is mined from placer deposits, but when they are found in igneous host rocks, textural and chemical evidence often indicates they are xenocrysts and their genesis is uncertain (Giuliani, Ohnenstetter, Fallick, Groat, & Fagan, 2014). Are they igneous or metamorphic? Did they crystallize in the deep crust or mantle, from primitive or evolved magmas that have undergone crustal interactions? Evaluating oxygen isotope fractionation between co-existing minerals is a useful technique for understanding mineral paragenesis and crystallization temperature.

The fractionation of $^{18}O/^{16}O$ among mineral pairs equilibrated at a given temperature is commonly used as a thermometer (Hoefs, 2018; O'Neil, 1986; Valley, 2001). This relation can be represented by a linear, one-coefficient equation:

$$1000 \ln \alpha(a-b) = \frac{A(a-b) \times 10^6}{T^2} \quad (1)$$

where α(a-b) is the fractionation factor, A(a-b) is a constant referred to as the A-factor, T is temperature (in Kelvin), and "a" and "b" are the two minerals (for mineral abbreviations used in this study, see Table 1). Values of 1000lnα(a-b) can be approximated by $\delta^{18}O(a) - \delta^{18}O(b)$ (= $\Delta^{18}O(a\text{-}b)$). Thus, equilibration temperature can be calculated from the oxygen isotope ratios of two minerals if they preserve isotope equilibrium and the A-factor is known.

Calcite-corundum oxygen isotope fractionation has been estimated from modified increment method calculations of corundum-water and calcite-water fractionation with three coefficients (Zheng, 1991, 1994), which equates to:

$$1000 \ln \alpha(Cc - Crn) = \left(\frac{1.77 \times 10^6}{T^2} + \frac{9.05 \times 10^3}{T} - 4.34 \right) \quad (2)$$

At 1000 K (727°C) Equation 2 gives $\Delta_{18}O$(Cc-Crn) = 6.5‰, and Eq. (1) can then be solved to show that this value equates to the A-factor (A(Cc-Crn)). However, the fractionations from equation (2) have been questioned as yielding temperatures that are unreasonably high (Yui, Zaw, & Wu, 2008). Likewise, Fallick et al. (2019) evaluate the modified increment fractionation factors for $\Delta_{18}O$(Cc-spinel) from marbles and also conclude that the fractionation factors yield unreasonably high metamorphic temperatures. Since there is no experimental calibration of oxygen isotope fractionation in corundum, the approach taken here is to calibrate 1000lnα(Cc-Crn) using measured data in comparison to isograd temperatures in metamorphic calcite-corundum rocks.

Metamorphic minerals are often zoned or heterogeneous in $\delta_{18}O$ (Ferry, Kitajima, Strickland, & Valley, 2014) reflecting a range of prograde and retrograde processes. Minerals with slow rates of oxygen diffusion can be homogeneous or preserve growth zoning if crystallized below their Dodson closure temperature. Minerals with faster diffusion can be reset by exchange during cooling, which frequently leads to retrograde zoning patterns (Eiler, Baumgartner, & Valley, 1992; Eiler, Valley, & Baumgartner, 1993). Under ideal conditions, the effects of diffusion, which are deleterious for thermometry, can be avoided by analysis of a "refractory" mineral with slow diffusion that is modally minor and crystallized in a rock dominated by a mineral with fast diffusion (Valley, 2001). Such refractory accessory mineral (RAM) thermometry can be applied to accessory minerals such as corundum, aluminosilicates, magnetite, pyroxene or garnet in marble, quartzite, or anorthosite for $\delta_{18}O$; or graphite in marble for $\delta_{13}C$.

In appropriate rocks, RAM thermometry can be used without calculating diffusion effects because the fast-exchanging mineral is modally abundant. In the absence of fluid flow, it does not change significantly in $\delta^{18}O$ due to mass-balance. The slow-exchanging accessory mineral preserves its $\delta^{18}O$ value and thus the $\Delta^{18}O$ from crystallization. Although RAM thermometry has been successfully applied in a range of rocks at mm- to cm-scale using bulk-analysis techniques (Kitchen & Valley, 1995; Putlitz et al., 2002; Valley 2001), the effects of overprinting events can be confounding. More recently, it has become possible to evaluate such formerly cryptic effects by employing *in situ* analysis at μm-scale by Secondary Ion Mass Spectrometry (SIMS) (Bowman, Valley, & Kita, 2009; Errico, Barnes, Strickland, & Valley, 2013; Ferry, Ushikubo, Kita, & Valley, 2010; Ferry et al., 2014; Gordon et al., 2012; Page, Essene, Mukasa, & Valley, 2014; Quinn, Kitajima, Nakashima, Spicuzza, & Valley, 2017; Russell et al., 2013; Valley 2001; Valley & Kita 2009; Vielzeuf, Champenois, Valley, Brunet, & Devidal, 2005).

Corundum and calcite in the metamorphosed karst-bauxite emery from Naxos, Greece (Figure 1) provide a promising setting for RAM thermometry, or alternatively, for empirical calibration of the calcite-corundum A-factor. The samples in this study approximate bi-mineral assemblages that are suitable for RAM thermometry. SIMS measurements were made on a local scale in domains of ~500 × 500 μm. The metamorphic temperatures have been independently determined by mineral isograds to increase from 400 °C in the SE to 700 °C at the migmatite dome in the NW part of the island (Figure 1; Feenstra, 1985). Details of mineral isograds are discussed in section 2.

In an earlier attempt to calibrate the A-factor using rocks from Naxos, oxygen isotope ratios were measured in bulk mineral-separates from volumes of one cubic centimeter or larger by laser-fluorination (corundum; Table S1) and acid-solution (calcite; Table S2) techniques (Katzir &

66 Valley, 2001). However, these analyses homogenized mineral grains that might have been zoned
67 or contained inclusions and veins. Fractionations, $\Delta_{18}O$(Cc-Crn), ranged by over 10‰ from -2.0
68 to +8.4‰ in 17 rocks (Appendix S1; Table S1.1). These fractionations include reversals from
69 negative to positive and are not consistent with sample temperature estimates of ~420 to 590 °C,
70 based on mineral isograds for M2 metamorphism (see section 2) of corundum-bearing rocks
71 across Naxos.
72 In the current study we analyzed samples using SIMS (10-μm spots) in order to test for isotopic
73 zonation and alteration that would impact the determination of equilibrium $\delta_{18}O$ values of calcite
74 and corundum. Samples were imaged by SEM-based cathodoluminescence (CL), secondary
75 electrons (SE), and back-scattered electrons (BSE) to guide *in situ* measurements. The textural
76 and isotopic complexity of the Naxos emery samples (Figures 2-5) indicate the need to make
77 oxygen isotope analyses *in situ* by SIMS in order to avoid micro-inclusions, prograde- and
78 retrograde-growth zones, and secondary minerals like vein calcite that do not relate to the high-
79 temperature equilibrium attained during metamorphism.
80 Microanalysis by SIMS allows evaluation of possible variability and disequilibrium of $\delta_{18}O$
81 within volumes smaller than analyzed at the mm-scale. Analyses of close pairs of corundum and
82 calcite grains are compared to the isograd temperatures in order to empirically calibrate the A-
83 factor in equation (1). From published data for calcite-mineral fractionation factors (Chacko,
84 Cole, & Horita, 2001; Valley, 2003), the A-factor for corundum versus other minerals can then
85 be calculated. We apply these new calibrations to explore the genesis of other corundum
86 deposits, especially basalt-hosted sapphires.

2 NAXOS GEOLOGY AND SAMPLE SELECTION

The island of Naxos, Greece, consists of mostly schist, gneiss, and marble (the main host of metabauxite lenses). Sediments were originally deposited in a shallow-sea environment (Aydoğan & Moazzen, 2012) that was later exposed as karst topography to subaerial weathering and lateritic infilling. Naxos has experienced two major metamorphic events that turned the karst bauxite to marble and emery: M1, an Eocene blueschist- to eclogite-facies event, and M2, a Miocene greenschist- to amphibolite-facies event (Avigad, 1998; Bolhar, Ring & Ireland, 2017; Keay, Lister, & Buick, 2001; Martin, Duchéne, Deloule, & Vanderheaghe, 2006; Wijbrans & McDougall, 1988). The M2 metamorphism overprinted M1 assemblages and resulted in a metamorphic thermal gradient on the island of Naxos that is reflected in a series of mineral isograds.

From low- to high-grade metamorphism, the isograds divide the rocks on Naxos into a series of metamorphic zones (zones I-VI, Figure 1), which are defined based on the characteristic mineral assemblages in the pelitic schists and metabauxites. Pressures for M2 on Naxos range from 5 to 7 kbar (Buick, 1988; Jansen & Schuiling, 1976) and isograd temperatures range from 420 to 700 ±50 °C (Buick, 1988, Buick & Holland, 1989). Mineral isograds were first mapped by Schuiling and Oosterom (1967), and then refined by Jansen and Schuiling (1976) and Buick (1988). Isograd index minerals were mapped based on field observations and verified in the lab with thin sections and X-ray diffraction (Jansen, 1977). Isograd temperatures are consistent with those obtained by garnet-biotite exchange thermometry by Duchêne, Aïssa, and Vanderhaeghe (2006). This information is summarized here in terms of the metabauxite mineral assemblages from each zone, the occurrence of index minerals, and the characteristic reactions for each mineral isograd separating the zones.

Zone I is the diaspore-chloritoid zone, where metabauxites contain diaspore, chloritoid, Fe-Ti oxides, rutile ± calcite (in the outer rims and, locally, central parts of the metabauxite bodies; Feenstra, 1985). The pelitic schists have a greenschist-facies assemblage of albite-quartz-chlorite-sericite (Jansen & Schuiling, 1976). The first isograd, corundum-in, is defined by the reaction of diaspore to corundum and water; it was mapped based on the appearance of corundum in 25 metabauxite occurrences (Jansen & Schuiling, 1976). On Naxos, this reaction occurs at approximately 5 kbar and 420 °C (Feenstra 1985; Rye, Schuiling, Rye, & Jansen, 1976).

The corundum-in isograd marks the beginning of zone II, the chlorite-sericite zone. Metabauxites in zone II contain mainly corundum-chloritoid-Fe-oxide (Feenstra, 1985), but also have calcite near marble-metabauxite contacts (samples 7 and 8, this study). Minerals in the schists are similar to those in zone I schists (Jansen & Schuiling, 1976).

The next isograd, biotite-in, is mapped based on 30 field observations of biotite in pelites (Jansen & Schuiling, 1976). The biotite-in isograd marks the beginning of zone III: the biotite-chloritoid zone. Biotite may be formed by the breakdown of chlorite and muscovite (Schuiling & Oosterom, 1967). This occurs at approximately 450 °C on Naxos (Baker & Matthews, 1995; Jansen, 1977). Biotite was not detected in the zone III metabauxites (Feenstra, 1985). The metabauxite deposits in this zone have a characteristic assemblage of corundum, calcite, margarite, and chloritoid at their contact with the marble (Jansen & Schuiling, 1976). Feenstra (1985) reports the middle of zone III as the first occurrence of magnetite in the Fe-Ti oxide assemblages, which contradicts Jansen and Schuiling (1976) who report the middle of zone II as the hematite-magnetite transition.

The staurolite-in isograd marks the beginning of zone IV, the corundum-staurolite zone, and is based on the first appearance of Fe-rich staurolite in the metabauxites and pelites (Feenstra, 1996; Feenstra & Wunder, 2002). It was originally mapped as the chloritoid-out isograd based on the disappearance of chloritoid in the pelites and metabauxites (Jansen & Schuiling, 1967), but Feenstra (1985) found chloritoid persisted in a few of the zone IV metabauxites. As the disappearance of chloritoid corresponds to the appearance of staurolite, the first metabauxite staurolite may have formed by the reaction of chloritoid and rutile to form staurolite, chlorite, corundum, ilmenite, and water (Feenstra, 1985). The isograd was originally mapped based on 10 observations of the disappearance of chloritoid in the pelites and metabauxites; it does not appear to have changed in position when it was redefined as the staurolite-in isograd. On Naxos, this reaction occurs at approximately 540 °C (Feenstra & Wunder, 2002; Jansen & Schuiling, 1976). The characteristic metabauxite assemblage is corundum + kyanite + staurolite + biotite + margarite ± anorthite ± muscovite + Fe-Ti oxides (Feenstra, 1985). At emery-marble contacts the assemblage of margarite-anorthite-corundum occurs (Jansen & Schuiling, 1976) along with calcite (this study).

The next isograd, sillimanite-in, marks the beginning of zone V and is based on the first appearance of sillimanite in metapelites. On Naxos, at pressures of 6 to 7 kbar, this occurs at approximately 620 °C (Buick, 1988; Jansen & Schuiling, 1976; Rye et al., 1976). Zone V is the kyanite-sillimanite transition zone. Metabauxite deposits are rare, but generally have the same mineralogy as metabauxites from zone IV; at the metabauxite-marble contacts, the assemblage is anorthite-calcite-corundum (Jansen & Schuiling, 1976). Zone V was previously subdivided into A/B based on the disappearance of kyanite, but this was not supported by the work of Buick

(1988) and was removed from later maps (Baker & Matthews 1995) so zones V-A and V-B are not included in Figure 1.

The melt-in isograd, or migmatite limit, is mapped based on the beginning of partial melting in the pelitic gneisses (660-690 °C, Jansen & Schuiling, 1976). The migmatite dome (zone VI) reached the highest metamorphic grade, with pressures of ~7 kbar and temperatures around 700 °C (Buick, 1988; Buick & Holland, 1989; Katzir, Avigad, Matthews, Garfunkel, & Evans, 1999; Katzir, Valley, & Matthews, 2002).

Samples were collected during several field excursions by Valley (1996), Katzir (2000, 2003) and Turnier (2016) from the metabauxite emery deposits marked with triangles on Figure 1 (extra localities and GPS in Table S3.1 are shown in Figure S3.2). These samples are from zones II and IV, and span a range of temperatures, from approximately 420 to 600 °C (zone II avg = 424 °C, n=2 samples; zone IV avg = 575 °C, n=6 samples; see section 4.1 for a discussion of isograd temperatures). Sample localities, mineral assemblages and a summary of oxygen isotope results are presented in Table 1 and the modal abundance of minerals in each sample are shown in Table 2.

3 METHODS

Rocks collected from Naxos were cut into ~2.5 cm chips. After flattening one face, chips were cast into 2.54-cm round epoxy mounts (Figure S3.1) to fit within the SIMS sample holder for analysis. Holes for standards (1-mm dia.) were drilled in the middle of the epoxy-held rock chip, then standards UWCrn9 (corundum) and UWC-3 (calcite) were top mounted with epoxy in the holes. The samples were polished progressively from 6 to 1 μm with diamond suspensions and a final polish of 0.05 μm with colloidal alumina. The mounts were then gently cleaned by rinsing with alkaline soap and swirling with ethanol in a beaker. To remove adsorbed water, the sample

was first dried with a blast of nitrogen gas and then placed in a vacuum oven at 40 °C for at least three hours before carbon coating for imaging.

3.1 SEM

Samples were imaged with a Hitachi S-3400N variable pressure scanning electron microscope (SEM) in the Ray and Mary Wilcox SEM Laboratory at UW-Madison using backscattered electron (BSE), secondary electron (SE), and cathodoluminescence (CL) detectors. Mineral identification was aided by energy-dispersive spectrometry (EDS). Samples were coated with 4-5 nm of carbon for CL imaging. A 20-nm carbon coat was used for BSE, SE, and post-SIMS imaging. Images and EDS were acquired under high vacuum. The EDS system consists of a Si(Li) detector and thin-film window to allow detection of light elements down to carbon. BSE and SE images were mostly made with a 15-kV accelerating voltage, 50-70 nA current, and a working distance of 10 mm; these settings were sometimes varied slightly to optimize the image. CL images were collected using a Gatan PanaCL/F detector with the blue filter inserted to remove streaking from carbonate luminescence (Reed & Milliken, 2003).

3.2 EPMA

Electron probe microanalysis (EPMA) was performed with a CAMECA SX51 electron microprobe in the Eugene N. Cameron Microscopy and Microanalysis Laboratory at UW-Madison with Probe for EPMA software v. 9.6.4 (Donovan, Kremser, Fournelle, & Goemann, 2018). Calcite was analyzed for Mg, Ca, Mn, and Fe. Four WDS spectrometers were used to perform the measurements: a TAP monochromator crystal (2d spacing = 25.745 Å; Mg Kα), two PET crystals (2d = 8.75 Å; Ca Kα and Mn Kα), and a LIF crystal (2d = 4.0267 Å; Fe Kα). Oxygen and carbon were determined by stoichiometry. Samples were coated with a 20-nm

199 carbon coat and at least three EPMA spots were placed around each SIMS calcite pit to obtain
200 enough counts for statistics to optimize precision for trace and minor elements (Fe, Mn, and Mg)
201 while maintaining a low dwell time to minimize specimen damage. The beam diameter was
202 approximately 5 μm with a 15-kV accelerating voltage and 20-nA beam current.
203 Peak count times were 120 seconds for minor elements (Mg, Mn, and Fe) and 12 seconds for Ca.
204 Standards used were: Dolomite (Mg), Calcite (Ca), Rhodochrosite (Mn), and Siderite (Fe). A
205 Time Dependent Intensity (TDI) correction procedure was used to determine peak intensities due
206 to specimen damage in calcite. Initially, on- and off-peak counts were used to determine
207 background (sample mounts 2, 4, and 6). Background was counted for 60 seconds for minor
208 elements and 6 seconds for Ca. Later, to reduce the analysis time, the Mean Atomic Number
209 (MAN) correction procedure was used to determine background (sample mounts 1, 3, 5, 6, 7 and
210 8). Phi-Rho-Z matrix correction (Pouchou & Pichoir, 1991) was used to calculate compositions
211 from k-ratios. Compositions with analytical totals lower than 98% or greater than 102% were
212 excluded (avg. total = 99.5%, n=345).

213 **3.3 Corundum Standard Development**

214 SIMS analysis of $\delta^{18}O$ requires a matrix- and chemistry-matched comparison standards (Eiler,
215 Graham, & Valley, 1997; Hervig, Williams, Thomas, Schauer, & Steele, 1992; Valley & Kita,
216 2009). Standards must be homogeneous in $\delta^{18}O$ and chemical composition, and available in
217 sufficient quantity to calibrate by conventional gas-source mass spectrometry. A total of 10
218 natural and synthetic gem corundum samples were examined. UWCrn9 is the most homogeneous
219 sample in $\delta^{18}O$ by SIMS (±0.29 ‰ 2SD; Table S3) and was analyzed 5 times by laser
220 fluorination/gas-source mass spectrometry to calibrate its $\delta^{18}O$ value (4.94 ±0.10‰ avg. 2SD

VSMOW, Vienna Standard Mean Ocean Water). UWCrn9 was mounted in every sample and used as a running standard for all corundum analyses to correct for any SIMS instrument drift and calibrate the measurements with respect to VSMOW. Details of standard development can be found in Appendix S2.

3.4 SIMS

Secondary Ion Mass Spectrometry (SIMS) measurements of $\delta^{18}O$ were made in the WiscSIMS Lab (Wisconsin Secondary Ion Mass Spectrometry), Department of Geoscience, UW-Madison on a CAMECA IMS 1280 ion microprobe. Measurements were conducted with a primary beam of $^{133}Cs^+$, 10 kV accelerating voltage, 20 kV total impact potential, ~2 nA sample current, and 10-µm diameter spot size (1-2 µm deep). Three Faraday cups were used to measure $^{16}O^-$, $^{18}O^-$, and $^{16}OH^-$. Tuning parameters are described by Śliwiński et al. (2016) for calcite and Valley and Kita (2009) for corundum. Typical $^{16}O^-$ count rates were 2.5×10^9 counts per second (cps) for corundum (~2 nA primary beam) and 2×10^9 cps for calcite (~1 nA primary beam).

The analytical standards used to calibrate raw SIMS $\delta^{18}O$ measurements onto the VSMOW scale were UWC-3 for calcite (Kozdon, Ushikubo, Kita, Spicuzza, & Valley, 2009) and UWCrn9 for corundum (Appendix S2). To evaluate any instrument drift, four standard analyses were acquired before and after each bracketed group of ten unknown analyses. Analytical precision was determined from the 2SD of bracketing standard analyses. The average precision (2SD) is ±0.25‰ for calcite measurements (max = 0.45‰, sample 6) and ±0.26‰ for corundum (max = 0.51‰, sample 2; Table S3.2). When propagating analytical precision to the fractionation, the standard deviation of each paired calcite and corundum measurement were added in quadrature (range of propagated 2SD = 0.30 to 0.59‰). After SIMS analysis, pits in both samples and

243 standards were examined by SEM to confirm that cracks, other minerals, and μm-scale
244 inclusions were avoided.
245 Raw $\delta^{18}O$ values measured in calcite were corrected for matrix effects due to differences in the
246 amounts of Fe, Mn, and Mg measured in samples versus standard. While corrections in this study
247 were minor (i.e., avg = 0.45‰, max = 1.2‰; Appendix S3.12), a difference of 5 mol% $MgCO_3$
248 would change SIMS bias (or instrumental mass fractionation, IMF) by ~0.5‰ (Valley and Kita,
249 2009). Likewise, matrix effects due to Mg-Fe substitution in dolomite are significant (Śliwiński
250 et al., 2016) and Ca-Fe and Ca-Mn might be significant in calcite. In this study, bias* corrections
251 refer to $\delta^{18}O$ bias values for standards that have been normalized with respect to UWC-1 (end-
252 member calcite) for minor element corrections.
253 To correct for bias*, calcite standards of varying minor element composition were analyzed
254 during each carbonate SIMS session (Turnier, 2017; Appendix A5). Using this suite of calcite
255 standards, the $\delta^{18}O$ values of individual calcite SIMS analyses were corrected using sample
256 compositions obtained by EPMA (Table S5). The procedure for these corrections is summarized
257 in Appendix S4. The bias effects are relatively small because the bias for Ca-Mg is opposite in
258 sign and partly counteracts the bias for Ca-Fe and Ca-Mn. For the Naxos samples, the minor
259 element compositions of calcite within each sample cluster with respect to Fe, Mn, Mg, and Ca
260 (Figure 6). Low-temperature samples 7 and 8 have the lowest amounts of Fe, Mn, and Mg. In
261 this study, differences are minimal between standardization with UWC-3 only versus complex
262 standardization with a range of carbonates (average = 0.45‰). Corrections are greatest for
263 calcite with larger amounts of Fe (Figure S3.12).
264 For an empirical calibration of the calcite-corundum A-factor, it is necessary to obtain values of
265 fractionation for minerals that preserve peak-metamorphic equilibrium at the scale of analysis, so

SIMS analyses of calcite and corundum are placed as close together as possible while avoiding cracks and inclusions. These are referred to as "close pairs" of calcite and corundum. Typically, close pairs were less than 100 μm apart. The within-sample fractionations are evaluated for consistency—if representative of equilibrated pairs, fractionation should not vary by more than approximately 0.6‰ within a single sample that preserves peak metamorphic calcite-corundum isotope fractionation. The limit of 0.6‰ was defined as the 3SD of propagated analytical precision for fractionation values. Variability outside of this limit could be due to effects such as incomplete equilibration or retrogression.

In this study, fractionation consistency is statistically represented by the 2SD of fractionation (Δ(Cc-Crn)) values, which includes any real variability within the samples. This is not the same as the propagated analytical precision for fractionation, which is based on analysis of homogeneous standards. The 2SD of Δ(Cc-Crn) is determined by the standard deviation of within-sample fractionations; it is calculated for each sample based on the number of analyses and deviation of each value from the mean. This is summarized in Table 1 for each sample.

4 RESULTS

Data from this study are summarized in Table 1. Details are given for: mineralogy and modal abundances (Table 2), CL and BSE images (Figures 2-5), and any isotopic variability (Figures 2 and 5). All bulk and SIMS data are found in the appendix (Tables S1, S2, and S4) and a tabulation of each paired set of calcite and corundum measurements used to determine fractionation are in Table S3.2. Paired BSE and CL images for samples that are not shown in the main text are included in the appendix (Figures S3.3 to S3.9).

4.1 Isograds & Estimation of Temperature

Peak metamorphic temperature for each sample was approximated by linear interpolation of metamorphic gradients between isograds. Isograd temperatures were compared to oxygen isotope fractionations for quartz-kyanite pairs that satisfy the requirements for RAM thermometry in bi-mineral metamorphic veins in M2 pelites on Naxos (Putlitz et al., 2002). Quartz-kyanite pairs from zone-IV near the sillimanite-in isograd and zone-V yielded temperatures of 635 to 690 °C that match well with estimates from mineral isograds (620 to 700 °C for zone V; Δ(Qz-Ky) from Sharp, 1995). Also, the dehydration of margarite to corundum, anorthite, and water occurs at approximately 600 °C at 5.5 kbar (Rosing, Bird, & Dymek, 1987). The temperature estimated by linear interpolation between isograds for Sample 1 (593 °C), which contains margarite, corundum, and anorthite, matches well with the temperature at which this dehydration reaction occurs.

Another test of the accuracy of isograd temperatures is by comparison of the carbonate compositions with the calcite-dolomite solvus. None of the calcites in this study are buffered by dolomite and thus the solvus provides only a lower limit for metamorphic temperature. Samples 4 and 5 show the highest Mg content (4.0 to 5.3 mol % $MgCO_3$, Figure 6). Based on the position of the Cc-Dol solvus (Anovitz & Essene, 1987), this composition indicates a temperature greater than 550 °C for these rocks. This matches well with the temperature estimates from mineral isograds, which indicate a temperature of approximately 570 °C for these rocks.

4.2 Mineral Identification

EDS during SEM imaging was used to confirm mineral identification in the polished SIMS mounts for which transmitted light petrography is not possible. The modal mineralogy in

samples of this study are presented in Table 2 and agree with those identified by Feenstra (1985, 1996). Oxidation state was not determined for Fe, so both hematite and magnetite are referred to as "Fe-oxide", and oxides with various proportions of Fe and Ti are called "Fe-Ti oxides". For a detailed discussion of oxide and accessory mineralogy of these rocks, refer to Feenstra (1985), who reports magnetite as a major phase in the high-temperature samples (>540 ^{o}C, zones IV-V) and weakly magnetic Fe-Ti oxides and in the low-temperature samples (<540 ^{o}C, zones I-III; based on reflected-light microscopy and EPMA).

4.3 Modal Abundances

Modal abundances were approximated using ImageJ software and BSE images for areas approximately 600 × 1000 μm^2 in dimension. These abundances were used to assess the variation of major minerals at different metamorphic grades and to determine how well the samples approach conditions for RAM thermometry in terms of abundances for minerals with fast and slow rates of oxygen diffusion. The modes are summarized for each sample in Table 2. Areas with representative amounts of major minerals were chosen, but accessory mineral modes are not necessarily representative of the whole sample. In discrete areas, approximately bi-mineral abundances of calcite and corundum are present within a sample that otherwise can have moderate amounts of other minerals when considering a larger domain in the rock.

For samples in this study, mineral modes average 52% calcite, 25% corundum, and 13% or less for other accessory minerals. Oxygen diffuses much more quickly in calcite than in corundum, which is below its closure temperature (Yui et al., 2008) during metamorphism on Naxos. This limits isotopic alteration because retrograde exchange in the rock is dominated by the $\delta^{18}O$ of the fast-diffusing mineral and the slow-diffusing mineral will preserve its isotopic value if it formed

below its blocking temperature. Oxygen also diffuses quickly in some of the other minerals, notably muscovite and anorthite (Cole & Chakraborty, 2001; Fortier & Giletti, 1991). Hematite and magnetite are common accessory minerals and inclusions in the corundum, but oxygen diffuses relatively slowly. Overall, the diffusivity rates of oxygen decrease: anorthite > muscovite > calcite > magnetite > hematite > corundum.

Since oxygen diffuses relatively fast in calcite, its potential to exchange oxygen isotopes with other minerals is greater than corundum. Also, calcite in the low-grade rocks is close to its closure temperature (~400 °C; Farver, 1994). Using existing data on mineral-calcite fractionation, the isotope fractionation, or $\Delta_{18}O$(Cc-Mineral), calculated for these accessory minerals at 500 °C is: 9.9‰ (ΔCc-Mt; Chiba, Chacko, Clayton, & Goldsmith, 1989), 4.6‰ (ΔCc-Mrg; Hoffbauer, Hoernes, & Fiorentini, 1994), 3.5‰ (ΔCc-Msc; Hoffbauer et al., 1994), and 2.7‰ (ΔCc-An; Chiba et al., 1989). Mica is the most abundant mineral after calcite and corundum, and retrograde exchange of mica and calcite would raise the $\delta_{18}O$ value of calcite. The 2SD of Δ(Cc-Crn) values (Table 1) correlates with the mica to calcite ratio (mineral modes, Table 2); samples with higher ratios have greater fractionation variability (samples 2, 4, and 5). At Naxos, $\delta_{18}O$ variability of calcite (excluding vein calcite) is within 3SD of analytical precision near mica and other accessory minerals, suggesting minimal diffusion, but this nonetheless could contribute to some of the minor differences in $\delta_{18}O$ measured among calcite from discrete areas with multiple SIMS analyses. Sample 3 has the best modal abundances for RAM thermometry (78% calcite, 9% corundum, 8% tourmaline, 4% mica, and 1% oxides; Table 2) and thus has the least potential for isotopic exchange between calcite and other fast-diffusing minerals. Indeed, sample 3 also has the most consistent values of Δ(Cc-Crn) when comparing fractionations from area-to-area within the same sample (2SD of Δ(Cc-Crn) = 0.33‰; Table 1).

Corundum $\delta^{18}O$ is more variable than calcite in most samples, so fractionation variability must be influenced by factors other than oxygen diffusion in calcite.

4.4 CL Textures and Isotope Zonation

CL textures in corundum vary among high- and low-grade samples, either among grains within a single sample and among samples crystallized at similar metamorphic grade. Three main textural types are observed: 1) concentric zoning, 2) mottled zoning, and 3) linear zoning. Concentric zoning occurs as evenly distributed growth domains along the crystallographic faces (Figure 3c). Mottled zoning occurs as patchy zones of varying CL intensity (Figure 4a). Linear zoning appears as lines of different CL intensity cutting across a corundum grain (Figure 4c). These CL textures could have formed by a range of processes, including healed fractures, Ostwald ripening, deformation, growth zoning, or a combination of these processes. Images of zoning are shown for low-grade samples (Figure 3) and for high-grade samples (Figure 4). In general, corundum grains are larger in high-grade samples, but CL textures are variable among samples from a single metamorphic grade.

Despite the variety of CL textures, $\delta^{18}O$ values are consistent in most grains and do not correlate with specific domains of different CL intensity. Dark zones in corundum CL are not systematically different in $\delta^{18}O$ than more brightly luminescing counterparts. The largest isotopic gradients are 1.1‰/60 μm in corundum (Figure 5a) and 0.6‰/150 μm in calcite (Figure 5b). Calcite can sometimes exhibit bright luminescence, but no textural CL zoning was observed in this study. On average, the 2SD of $\delta^{18}O$ for single grains is 0.3‰ for calcite and 0.5‰ for corundum. Within ~500 × 500 μm areas in each sample, the average 2SD of $\delta^{18}O$ values is 0.5‰ for calcite and 0.6‰ for corundum. The larger $\delta^{18}O$ variability in corundum, which is below its

376 closure temperature, could be due to growth zoning. But this is within 3SD of analytical
377 precision and is considered insignificant.

378 **4.5 Secondary Veins and Disequilibrium**

379 Fluid flow was limited within the emery pockets on Naxos, as the impermeability of the
380 surrounding marble restricted the migration of externally derived fluids. Instead, fluid in the
381 emery pockets was mostly produced by the dehydration of diaspore to corundum and water
382 (Feenstra & Wunder, 2002). Infrequent calcite veins encountered in low-grade emery are
383 presumed to be secondary because of their fracture-filling textures and variable $\delta^{18}O$ values.
384 While syn-metamorphic veins can contain equilibrated mineral pairs, e.g., Putlitz et al. (2002),
385 secondary veins can be texturally and isotopically distinct; often the mineral pairs are not
386 isotopically equilibrated. Figure 7a shows an example of a low-temperature sample (NOA-2-3a)
387 with calcite forming a cross-cutting vein. The analyses from this sample yield large and variable
388 values of fractionation even for close mineral pairs (Δ(Cc-Crn) = 6.3 to 9.9‰, 2SD = 3.2‰).
389 Because vein calcite is not equilibrated with the corundum, these analyses cannot be used in A-
390 factor calibration. In contrast, Figure 8 shows high-temperature sample 1 with much less variable
391 SIMS analyses from calcite and corundum. The values of fractionation are consistent, even
392 among different CL zones in the corundum (avg. Δ(Cc-Crn) = 3.4‰, 2SD = 0.67‰; Table 1).
393 Most samples contain massive calcite associated with the corundum; three samples (NOA-379,
394 NOA-2-12a, and NZ-2-427) contained only vein calcite. These all occurred in the low-grade
395 rocks and were excluded from the thermometry calibration. All other eight samples contained
396 equilibrated assemblages with consistent oxygen isotope fractionation.

5 DISCUSSION

SIMS analysis allows avoidance of inclusions and secondary veins. Measurements target mineral pairs that texturally appear to have crystallized at peak metamorphic temperature. Fractionations among close pairs of calcite and corundum, measured by SIMS, have minimal variability. Low-temperature samples have Δ(Cc-Crn) values of 6.3 and 7.2‰ (2SD = 0.91‰); high-temperature samples range from 2.9 to 3.8‰ (2SD = 0.87‰). Values of Δ(Cc-Crn) contrast with the wide range of fractionations calculated from the previous bulk data of high- and low-temperature samples (-2.0 to 6.0‰ and 0.7 to 8.4‰, respectively). Given the variability of vein calcite $\delta^{18}O$ values obtained by SIMS, it is clear that bulk analysis averages peak metamorphic minerals with secondary veins and inclusions in corundum, contributing to the scatter of bulk measurements.

5.1 Evaluating Equilibrium

To examine possible equilibrium versus retrograde exchange, values of $\delta^{18}O$(Crn) vs. $\delta^{18}O$(Cc) are graphed in Figure 9. Such plots have been used to evaluate equilibrium or determine open-system exchange (Gregory & Criss, 1986). If a group of rocks has equilibrated at a constant metamorphic temperature, even though the whole rock $\delta^{18}O$ may be different for each rock, $\delta^{18}O$(a) vs. $\delta^{18}O$(b) will plot along an isopleth with a slope of one. This is because the value of $\Delta^{18}O$(a-b) is constant at a single temperature even though the $\delta^{18}O$ values may differ when the whole-rock values are different.

Thus, analyses from rocks that preserve equilibration at a constant temperature will form a linear array along an isotherm with constant Δ(Cc-Crn). Analyses from rocks preserving a different metamorphic temperature would plot along a different isotherm. These relations allow the

419 evaluation of data quality and whether each sample is consistent with local equilibrium at the
420 peak of metamorphism. Samples that pass this test can be compared to metamorphic
421 temperatures to create an empirical calibration of the A-factor versus temperature. While it is
422 difficult to prove equilibrium, mineral pairs that pass this test are consistent with equilibrium.
423 Alternatively, pairs that do not pass this test are proven to not be equilibrated at the scale of the
424 measurement.
425 Samples with calcite occurring in veins give erratic and variable values and are not equilibrated
426 at peak metamorphic temperatures. They plot away from the isotherms (Figure S3.10) and are
427 not used to calibrate calcite-corundum fractionation. The values of $\delta_{18}O$(Crn) vs. $\delta_{18}O$(Cc) for
428 close mineral pairs from the *in situ* SIMS analyses plot along isotherms for the average
429 temperature of high- and low- grade samples (avg. Δ(Cc-Crn) = 3.3 and 6.8‰, respectively;
430 Figure 9). In detail, individual data points within equilibrated samples will have some scatter, as
431 noted during the previous discussions of isotope zoning, diffusion, and RAM thermometry, but
432 the mean of these data for each sample plots along the isotherms.

433 **5.2 Disequilibrium effects**

434 Ideal calibration samples will have fractionation variability below 0.6‰, the propagated
435 analytical 3SD of Δ(Cc-Crn). Samples with variability outside of this are not necessarily
436 excluded but require evaluation. There are several potential causes of variability outside of
437 analytical precision, including retrograde diffusion, secondary mineral generations, and growth
438 zoning.
439 Secondary mineral generations are highly variable and distinct (2SD = 3.2‰, Figure S3.10), but
440 effects from diffusion or growth zoning are more subtle. Oxygen diffuses quickly in calcite, so
441 the potential for calcite $\delta_{18}O$ alteration increases if other minerals with fast oxygen diffusion are

442 locally abundant. These effects appear minimal since the 2SD of calcite $\delta^{18}O$ values is low
443 (range = 0.3 to 0.9‰, Avg. = 0.6‰; Table 1) even though the low-grade calcite is near its
444 closure temperature (~400 ^{o}C). Growth zoning appears to be more abundant in corundum (which
445 is below its closure temperature), though it is not consistent among CL domains. Corundum $\delta^{18}O$
446 2SD ranges from 0.5 to 1.2‰ (Avg. = 0.7‰; Table 1).
447 The interplay of effects on calcite and corundum variability within individual samples results in
448 greater 2SD Δ(Cc-Crn) for some samples (sample mounts 2, 3, 4, 5, 8). Despite this, the self-
449 consistency of fractionation values among rocks from a single grade suggest disequilibrium
450 effects are minor and the main effects on calcite-corundum fractionation are equilibrium
451 processes.

452 **5.3 Calibration of $\Delta^{18}O$(Cc-Crn)**

453 As discussed above, the $\delta^{18}O$ of fine-grained textures present in these rocks can only be resolved
454 using SIMS analyses in calcite and corundum. Calcite-corundum fractionations calculated from
455 SIMS data yield sample averages that range from 2.93 to 3.77‰ (Table 1) among six different
456 high-grade samples with a similar peak metamorphic temperature. This is reasonable, since
457 linear interpolation between isograds indicates a difference of 25°C among these samples (568 to
458 593 °C). The two low-grade samples have values of 6.33 and 7.20‰ (Table 1) and are from
459 rocks of equivalent metamorphic temperature (~425 °C, Table 1).
460 Measured calcite-corundum fractionations are self-consistent for close pairs within each sample.
461 The 2SE value of fractionation is a good representation of the uncertainty of average
462 fractionation values because it considers the number of analyses; from sample-to-sample, this
463 averages 0.26‰ (range = 0.10 to 0.56‰; Table S4). To determine the A-factor for calcite-

corundum fractionation, the average fractionation for each sample (Table 1) is plotted versus the metamorphic temperatures estimated from isograds (1000lnα(Cc-Crn) vs. $1/T_2$, Figure 10). In many circumstances, Δ(Cc-Crn), or $\delta_{18}O(a) - \delta_{18}O(b)$, is a good approximation for 1000lnα(a-b). For these metamorphic rocks, the differences between 1000lnα(Cc-Crn) and Δ(Cc-Crn) range from 0.06 to 0.16‰ (Avg. = 0.09‰), which is within analytical precision. The groups of high- and low-temperature samples cluster in 1000lnα(Cc-Crn) vs. $1/T_2$ space (Figure S3.11) and, taken together, define the slope, yielding an A-factor of 2.72 ±0.34 2SE (Eq. 1), assuming 0 fractionation at infinite temperature. The dashed lines in Figure 10 show the boundaries equivalent to ±0.34‰, the 2SE of the linear regression through the origin and eight data points for sample averages.

The slight non-linearity of the data could indicate a change in slope or more disequilibrium at lower temperatures. For most samples, corundum is more variable than calcite so it could be preserving some growth zoning. Corundum is below its closure temperature, so it is less likely to be affected by retrograde alteration than growth zoning. Another potential factor is the accuracy of the corundum-in isograd temperature. If the isograd temperature is lower, it would shift the fractionation closer to the linear regression.

Despite this, all eight samples are within analytical uncertainty of the linear regression. The median of low-temperature sample 7 plots above the line but is within error. If only the high-temperature data and origin are used to define the slope, a slightly smaller A-factor of 2.36 results, but this value is approximately within error of the linear regression 2SE. The isograd temperatures are estimated to be accurate to ±50 ^{o}C, providing an additional uncertainty based on the placement of isograds and determination of their temperatures.

The fractionations determined empirically in this study result in a calibration of the 1000lnα(Cc-Crn) vs. temperature. This is compared to the polynomial curve calculated using the modified increment method (Zheng 1991, 1994) in Figure 10. At 1000 K the modified increment method derives a fractionation of 6.5‰, which is more than twice the value of 2.7‰ empirically derived in this study. If the modified increment fractionation is applied to the values of Δ_{18}O(Cc-Crn) measured in this study by SIMS, estimated temperatures are unreasonably high when compared to the metamorphic mineral equilibria at Naxos, Greece. The high-temperature samples from zone IV have calculated temperatures of 975 to 1140 °C for rocks collected between the staurolite-in isograd (540 ^{o}C) and the sillimanite-in isograd (620 ^{o}C). Furthermore, these temperatures would be significantly above the temperature of partial melting (migmatite limit, ~700 °C; Figure 1). As such, the modified increment calibration is not consistent with reasonable metamorphic temperatures and the values of Δ_{18}O(Cc-Crn) measured for close pairs of calcite and corundum.

5.4 Mineral-Corundum A-factors

The empirical calcite-corundum A-factor of this study for oxygen isotope fractionation can be combined with other data to derive a suite of mineral-corundum A-factors (left column, Table 3). The oxygen isotope fractionation of calcite has been calibrated against a range of other minerals by experimental, theoretical, and empirical methods (Chacko et al., 2001; Fallick et al., 2019; O'Neil, Clayton, & Mayeda, 1969; Valley, 2003; Zheng, 1994). These calibrations allow derivation of mineral-corundum A-factors:

$$A(a-c) = A(a-b) + A(b-c) \quad (3)$$

506 where “a”, “b”, and “c” are minerals and “A” is the A-factor for each particular mineral-mineral
507 pair. In the case of this study, mineral “b” is calcite and “c” is corundum, and they can be used to
508 derive A-factors between corundum and other minerals (“a”).
509 If there are available data for a mineral-calcite system of interest and the linear A-factor
510 approximation is valid (Eq.1) these mineral-calcite A-factors can be used in Eq. 3 to derive the
511 A-factors for other minerals. The matrix of mineral-corundum A-factors in Table 3 is based on
512 calcite-mineral fractionations from Valley (2003) and references therein. Additional spinel-
513 mineral A-factors were calculated from the value of equilibrium $\Delta_{18}O$(Cc-spinel) reported in
514 Fallick et al. (2019; $\Delta_{18}O$(Cc-spinel) = 3.7‰ at T = 620 ^{o}C) and mineral-corundum A-factors
515 from the current study.

516 **5.5 Genesis of Basalt-Hosted Sapphire**

517 The A-factor for zircon-corundum (A(Zrc-Crn) = 0.46, Table 3) provides new insight for
518 evaluating corundum genesis. Wong and Verdel (2017) include a catalog of sapphire $\delta_{18}O$ values
519 from different rock types. These data (Figure 11) are from 74 localities among 19 countries,
520 detailing the $\delta_{18}O$ variation among gem corundum found in metamorphic, metasomatic, and
521 mafic to ultramafic igneous deposits. The $\delta_{18}O$ values range from 1.7 to 19.9‰ (Avg. = 6.7‰).
522 Of these data, corundum from metamorphic and metasomatic deposits range from 1.7 to 19.9‰
523 (Avg. = 9.7‰), and corundum associated with mafic to ultramafic deposits range from 2.7‰ to
524 13.9‰ (Avg. = 5.7‰). Zircons equilibrated at magmatic temperatures with typical mantle have
525 $\delta_{18}O$ = 4.7 to 5.9‰ (5.3 ±0.6‰ 2SD, Valley et al., 2005). Thus, corundum equilibrated with this
526 mantle value will have an average $\delta_{18}O$ of 5.1 ±0.6‰ 2SD at 1200 °C and range from 4.4 to
527 5.7‰.

528 This range of values calculated for primitive-mantle-like corundum is shown by a grey bar on a
529 histogram of gem corundum $\delta^{18}O$ values (Figure 11). The top histogram shows the distribution
530 in $\delta^{18}O$ of corundum associated with mafic and ultra-mafic rocks (including basalt, lamprophyre,
531 pyroxenite, and basanite), which are plotted together because they have similar $\delta^{18}O$ values.
532 Even though the host rocks for corundum are mantle-related, the corundum $\delta^{18}O$ ranges to higher
533 values than mantle-like corundum, overlapping with $\delta^{18}O$ values seen in corundum from
534 metamorphic and metasomatic deposits (bottom histogram, Figure 11). The high-$\delta^{18}O$ corundum
535 could not have crystallized from primitive mantle magmas. Furthermore, the textures suggest
536 that the corundum is not in equilibrium with the host magma, making the corundum inherently
537 xenocrystic.
538 Though most of the sapphires plotted in Figure 11 are found in placer deposits, they are thought
539 to originate from nearby rock types (e.g., basalt, lamprophyre, and basanite). Even within a
540 single corundum locality, the $\delta^{18}O$ can be quite variable. Among the localities in Figure 11,
541 placer corundum associated with basalt fields from Madagascar, the French Massif Central, and
542 Thailand are the most variable. The $\delta^{18}O$ value of gem sapphire ranges from 3.9 to 9.5‰ at
543 Vatromandry, Madagascar; 2.7 to 6.9‰ at Antisrabe, Madagascar; 4.7 to 8.4‰ at Denchai,
544 Thailand; and 4.9 to 10.3‰ at Le Mont Coupet, French Massif Central.
545 The variability within single localities and the overall range of $\delta^{18}O$ indicates that many of these
546 sapphires did not crystallize from primitive mantle-derived melt. Instead, it suggests that
547 sapphire formed from variable protoliths at different stages of melt evolution and crustal
548 contamination. Insights from the application of oxygen isotope equilibrium and thermometry will
549 allow us to better understand the nature and evolution of these enigmatic corundum deposits.

6 CONCLUSIONS

The emery deposits of Naxos, Greece provide an excellent opportunity to calibrate the A-factor for close mineral pairs of corundum and calcite by SIMS. The metamorphic isograds mapped in the emery deposits and surrounding pelitic schists provide an independent estimate of peak metamorphic temperature. Previous attempts to assess corundum-calcite fractionation using bulk analyses of mineral concentrates from these rocks were unsuccessful. In contrast, accurate and precise *in situ* analyses of $\delta^{18}O$ at a spatial resolution of 10 μm yield self-consistent values and variation in the calcite-corundum fractionations consistent with temperature estimates based on metamorphic isograds. Using SIMS analysis guided by CL and BSE imaging, inclusions in corundum, along with secondary, disequilibrium isotope zones, or late, retrograde minerals and veins, can be avoided. This allows for a consistent value of calcite-corundum fractionation from close mineral pairs to be obtained and interpreted to represent equilibrated peak metamorphic values.

When calibrated against temperature estimates from metamorphic isograds, data from this study yield an empirically determined A-factor of 2.72 ±0.3 (2SE) for the oxygen isotope fractionation between calcite and corundum. This value (2.72) is significantly smaller than that calculated from previous theoretically determined values ($1000\ln\alpha(Cc\text{-}Crn) = 6.5‰$ at 1000 K). Using the new A-factor, crystallization temperatures for corundum in equilibrium with other mineral species were calculated for a variety of different minerals. In addition, the $\delta^{18}O$ of minerals crystallized in equilibrium can be determined from independent temperature estimates.

The corundum-zircon fractionation was used in conjunction with compositions of zircon from primitive mantle to find the $\delta^{18}O$ range of mantle-like corundum (5.1 ±0.6‰). Based on the $\delta^{18}O$ range of sapphire hosted in mafic and ultramafic rocks, we propose that many of these sapphires

573 crystallized in association with evolved magmas that interacted with the crust and are thus
574 xenocrystic to the mantle rocks in which they are found.
575
576 **ACKNOWLEDGEMENTS**
577 We thank Brian Hess for sample preparation, the WiscSIMS group for SIMS support, John
578 Fournelle and Aurélien Moy for EPMA help, Bil Schneider and Phil Gopon for SEM training
579 and aid, Maciej Sliwinski for corrections of SIMS bias for carbonates, and Noriko Kita for SIMS
580 advice. We also thank Alan Matthews for helpful discussions. This work was supported by
581 National Science Foundation (EAR-1525336). WiscSIMS is supported by NSF (EAR-1355590,
582 1658823) and UW-Madison. RT received a UW-Madison Advanced Opportunity Fellowship.
583 Fieldwork was aided by the UW Geoscience Department.

584 **References**

585

586 Anovitz, L. M., & Essene, E. J. (1987). Phase equilibria in the system $CaCO_3$-$MgCO_3$-$FeCO_3$.
587 *Journal of Petrology, 28,* 389–415.

588 Avigad, D. (1998). High-pressure metamorphism and cooling on SE Naxos. *European Journal of*
589 *Mineralogy, 10,* 1309-1319.

590 Aydoğan, M. S., & Moazzen, M. (2012). Origin and Metamorphism of Corundum-Rich
591 Metabauxites at Mt. Ismail in the Southern Menderes Massif, SW Turkey. *Resource*
592 *Geology, 62,* 243–262.

593 Baker, J., & Matthews, A. (1994). Textural and isotopic development of marble assemblages
594 during the Barrovian-style M2 metamorphic event, Naxos, Greece. *Contributions to*
595 *Mineralogy and Petrology, 116,* 130-144.

596 Bolhar, R., Ring, U., & Ireland, T. R. (2017). Zircon in amphibolite from Naxos, Aegean Sea,
597 Greece: Origin, significance and tectonic setting. *Journal of Metamorphic Geology, 35,*
598 413–434.

599 Bowman, J. R., Valley, J. W., & Kita, N. T. (2009). Mechanisms of oxygen isotopic exchange
600 and isotopic evolution of $^{18}O/^{16}O$-depleted periclase zone marbles in the Alta aureole,
601 Utah: insights from ion microprobe analysis of calcite. *Contributions to Mineralogy and*
602 *Petrology, 157,* 77–93.

603 Buick, I. S. (1988). The Metamorphic and Structural Evolution of the Barrovian overprint,
604 Naxos, Cyclades, Greece. *Unpublished doctoral dissertation, University of Cambridge.* p.
605 235.

606 Buick, I. S., & Holland, T. J. B. (1989). The P-T-t path associated with crustal extension, Naxos,
607 Cyclades, Greece. *Geological Society of London Special Publication, 43,* 365–369.

608 Chacko, T., Cole, D. R., & Horita, J. (2001). Equilibrium Oxygen, Hydrogen and Carbon Isotope
609 Fractionation Factors Applicable to Geologic Systems. *Reviews in Mineralogy and*
610 *Geochemistry, 43,* 1–81.

611 Chiba, H., Chacko, T., Clayton, R. N., & Goldsmith, J. R. (1989). Oxygen isotope fractionations
612 involving diopside, forsterite, magnetite, and calcite: Application to geothermometry.
613 *Geochimica et Cosmochimica Acta, 53,* 2985–2995.

614 Cole, D. R., & Chakraborty, S. (2001). Rates and Mechanisms of Isotopic Exchange. *Reviews in*
615 *Mineralogy and Geochemistry, 43,* 83–223.

616 Donovan, J., Kremser, D., Fournelle, J., & Goemann, K. (2018). *Probe for Windows User's*
617 *Guide and Reference, Enterprise Edition*, Probe Software, Inc., Eugene, OR. p. 431.

618 Duchêne, S., Aïssa, R., & Vanderhaeghe, O. (2006). Pressure-temperature-time evolution of
619 metamorphic rocks from Naxos (Cyclades, Greece): Constraints from thermobarometry
620 and Rb/Sr dating, *Geodinamica Acta, 19*(5), 301–321.

621 Eiler, J. M., Baumgartner, L. P., & Valley, J. W. (1992). Intercrystalline stable isotope diffusion:
622 a fast grain boundary model. *Contributions to Mineralogy and Petrology, 112,* 543–557.

623 Eiler, J. M., Graham, C., & Valley, J. W. (1997). SIMS analysis of oxygen isotopes: matrix
624 effects in complex minerals and glasses. *Chemical Geology, 138,* 221–244.

625 Eiler, J. M., Valley, J. W., & Baumgartner, L. P. (1993). A new look at stable isotope
626 thermometry. *Geochimica et Cosmochimica Acta, 57,* 2571–2583.

627 Errico, J. C., Barnes, J. D., Strickland, A., & Valley, J. W. (2013). Oxygen isotope zoning in
628 garnets from Franciscan eclogite blocks: evidence for rock–buffered fluid interaction in
629 the mantle wedge. *Contributions to Mineralogy and Petrology, 166,* 1161–1176.

630 Fallick, A., Giuliani, G., Rigaudier, T., Boyce, A. J., Long Pham, V., & Pardieu, V. (2019).
631 Remarkably uniform oxygen isotope systematics for co-existing pairs of gem-spinel and
632 calcite in marble, with special reference to Vietnamese deposits. *Comptes Rendus*
633 *Geoscience, 351,* 27–36.

634 Farver, J. R. (1994). Oxygen self-diffusion in calcite: Dependence on temperature and water
635 fugacity. *Earth and Planetary Science Letters, 121,* 575–587.

636 Feenstra, A. (1985). Metamorphism of bauxites on Naxos, Greece. *Geologica Ultraiectina, 39,*
637 1–206.

638 Feenstra, A. (1996). An EMP and TEM—AEM study of margarite, muscovite and paragonite in
639 polymetamorphic metabauxites of Naxos (Cyclades, Greece) and the implications of fine-
640 scale mica interlayering and multiple mica generations. *Journal of Petrology, 37,* 201–
641 233.

642 Feenstra, A., & Wunder, B. (2002). Dehydration of diasporite to corundite in nature and
643 experiment. *Geology, 30,* 119–122.

644 Ferry, J. M., Kitajima, K., Strickland, A., & Valley, J. W. (2014). Ion microprobe survey of the
645 grain-scale oxygen isotope geochemistry of minerals in metamorphic rocks. *Geochimica*
646 *et Cosmochimica Acta, 144,* 403–433.

647 Ferry, J. M., Ushikubo, T., Kita, N. T., & Valley, J. W. (2010). Assessment of grain-scale
648 homogeneity and equilibration of carbon and oxygen isotope compositions of minerals in
649 carbonate-bearing metamorphic rocks by ion microprobe. *Geochimica et Cosmochimica*
650 *Acta, 74,* 6517–6540.

651 Fortier, S. M., & Giletti, B. J. (1991). Volume self-diffusion of oxygen in biotite, muscovite, and
652 phlogopite micas. *Geochimica et Cosmochimica Acta, 55,* 1319–1330.

653 Giuliani, G., Ohnenstetter, D., Fallick, A. E., Groat, L.A., & Fagan, A. J. (2014). The Geology
654 and Genesis of Gem Corundum Deposits. *Mineralogical Association of Canada Short*
655 *Course, 44,* 23–112.

656 Gregory, R. T., & Criss, R. E. (1986). Isotopic Exchange in Open and Closed Systems. *Reviews*
657 *in Mineralogy, 16,* 91–127.

658 Gordon, S. M., Luffi, P., Hacker, B., Valley, J., Spicuzza, M., Kozdon, R., Kelemen, P.,
659 Ratshbacher, L., & Minaev, V. (2012). The thermal structure of continental crust in
660 active orogens: insight from Miocene eclogite and granulite xenoliths of the Pamir
661 Mountains. *Journal of Metamorphic Geology, 30,* 413–434.

662 Hervig, R. L., Williams, P., Thomas, R. M., Schauer, S. N., & Steele, I. M. (1992).
663 Microanalysis of oxygen isotopes in insulators by secondary ion mass spectrometry.
664 *International Journal of Mass Spectrometry and Ion Processes, 120,* 45–63.

665 Hoefs, J. (2018). *Stable Isotope Geochemistry*. New York: Springer International Publishing. p.
666 437.

667 Hoffbauer, R., Hoernes, S., & Fiorentini, E. (1994). Oxygen isotope thermometry based on a
668 refined increment method and its application to granulite-grade rocks from Sri Lanka.
669 *Precambrian Research, 66,* 199–220.

670 Jansen, J. B. H., & Schuiling, R. D. (1976). Metamorphism on Naxos; petrology and geothermal
671 gradients. *American Journal of Science, 276,* 1225–1253.

672 Jansen, J. B. H. (1977). *The Geology of Naxos.* Athens: Institute of geological and mining
673 research*, 19*(1-3), p. 100.

674 Katzir, Y., Avigad, D., Matthews, A., Garfunkel, Z., & Evans, B. W. (1999). Origin and
675 metamorphism of ultrabasic rocks associated with a subducted continental margin, Naxos
676 (Cyclades, Greece). *Journal of Metamorphic Geology, 17,* 301–318.

677 Katzir, Y., & Valley, J. W. (2001). Calcite-corundum oxygen isotope fractionations in Naxos
678 metabauxites; selecting samples for thermometry. *Geological Society of America, Annual*
679 *Meeting Abstract*, *#25470*.

680 Katzir, Y., Valley, J. W., & Matthews, A. (2002). Tracking fluid flow during deep crustal
681 anatexis: metasomatism of peridotites (Naxos, Greece). *Contributions to Mineralogy and*
682 *Petrology, 142,* 700–713.

683 Keay, S., Lister, G., & Buick, I. S. (2001). The timing of partial melting, Barrovian
684 metamorphism and granite intrusion in the Naxos metamorphic core complex, Cyclades,
685 Aegean Sea, Greece. *Tectonophysics, 342,* 275-312.

686 Kitchen, N. E., & Valley, J. W. (1995). Carbon isotope thermometry in marbles of the
687 Adirondack Mountains, New York. *Journal of Metamorphic Geology, 13,* 577–594.

688 Kozdon, R., Ushikubo, T., Kita, N. T., Spicuzza, M., & Valley, J. W. (2009). Intratest oxygen
689 isotope variability in the planktonic foraminifer N. pachyderma: Real vs. apparent vital
690 effects by ion microprobe. *Chemical Geology, 258,* 327–337.

691 Martin, L., Duchéne, S., Deloule, E., & Vanderheaghe, O. (2006). The isotopic composition of
692 zircon and garnet: a record of the metamorphic history of Naxos, Greece. *Lithos, 87,* 174-
693 192.

694 O'Neil, J. R. (1986). Theoretical and Experimental Aspects of Isotopic Fractionation. *Reviews in*
695 *Mineralogy, 16,* 1–40.

696 O'Neil, J. R., Clayton, R. N., & Mayeda, T. K. (1969). Oxygen isotope fractionation in divalent
697 metal carbonates. *Journal of Chemical Physics, 51,* 5547–5558.

698 Page, F. Z., Essene, E. J., Mukasa, S. B., & Valley, J. W. (2014). A garnet–zircon oxygen
699 isotope record of subduction and exhumation fluids from the Franciscan Complex,
700 California. *Journal of Petrology, 55,* 103–131.

Pouchou, J. L., & Pichoir, F. (1991). Quantitative analysis of homogenous or stratified microvolumes applying the model "PAP". K. F. J. Heinrich and D. E. Newbury, Eds. *Electron Probe Quantitation*, 31–75.

Putlitz, B., Valley, J. W., Matthews, A., & Katzir, Y. (2002). Oxygen isotope thermometry of quartz–Al_2SiO_5 veins in high-grade metamorphic rocks on Naxos island (Greece). *Contributions to Mineralogy and Petrology, 143,* 350–359.

Quinn, R. J., Kitajima, K., Nakashima, D., Spicuzza, M. J., & Valley, J. W. (2017). Oxygen isotope thermometry using quartz inclusions in garnet. *Journal of Metamorphic Geology, 35,* 231–252.

Reed, R. M., & Milliken, K. L. (2003). How to overcome imaging problems associated with carbonate minerals on SEM-based cathodoluminescence systems. *Journal of Sedimentary Research, 73,* 328–332.

Rosing, M. T., Bird, D. K., & Dymek, R. F. (1987). Hydration of corundum-bearing xenoliths in the Qôrqut Granite Complex, Godthåbsfjord, West Greenland. *American Mineralogist, 72,* 29–38.

Russell, A. K., Kitajima, K., Strickland, A., Medaris, L. G., Schulze, D. J., & Valley, J. W. (2013). Eclogite-facies fluid infiltration: constraints from $\delta^{18}O$ zoning in garnet. *Contributions to Mineralogy and Petrology, 165,* 103–116.

Rye, R. O., Schuiling, R. D., Rye, D. M., & Jansen, J. B. H. (1976). Carbon, hydrogen, and oxygen isotope studies of the regional metamorphic complex at Naxos, Greece. *Geochimica et Cosmochimica Acta, 40,* 1031–1049.

722 Schuiling, R. D., & Oosterom, M. G. (1967). The metamorphic complex on Naxos (Greece) and
723 the strontium and barium content of its carbonate rocks. *Proceedings of the Koninklijke*
724 *Nederlandse Akademie van Wetenschappen, 70*(2), 165–175.

725 Sharp, Z. D. (1995). Oxygen isotope geochemistry of the Al_2SiO_5 polymorphs. *American*
726 *Journal of Science, 295,* 1058–1076.
727
728 Śliwiński, M. G., Kitajima, K., Kozdon, R., Spicuzza, M. J., Fournelle, J. H., Denny, A., &
729 Valley, J. W. (2016). Secondary ion mass spectrometry bias on isotope ratios in
730 dolomite–ankerite, Part I: $\delta_{18}O$ Matrix Effects. *Geostandards and Geoanalytical*
731 *Research, 40,* 157–172.

732 Turnier, R. B. (2017). Calibration of Oxygen Isotope Fractionation and Corundum-Calcite
733 Thermometry in Emery at Naxos, Greece: *In Situ* Versus Bulk Analysis. *Unpublished M.S.*
734 *Thesis, University of Wisconsin-Madison.* p. 53.

735 Valley, J. W. (2001). Stable Isotope Thermometry at High Temperatures. *Reviews in Mineralogy*
736 *and Geochemistry, 43,* 365–413.

737 Valley, J. W. (2003). Oxygen Isotopes in Zircon. *Reviews in Mineralogy and Geochemistry, 53,*
738 343–385.

739 Valley, J. W., & Kita, N. T. (2009). In Situ Oxygen Isotope Geochemistry by Ion Microprobe.
740 *Mineralogical Association of Canada Short Course, 41,* 19–63.

741 Valley, J. W., Lackey, J. S., Cavosie, A. J., Clechenko, C. C., Spicuzza, M. J., Basei, M. A. S.,
742 Bindeman, I. N., Ferreira, V. P., Sial, A. N., King, E. M., Peck, W. H., Sinha, A. K., &

743 Wei, C. S. (2005). 4.4 billion years of crustal maturation: oxygen isotope ratios of
744 magmatic zircon. *Contributions to Mineralogy and Petrology, 150,* 561–580.

745 Vielzeuf, D., Champenois, M., Valley, J. W., Brunet, F., & Devidal, J. L. (2005). SIMS analyses
746 of oxygen isotopes: Matrix effects in Fe–Mg–Ca garnets. *Chemical Geology, 223,* 208–
747 226.

748 Wijbrans, J. R., & McDougall, I., 1988. Metamorphic evolution of the Attic-Cycladic
749 metamorphic belt on Naxos (Cyclades, Greece) utilizing $^{40}Ar/^{39}Ar$ age spectrum
750 measurements. *Journal of Metamorphic Geology, 6,* 571-594.

751 Wong, J., & Verdel, C. (2017). Tectonic environments of sapphire and ruby revealed by a global
752 oxygen isotope compilation. *International Geology Review, 60*(2), 188–195.

753 Yui, T.-F., Zaw, K., & Wu, C.-M. (2008). A preliminary stable isotope study on Mogok Ruby,
754 Myanmar. *Ore Geology Reviews, 34,* 192–199.

755 Zheng Y.-F. (1991). Calculation of oxygen isotope fractionation in metal oxides. *Geochimica et*
756 *Cosmochimica Acta, 55,* 2299–2307.

757 Zheng Y.-F. (1994). Oxygen isotope fractionation in metal monoxides. *Mineralogical Magazine,*
758 *58A,* 1000–1001.

759 **SUPPORTING INFORMATION**

760 Additional Supporting Information may be found online in the supporting information tab for
761 this article.

762 Suppinfo.pdf

Appendix S1. Tabulated Bulk Fractionation

Table S1.1. Tables of calcite-corundum fractionation for each hand-sample. These data were acquired from 2001-2002 by laser fluorination (corundum) and acid reaction (calcite) at the University of Wisconsin-Madison. The 2SD listed for corundum, calcite, and fractionation ($\Delta_{18}O$(Cc-Crn)), report the variability of samples and are not analytical precision. The 2SD of calcite and corundum $\delta_{18}O$ values are used to calculate the propagated 2SD for $\Delta_{18}O$(Cc-Crn), which is calculated from the square root of calcite and corundum $\delta_{18}O$ 2SD values added in quadrature. These data and analytical precision 2SD are tabulated in Table S1 and S2. Crn = corundum and Cc = calcite.

Appendix S2. Corundum Standard Development

Table S2.1. List of all potential corundum standards and any known information about their locality, characteristics, and mount number. Most samples analyzed have an acceptable 2SD for a standard (except UWCrn8). UWCrn9 shows the lowest variability.

Figure S2.1. Image of epoxy mount GR1 with natural corundum grains investigated as potential standards.

Table S2.2. Table summarizes SIMS data for homogeneity test of UWCrn9 (selected and used as a working standard for all corundum SIMS analyses in this study).

Table S2.3. Table summarizes laser fluorination data for UWCrn9.

Figure S2.2. Image of epoxy mount GR2 with synthetic and natural corundum grains investigated as potential standards. Width of epoxy mount is 2.54 cm.

Figure S2.3. BSE image of UWCrn9 grain 4.

Figure S2.4. CL images of UWCrn9 grains 2, 4, 10, and 11.

Appendix S3. Naxos SIMS Supplementary Material

Figure S3.1. Images showing samples used for SIMS analysis and calcite-corundum A-factor calibration (8 out of 15 mounts prepared for calcite-corundum pairs; other mounts had either vein calcite or were from a location within the metabauxite lens that did not have both calcite and corundum). Mount names (top label) are shown along with sample names (bottom label) for reference. Standards UWCrn9 and UWC-3 are mounted in these samples.

Table S3.1. List of sample names and coordinates for all rocks analyzed by SIMS from Naxos, Greece.

Figure S3.2. Supplementary geological map of Naxos, Greece. Open circles show the location of emery deposits. Samples used in this study are located in Figure 1. Blue stars indicate the location of extra samples that were not used in A-factor calibration because of disequilibrium textures (e.g., vein calcite) or a lack of within-session standardization for the carbonate minor element bias correction; GPS coordinates for these samples are listed in Table S3.1. Map also shows the grouping of Naxos rock units into the Upper Series, Lower Series, and migmatite (leucogneiss core).

Figure S3.3. Representative CL/SE and BSE image of sample 2 (NL-4-351) showing SIMS data for $\delta^{18}O$ in calcite and corundum (circles and accompanying numbers). The partial black box in panel a) denotes the location of magnified CL/SE image in panel b); part of the image in b) extends beyond the field of view in a).

Figure S3.4. Representative CL/SE and BSE image of sample 3 (NL-7-358), including SIMS data for $\delta^{18}O$ in calcite and corundum (circles and accompanying numbers). Circle with "x" through it marks location of bad analysis. Panel B highlights corundum CL and $\delta^{18}O$, showing limited growth texture. Ap = apatite, Crn = corundum, Cc = calcite, Rt = rutile, Mrg = margarite, and Msc = muscovite.

Figure S3.5. Representative CL/SE and BSE image of sample 4 (NL-3-40Aa) showing SIMS data for $\delta^{18}O$ in calcite and corundum (circles and accompanying numbers). Crn = corundum, Cc = calcite, Mrg = margarite, and Ap = apatite.

Figure S3.6. Representative CL/SE and BSE image of sample 6 (NL-8-359) showing SIMS data for $\delta^{18}O$ in calcite and corundum (circles and accompanying numbers). Crn = corundum, Cc = calcite, Msc = muscovite, Rt = rutile, and Gahnitic Spi = spinel with Zn.

Figure S3.7. Representative CL/SE and BSE image of sample 7 (NOA-381) showing SIMS data for $\delta^{18}O$ in calcite and corundum (circles and accompanying numbers). Crn = corundum, Cc = calcite, Mrg = margarite, Cld = chloritoid, Tur = tourmaline, Msc = muscovite, and Dsp = diaspore.

Figure S3.8. Representative CL/SE and BSE image of sample 8 (NZ-3-434) showing SIMS data for $\delta^{18}O$ in calcite and corundum (circles and accompanying numbers). Circle with black "x" indicates bad data point. Crn = corundum, Cc = calcite, Cld = chloritoid, and Dsp = diaspore.

Figure S3.9. Representative CL/SE and BSE image of sample 8 (NZ-3-434) showing SIMS data for $\delta^{18}O$ in calcite and corundum (circles and accompanying numbers). Crn = corundum, Cc = calcite, Fe-oxide = iron oxide, Msc = muscovite, Mrg = margarite, and Cld = chloritoid. CL/SE image shows slight isotopic zonation covarying with CL intensity.

Table S3.2. Tabulation of SIMS data for touching calcite-corundum mineral pairs used in A-factor calibration, with analytical 2SD values for calcite and corundum from SIMS precisions; fractionation 2SD propagated (prop.) is calculated from the square root of calcite and corundum analytical 2SD added in quadrature. The analytical 2SD values reported in "Averages" for measurements of calcite, corundum, and fractionation, are the maximum 2SD of all averaged

832 measurements for a single sample. The 2SE for Δ(Cc-Crn) values is not equivalent to the
833 analytical precision. It was determined from the 2SD of each sample's spot-to-spot fractionation
834 values divided by the square root of the number of measurements from that sample. SIMS calcite
835 data have been corrected for carbonate cation composition $\delta^{18}O$ bias.

836 **Figure S3.10.** Plot of $\delta^{18}O$(Cc) vs. $\delta^{18}O$(Crn) for calcite coexisting with corundum. All
837 pairs are close mineral pairs that are interpreted to be equilibrated, except green symbols that are
838 from texturally late vein calcite (BSE, CL images in Figure 7; sample NOA-2-3a).

839 **Figure S3.11.** Plot showing 1000lnα(Cc-Crn) vs. $1/T_2$ (K) of individual calcite-corundum
840 pairs for each sample with y-axis error bars from analytical 2SD and x-axis error bars from the
841 isograd temperature uncertainty (±50 °C). For reference, temperature in ^{o}C is included on the
842 upper x-axis. Based on this study's data, the line going through to the origin, whose slope is the
843 A-factor, shows value of 2.72.

844 **Figure S3.12.** Plots of the $\delta^{18}O$ (Cc) VSMOW difference (‰) between simple and minor
845 element carbonate bias correction versus mol % $MgCO_3$, $MnCO_3$, and $FeCO_3$. Mol %
846 concentrations are from EPMA measurements. The extent of $\delta^{18}O$ difference between
847 measurements corrected by the simple versus carbonate composition bias methodology varies
848 depending on calcite composition.

849 **Appendix S4**. SIMS Carbonate Composition Bias Correction

850 **Table S4.1.** Carbonate standard compositions (in mol %) determined by EPMA and
851 stable isotope ratios determined by reaction with concentrated phosphoric acid and gas-source
852 mass spectrometry at UW-Madison.

853

854 Dataset.xlsx

Table S1. Bulk Naxos $\delta^{18}O$ corundum LF data

Table S2. Bulk Naxos $\delta^{18}O$ acid dissolution calcite data

Table S3. Catalogue of all standard development SIMS data

Table S4. Catalogue of all Naxos A-factor calibration SIMS data. Discarded analyses are denoted with gray font and justified in the "comments" column.

Table S5. Catalogue of all Naxos calcite EPMA data for composition bias correction

Appendix S1. Tabulated Bulk Fractionation

Table S1.1. Tables of calcite-corundum fractionation for each hand-sample. These data were acquired from 2001-2002 by laser fluorination (corundum) and acid reaction (calcite) at the University of Wisconsin-Madison. The 2SD listed for corundum, calcite, and fractionation ($\Delta_{18}O$(Cc-Crn)), report the variability of samples and are not analytical precision. The 2SD of calcite and corundum $\delta_{18}O$ values are used to calculate the propagated 2SD for $\Delta_{18}O$(Cc-Crn), which is calculated from the square root of calcite and corundum $\delta_{18}O$ 2SD values added in quadrature. These data and analytical precision 2SD are tabulated in Table S1 and S2. Crn = corundum and Cc = calcite.

T= 581 °C

Sample No.	Phase	$\delta_{18}O$ VSMOW	Sample No.	Phase	$\delta_{18}O$ VSMOW
NL-3-347	Crn (150-500)	19.95	**NL-3-347 C**	Cc	24.34
NL-3-347	Crn (<150 micron)	20.26	**NL-3-347 F**	Cc	23.29
NL-3-347	Crn (<150 micron)	19.99	**NL-3-347a**	Cc	22.38
NL-3-347	Crn (picked)	20.08	**NL-3-347b**	Cc	21.83
NL-3-347	Crn (picked)	20.09			
	Crn avg:	**20.07**		**Cc avg:**	**22.96**
	2SD	***0.24***		***2SD***	***2.20***

$\Delta^{18}O$(Cc-Crn) and propagated 2SD: 2.89 ± 2.21

T= 581 °C

Sample No.	Phase	$\delta_{18}O$ VSMOW	Sample No.	Phase	$\delta_{18}O$ VSMOW
NL-3-349	Crn (blue)	22.18	**NL-3-349 F**	Cc	26.21
NL-3-349	Crn (blue)	22.09	**NL-4-349 coarse**	Cc	26.01
	Crn avg:	**22.14**		**Cc avg:**	**26.11**
	2SD	***0.13***		***2SD***	***0.28***

$\Delta^{18}O$(Cc-Crn) and propagated 2SD: 3.98 ± 0.31

T= 577 °C

Sample No.	Phase	$\delta_{18}O$ VSMOW	Sample No.	Phase	$\delta_{18}O$ VSMOW
NL-4-350	Crn	21.12	**NL-4-350 C**	Cc	26.19
NL-4-350	Crn	21.69	**NL-4-350 F**	Cc	25.93
	Crn avg:	**21.41**		**Cc avg:**	**26.06**
	2SD	***0.81***		***2SD***	***0.37***

$\Delta^{18}O$(Cc-Crn) and propagated 2SD: 4.66 ± 0.89

T= 577 °C

Sample No.	Phase	$\delta_{18}O$ VSMOW	Sample No.	Phase	$\delta_{18}O$ VSMOW
NL-4-351	Crn (or)	18.68	**NL-4-351 C**	Cc	21.72
NL-4-351	Crn (or)	18.75	**NL-4-351 F**	Cc	22.38
NL-4-351	Crn (or)	18.57	**NL-4-351a**	Cc	22.69
NL-4-351	Crn	18.71	**NL-4-351b**	Cc	22.63
NL-4-351	Crn	18.72	**NL-4-351c**	Cc	22.56
NL-4-351	Crn	18.56	**NL-4-351m**	Cc	22.01
	Crn avg:	**18.67**		**Cc avg:**	**22.33**
	2SD	***0.16***		***2SD***	***0.77***

$\Delta^{18}O$(Cc-Crn) and propagated 2SD: 3.67 ± 0.79

T= 577 °C

Sample No.	Phase	$\delta_{18}O$ VSMOW	Sample No.	Phase	$\delta_{18}O$ VSMOW
NL-4-354	Crn (picked after)	21.38	**NL-4-354-2**	Cc	25.18
NL-4-354	Crn (picked)	21.28	**NL-4-354-2 (100-500)**	Cc	25.18
NL-4-354-1	Crn	20.94			
NL-4-354-1	Crn	20.98			
NL-4-354-3	Crn	21.54			
NL-4-354-3	Crn	21.32			
NL-4-354-3	Crn	21.47			
NL-4-354-4	Crn (100-300)	20.92			
NL-4-354-4	Crn (<100)	21.10			
NL-4-354-4	Crn (<100)	21.24			
NL-4-354-4	Crn	21.13			
	Crn avg:	**21.21**		**Cc avg:**	**25.18**
	2SD	***0.43***		***2SD***	***0.00***

$\Delta^{18}O$(Cc-Crn) and propagated 2SD: 3.97 ± 0.43

T= 577 °C

Sample No.	Phase	$\delta_{18}O$ VSMOW	Sample No.	Phase	$\delta_{18}O$ VSMOW
NL-6-356	Crn (150-300)	18.38	**NL-6-356a**	Cc	23.44
NL-6-356	Crn (150-300)	18.41	**NL-6-356b**	Cc	23.24
NL-6-356	Crn (150-300)	18.54	**NL-6-356m**	Cc	21.60
NL-6-356	Crn	18.62			
NL-6-356	Crn	18.46			
	Crn avg:	**18.48**		**Cc avg:**	**22.76**
	2SD	***0.20***		***2SD***	***2.02***

$\Delta^{18}O$(Cc-Crn) and propagated 2SD: 4.28 ± 2.03

T= 574 °C

Sample No.	Phase	$\delta_{18}O$ VSMOW	Sample No.	Phase	$\delta_{18}O$ VSMOW
NL-7-357	Crn (150-300)	17.84	**NL-7-357 <150µm**	Cc	24.37
NL-7-357	Crn (150-300)	17.87	**NL-7-357 150-500µm**	Cc	24.37
	Crn avg:	**17.86**		**Cc avg:**	**24.37**
	2SD	***0.04***		***2SD***	***0.00***

$\Delta^{18}O$(Cc-Crn) and propagated 2SD: 6.52 ± 0.04

T= 568 °C

Sample No.	Phase	$\delta_{18}O$ VSMOW	Sample No.	Phase	$\delta_{18}O$ VSMOW
NL-8-359	Crn	18.19	NL-8-359 <150µm	Cc	18.50
NL-8-359	Crn	18.14	NL-8-359 150-500µm	Cc	21.90
			NL-8-359 F	Cc	18.54
			NL-8-359a	Cc	18.33
			NL-8-359b	Cc	20.90
			NL-8-359c	Cc	18.47
			NL-8-359d	Cc	19.23
			NL-8-359m	Cc	21.84
	Crn avg:	18.17		Cc avg:	19.71
	2SD	*0.07*		*2SD*	*3.14*

$\Delta^{18}O$(Cc-Crn) and propagated 2SD: 1.55 ± 3.14

T= 593 °C

Sample No.	Phase	$\delta_{18}O$ VSMOW	Sample No.	Phase	$\delta_{18}O$ VSMOW
NM-1-370-1	Crn	19.29	**NM-1-370-1**	Cc	23.23
NM-1-370-1	Crn	19.49	**NM-1-370-1 (100-500)**	Cc	23.33
NM-1-370-1	Crn	19.43			
NM-1-370-2	Crn	18.87			
NM-1-370-2	Crn	18.91			
	Crn avg:	**19.20**		**Cc avg:**	**23.28**
	2SD	***0.58***		***2SD***	***0.14***

$\Delta^{18}O$(Cc-Crn) and propagated 2SD: 4.08 ± 0.60

T= 593 °C

Sample No.	Phase	$\delta_{18}O$ VSMOW	Sample No.	Phase	$\delta_{18}O$ VSMOW
NM-2-373-1	Crn	16.27	**NM-2-373-1**	Cc	23.15
NM-2-373-1	Crn	16.22	**NM-2-373-1 (100-500)**	Cc	23.15
NM-2-373-1	Crn	16.36			
NM-2-373-2	Crn	17.31			
NM-2-373-2	Crn	17.35			
	Crn avg:	**16.70**		**Cc avg:**	**23.15**
	2SD	***1.15***		***2SD***	***0.00***

$\Delta^{18}O$(Cc-Crn) and propagated 2SD: 6.45 ± 1.15

T= 425 °C

Sample No.	Phase	$\delta_{18}O$ VSMOW	Sample No.	Phase	$\delta_{18}O$ VSMOW
NOA-378-1	Crn	14.80	**NOA-378-2**	Cc	23.22
NOA-378-1	Crn	14.83			
NOA-378-1	Crn	14.86			
NOA-378-2	Crn	14.91			
NOA-378-2	Crn	14.89			
	Crn avg:	**14.86**		**Cc avg:**	**23.22**
	2SD	***0.09***		***2SD***	***N/A***

$\Delta^{18}O$(Cc-Crn) and propagated 2SD: 8.36 ± 0.09

T= 425 °C

Sample No.	Phase	$\delta_{18}O$ VSMOW	Sample No.	Phase	$\delta_{18}O$ VSMOW
NOA-379-1	Crn	15.15	**NOA-379-1**	Cc	23.03
NOA-379-1	Crn	15.14			
NOA-379-2	Crn	15.37			
NOA-379-2	Crn	15.29			
NOA-379-2	Crn	15.24			
NOA-379-2	Crn	15.28			
	Crn avg:	**15.25**		**Cc avg:**	**23.03**
	2SD	***0.18***		***2SD***	***N/A***

$\Delta^{18}O$(Cc-Crn) and propagated 2SD: 7.79 ± 0.18

T= 425 °C

Sample No.	Phase	$\delta_{18}O$ VSMOW	Sample No.	Phase	$\delta_{18}O$ VSMOW
NOA-381-1	Crn	17.45	**NOA-381-3**	Cc	17.75
NOA-381-2	Crn	16.26	**NOA-381-3 (100-500)**	Cc	17.75
NOA-381-2	Crn	16.04			
NOA-381-2	Crn	16.15			
NOA-381-3	Crn	17.60			
NOA-381-3	Crn	17.58			
NOA-381-3	Crn	17.62			
NOA-381-3	Crn	17.58			
	Crn avg:	**17.04**		**Cc avg:**	**17.75**
	2SD	***1.47***		***2SD***	***0.00***

$\Delta^{18}O$(Cc-Crn) and propagated 2SD: 0.72 ± 1.47

T= 424 °C

Sample No.	Phase	$\delta_{18}O$ VSMOW	Sample No.	Phase	$\delta_{18}O$ VSMOW
NZ-2-428-4	Crn	21.41	**NZ-2-428-3**	Cc	25.07
NZ-2-428-5	Crn	21.03	**NZ-2-428-3 (100-500)**	Cc	25.07
	Crn avg:	**21.22**		**Cc avg:**	**25.07**
	2SD	***0.54***		***2SD***	***0.00***

$\Delta^{18}O$(Cc-Crn) and propagated 2SD: 3.85 ± 0.54

T= 571 °C

Sample No.	Phase	$\delta_{18}O$ VSMOW	Sample No.	Phase	$\delta_{18}O$ VSMOW
NL-10-366	Crn (B)	17.08	**NL-10-366 <150µm**	Cc	21.02
NL-10-366	Crn (w)	17.01			
NL-10-366	Crn (pink)	17.02			
NL-10-366	Crn (pink	17.13			
NL-10-366	Crn (pink)	17.23			
NL-10-366	Crn (blue)	17.23			
	Crn avg:	**17.12**		**Cc avg:**	**21.02**
	2SD	***0.196***		***SD***	***N/A***

$\Delta^{18}O$(Cc-Crn) and propagated 2SD: 3.90 ± 0.20

T= 581 °C

Sample No.	Phase	$\delta_{18}O$ VSMOW	Sample No.	Phase	$\delta_{18}O$ VSMOW
NL-3-348	Crn (<150 micron)	19.02	**NL-3-348 C**	Cc	23.47
NL-3-348	Crn (<150 micron)	19.12	**NL-3-348 F**	Cc	20.84
NL-3-348	Crn (150-500)	19.22	**NL-3-348-a**	Cc	18.34
NL-3-348	Crn (150-500	19.17	**NL-3-348b**	Cc	17.32
NL-3-348	Crn (150-500)	19.21	**NL-3-348c**	Cc	18.98
			NL-3-348m?	Cc	22.86
	Crn avg:	**19.15**		**Cc avg:**	**20.30**
	2SD	***0.163***		***2SD***	***5.009***

$\Delta^{18}O$(Cc-Crn) and propagated 2SD: 1.15 ± 5.01

T= 572 °C

Sample No.	Phase	$\delta_{18}O$ VSMOW	Sample No.	Phase	$\delta_{18}O$ VSMOW
NL-5-353	Crn (bl)	19.41	**NL-5-353 F**	Cc	17.12
NL-5-353	Crn (very fine)	21.95	**NL-5-353 F**	Cc	17.74
NL-5-353	Crn (very fine)	21.87	**NL-5-353c**	Cc	22.46
	Crn avg:	**21.08**		**Cc avg:**	**19.11**
	2SD	***2.888***		***2SD***	***5.841***

$\Delta^{18}O$(Cc-Crn) and propagated 2SD: -1.97 ± 6.52

Appendix S2. Corundum Standard Development

For a material to be used as a SIMS running standard for oxygen isotope ratios, it must be homogeneous in isotopic composition within analytical uncertainty and calibrated with respect to VSMOW by laser fluorination. In evaluating samples to develop as a standard, 10 sapphire samples were investigated (Table B.1). First, each of these samples was crushed and sieved (the 300 to 400 μm size fraction was collected). Twenty grains of each sample were chosen at random and mounted into epoxy along with two standards (UWQ-1 quartz and UWG-2 garnet). The 10 samples were divided among two epoxy mounts (GM1 and GM2). GM1 (Fig. B.1.1) consists of only natural samples and GM2 (Fig. B.1.2) contains natural and synthetic corundum samples. After mounting in epoxy, these were ground and polished to a final polishing step of 0.05 μm alumina grit.

The polished mounts were then imaged on a scanning electron microscope (SEM) using back-scattered electron (BSE) images to check for inclusions and cathodoluminescence (CL) to evaluate any within-grain textures (UWCrn9 BSE, Fig. B.1.3; CL, Fig. B.1.4) These samples were then analyzed for $\delta^{18}O$ by SIMS; the UWG-2 standard at the center of the mount was used to correct for any instrument drift. To test homogeneity, one SIMS analysis was collected on each of the 20 grains from a sample. If the sample is suitable for use as a standard, these analyses will be homogeneous within analytical uncertainty. Each of the samples in GM1 was tested for homogeneity along with one synthetic sapphire sample from GM2 (UWCrn8). The synthetic samples exhibited rhythmic CL zoning—likely from the crystal growth process. UWCrn8 (synthetic ruby) had a 2SD of 0.56‰ among only 6 of the grains analyzed, which was more variable than the other potential standards analyzed. Thus, the analyses were terminated, and other synthetic samples were not analyzed, especially since UWCrn9 had been analyzed earlier in the session and exhibited a lower 2SD (0.29‰). Two other potential standards (UWCrn3 and UWCrn5) had a 2SD lower than 0.35‰ but UWCrn9 exhibited the greatest homogeneity. All homogeneity-test SIMS data are reported in the appendix File B.2 and a data summary for UWCrn9 is provided in Table B.2, including the overall 2SE (±0.06‰) which was determined from the reproducibility (2SD) divided by the square root of the number of analyses.

After evaluating homogeneity, the least variable, UWCrn9, was analyzed five times by laser fluorination. UWG-2 (Valley et al. 1995; $\delta^{18}O$ = 5.8‰ VSMOW) was analyzed 7 to 9 times during each session and the average value was used to calibrate the $\delta^{18}O$ value of UWCrn9 with respect to VSMOW (4.94 ±0.10 2SD). These measurements are reported in Table B.3. UWCrn9 was used as a running standard for all corundum analyses to correct for instrument drift and calibrate all measurements with respect to VSMOW.

Reference

Valley, John W., Kitchen, Nami, Kohn, Matthew J., Niendorf, Christopher R., and Spicizza, Michael J. (1995) UWG-2, a garnet standard for oxygen isotope ratios: Strategies for high precision and accuracy with laser heating. Geochimica et Cosmochimica Acta, v. 59, n. 24, p. 5523-5531.

Table S2.1. List of all potential corundum standards and any known information about their locality, characteristics, and mount number. Most samples analyzed have an acceptable 2SD for a standard (except UWCrn8). UWCrn9 shows the lowest variability.

STD Name	Grain Mount	Description	Locality	From	No. SIMS Analyses	$\delta_{18}O$ drift corrected (‰)	2SD
UWCrn1	2	Synthetic ruby boule	N/A	UW Collection	None	—	—
UWCrn2	2	Natural corundum, colorless, likely placer	Unknown	UW Collection	None	—	—
UWCrn3	1	Orange-clear (oxidation?) natural, detrital	Umba, Tanzania	John Couch	20	5.78 to 6.36	0.34
UWCrn4	1	Reddish corundum, natural, detrital,	Umba, Tanzania	John Couch	20	5.18 to 5.90	0.38
UWCrn5	1	Ruby, natural, #46328, $\delta_{18}O$=4.65, from pegmatite associated with amphibolite and anorthosite	Fiskenaesset, Greenland	Brian Windley	20	2.73 to 3.33	0.33
UWCrn6	1	Pinkish natural sapphire	Unknown	UW Collection	20	5.41 to 6.01	0.36
UWCrn7	2	Ruby, synthetic, faceted	N/A	Online	None	—	—
UWCrn8	2	Pink sapphire, synthetic, faceted	N/A	Online	6	27.51 to 28.25	0.56
UWCrn9	1	Dark blue sapphire, natural	Unknown	UW Collection	20	3.03 to 3.77	0.29
UWCrn10	2	Umba (T) (A); colorless, detrital	Umba, Tanzania	John Couch	None	—	—

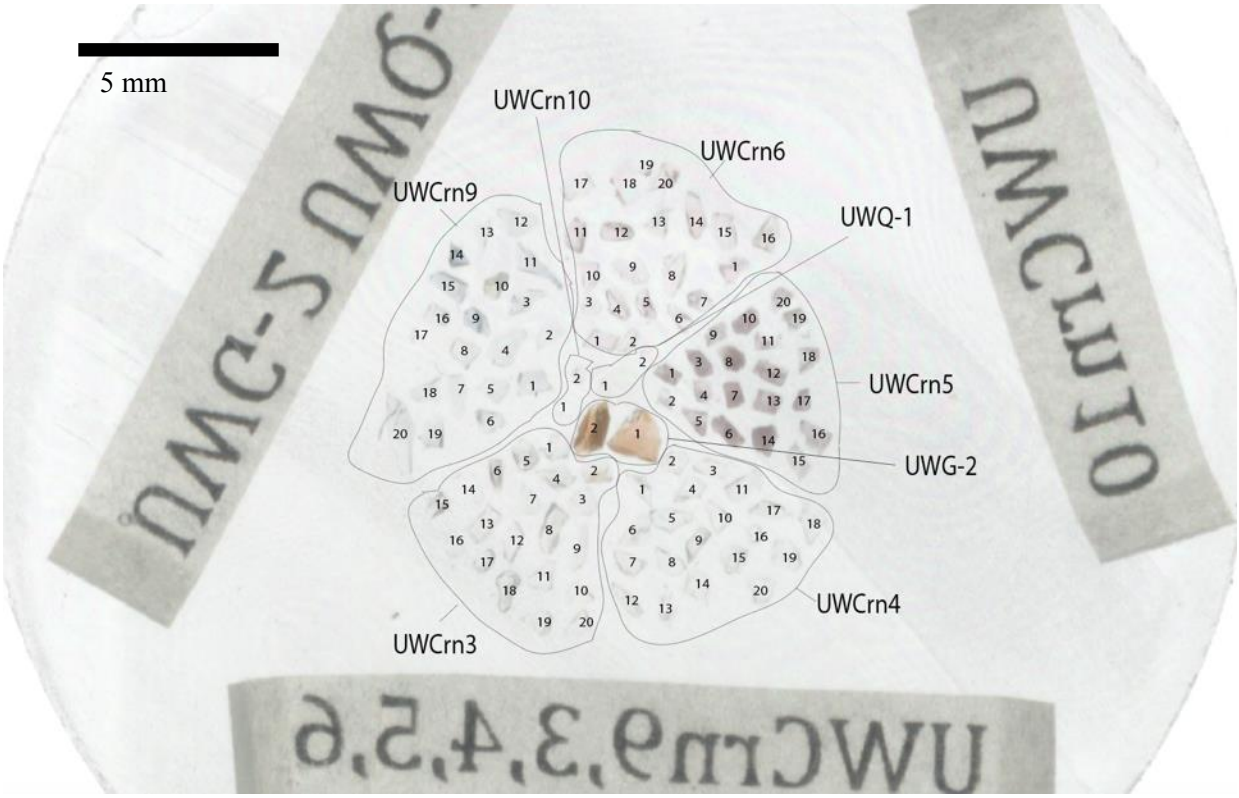

Figure S2.1. Image of epoxy mount GR1 with natural corundum grains investigated as potential standards.

Table S2.2. Table summarizes SIMS data for homogeneity test of UWCrn9 (selected and used as a working standard for all corundum SIMS analyses in this study).

Analysis No.	$\delta^{18}O$ drift corrected (‰)	2SD (‰)
UWCrn9 g1	3.38	0.39
UWCrn9 g2	3.36	0.39
UWCrn9 g3	3.48	0.39
UWCrn9 g4	3.61	0.39
UWCrn9 g5	3.36	0.39
UWCrn9 g6	3.38	0.39
UWCrn9 g7	3.38	0.39
UWCrn9 g8	3.43	0.39
UWCrn9 g9	3.46	0.39
UWCrn9 g10	3.03	0.39

Analysis No.	$\delta^{18}O$ drift corrected (‰)	2SD (‰)
UWCrn9 g11	3.47	0.24
UWCrn9 g12	3.64	0.24
UWCrn9 g13	3.60	0.24
UWCrn9 g14	3.51	0.24
UWCrn9 g15	3.44	0.24
UWCrn9 g16	3.46	0.24
UWCrn9 g18	3.49	0.24
UWCrn9 g19	3.77	0.24
UWCrn9 g20	3.43	0.24
UWCrn9 g20(2)	3.41	0.24

Average: 3.46‰
2SD of variability: 0.29
2SE of variability: 0.06

Table S2.3. Table summarizes laser fluorination data for UWCrn9 and running standard UWG-2 (Valley et al. 1995; $\delta_{18}O$ = 5.8‰ VSMOW).

LF Session Date	Standard	$\delta_{18}O$ raw (‰)	$\delta_{18}O$ VSMOW (‰)	Analytical 2SD (‰)
1/12/16	UWG-2	5.84		0.13
1/12/16	UWG-2	5.88		0.13
1/12/16	UWG-2	5.71		0.13
1/12/16	UWG-2	5.74		0.13
1/12/16	**UWCrn9**	**4.86**	**4.87**	**0.13**
1/12/16	UWG-2	5.80		0.13
1/12/16	UWG-2	5.74		0.13
2/11/16	UWG-2	5.82		0.15
2/11/16	UWG-2	5.60		0.15
2/11/16	UWG-2	5.59		0.15
2/11/16	UWG-2	5.72		0.15
2/11/16	UWG-2	5.71		0.15
2/11/16	UWG-2	5.72		0.15
2/11/16	UWG-2	5.65		0.15
2/11/16	UWG-2	5.74		0.15
2/11/16	**UWCrn9**	**4.87**	**4.98**	**0.15**
2/11/16	**UWCrn9**	**4.79**	**4.90**	**0.15**
2/11/16	**UWCrn9**	**4.83**	**4.94**	**0.15**
2/11/16	**UWCrn9**	**5.00**	**4.99**	**0.15**
UWCrn9 LF Average (accepted value) and 2SD			**4.94 ±0.10**	**0.15**

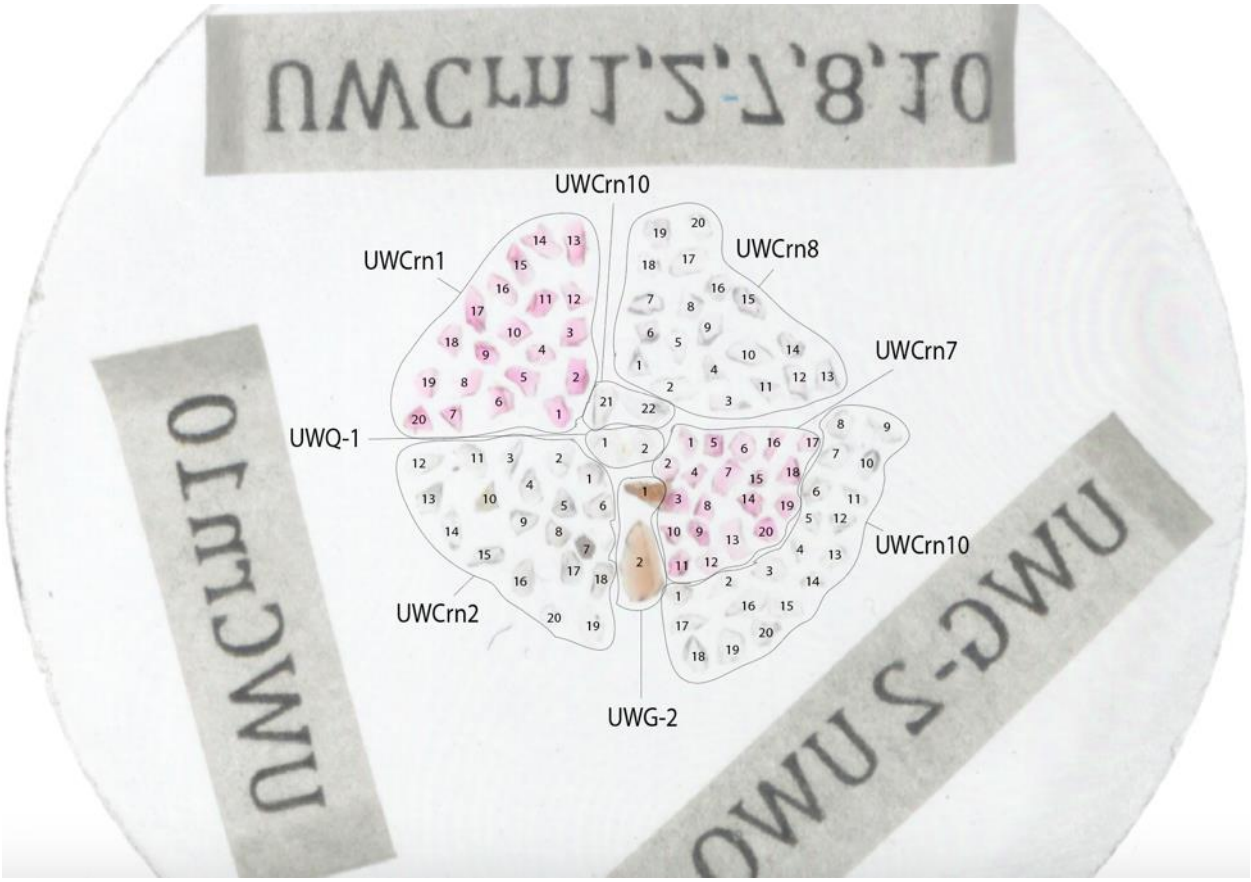

Figure S2.2. Image of epoxy mount GR2 with synthetic and natural corundum grains investigated as potential standards. Width of epoxy mount is 2.54 cm.

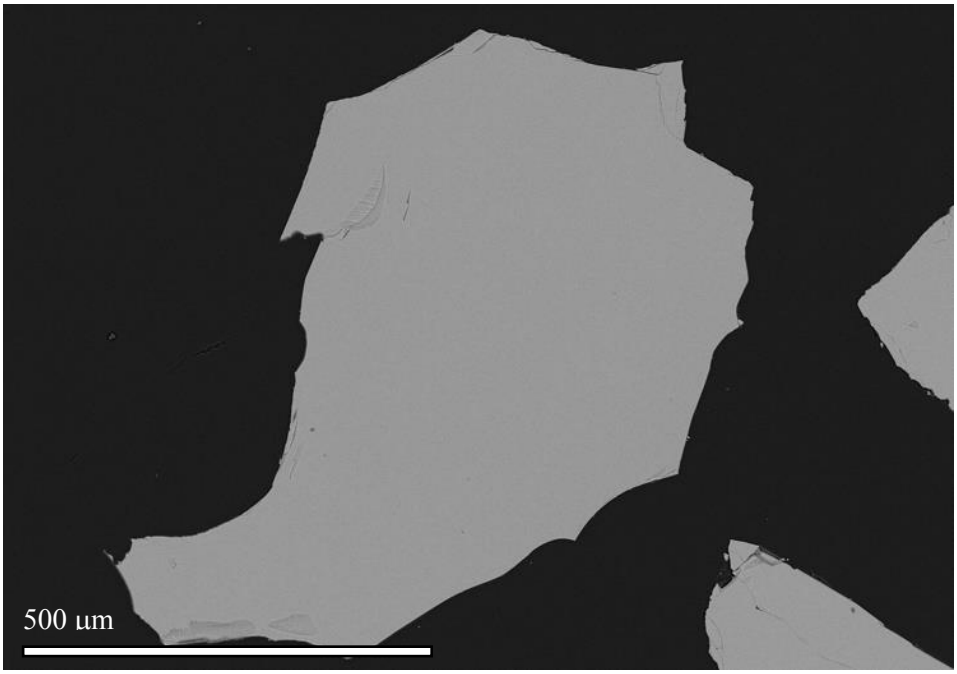

Figure S2.3. BSE image of UWCrn9 grain 4.

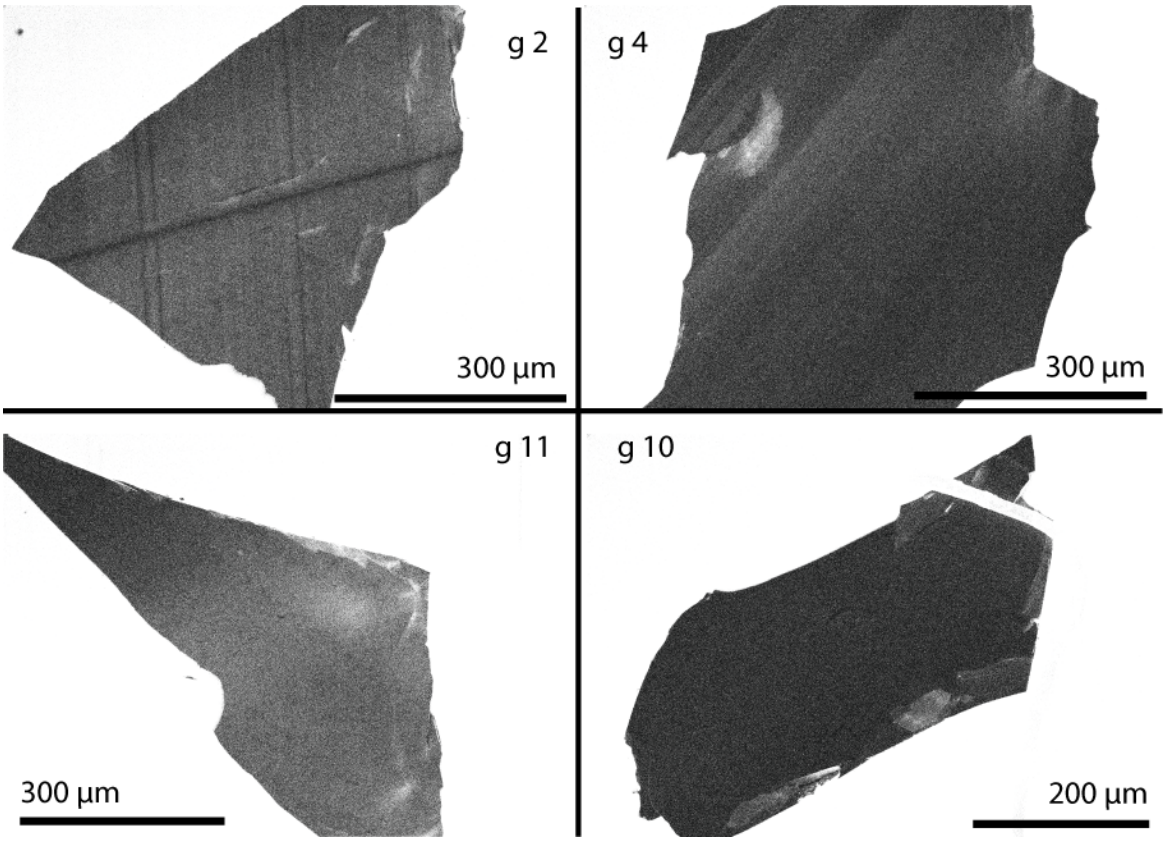

Figure S2.4. CL images of UWCrn9 grains 2, 4, 10, and 11.

Appendix S3. Naxos SIMS Supplementary Material

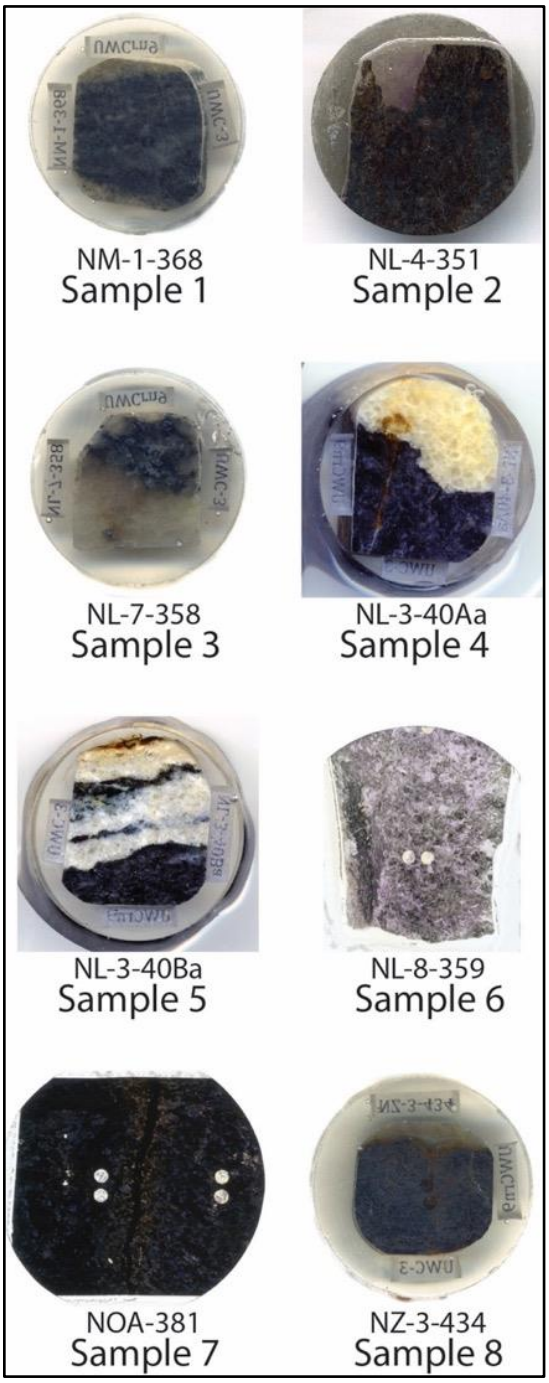

Figure S3.1. Images showing samples used for SIMS analysis and calcite-corundum A-factor calibration (8 out of 15 mounts prepared for calcite-corundum pairs; other mounts had vein calcite, were lacking within-session standardization for the carbonate minor element bias correction, or were from a location within the metabauxite lens that did not have both calcite and corundum). Mount names (top label) are shown along with sample names (bottom label) for reference. Standards UWCrn9 and UWC-3 are mounted in these samples.

Table S3.1. List of sample names and coordinates for all rocks analyzed by SIMS from Naxos, Greece.

Sample #	**Sample Name [Isograd T, °C]**	**Latitude**	**Longitude**	**Collected By:**
	Samples with calcite-corundum thermometry pairs:			
1	NM-1-368 [593]	37°6'42.00"N	25°32'24.48"E	YK (2000, 2003)
2	NL-4-351 [577]	37°7'56.16"N	25°33'49.05"E	YK (2000, 2003)
3	NL-7-358 [574]	37°8'3.91"N	25°34'2.73"E	YK (2000, 2003)
4	NL-3-40Aa [570]	37°7'28.98"N	25°33'55.20"E	RT (2016)
5	NL-3-40Ba [570]	37°7'28.98"N	25°33'55.20"E	RT (2016)
6	NL-8-359 [568]	37°7'39.94"N	25°33'53.75"E	YK (2000, 2003)
7	NOA-381 [425]	36°56'44.20"N	25°25'34.69"E	YK (2000, 2003)
8	NZ-3-434 [424]	36°58'42.99"N	25°28'26.04"E	YK (2000, 2003)
	Not used for thermometry:			
—	NL-4-351a	37°7'56.16"N	25°33'49.05"E	YK (2000, 2003)
—	NOA-2-12a	36°56'43.44"N	25°25'35.22"E	RT (2016)
—	NOA-2-3a	36°56'43.44"N	25°25'35.22"E	RT (2016)
—	NOA-379	36°56'44.20"N	25°25'34.69"E	YK (2000, 2003)
—	NOA-379 (b)	36°56'44.20"N	25°25'34.69"E	YK (2000, 2003)
—	NOA-380	36°56'44.20"N	25°25'34.69"E	YK (2000, 2003)
—	NZ-2-434	36°59'18.69"N	25°29'38.74"E	YK (2000, 2003)

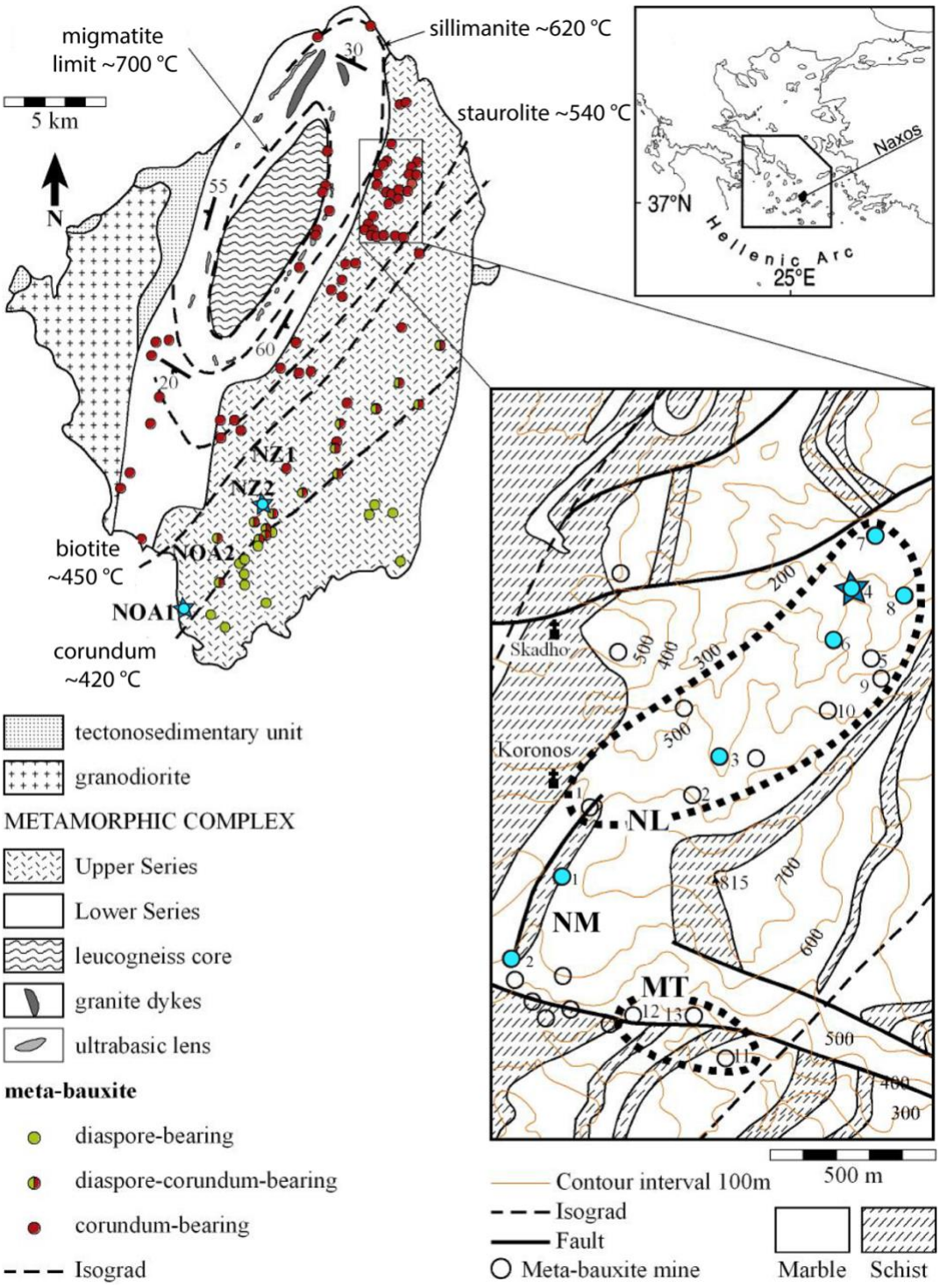

Figure S3.2. Supplementary geological map of Naxos, Greece. Open circles show the location of emery deposits. Samples used in this study are located in Figure 1. Blue stars indicate the location of extra SIMS samples that were not used in A-factor calibration because of disequilibrium textures (e.g., vein calcite) or a lack of within-session standardization for the carbonate minor element bias correction; GPS coordinates for these samples are listed in Table S3.1. Map also shows the grouping of Naxos rock units into the Upper Series, Lower Series, and migmatite (leucogneiss core). Blue circles indicate the location of bulk analysis samples.

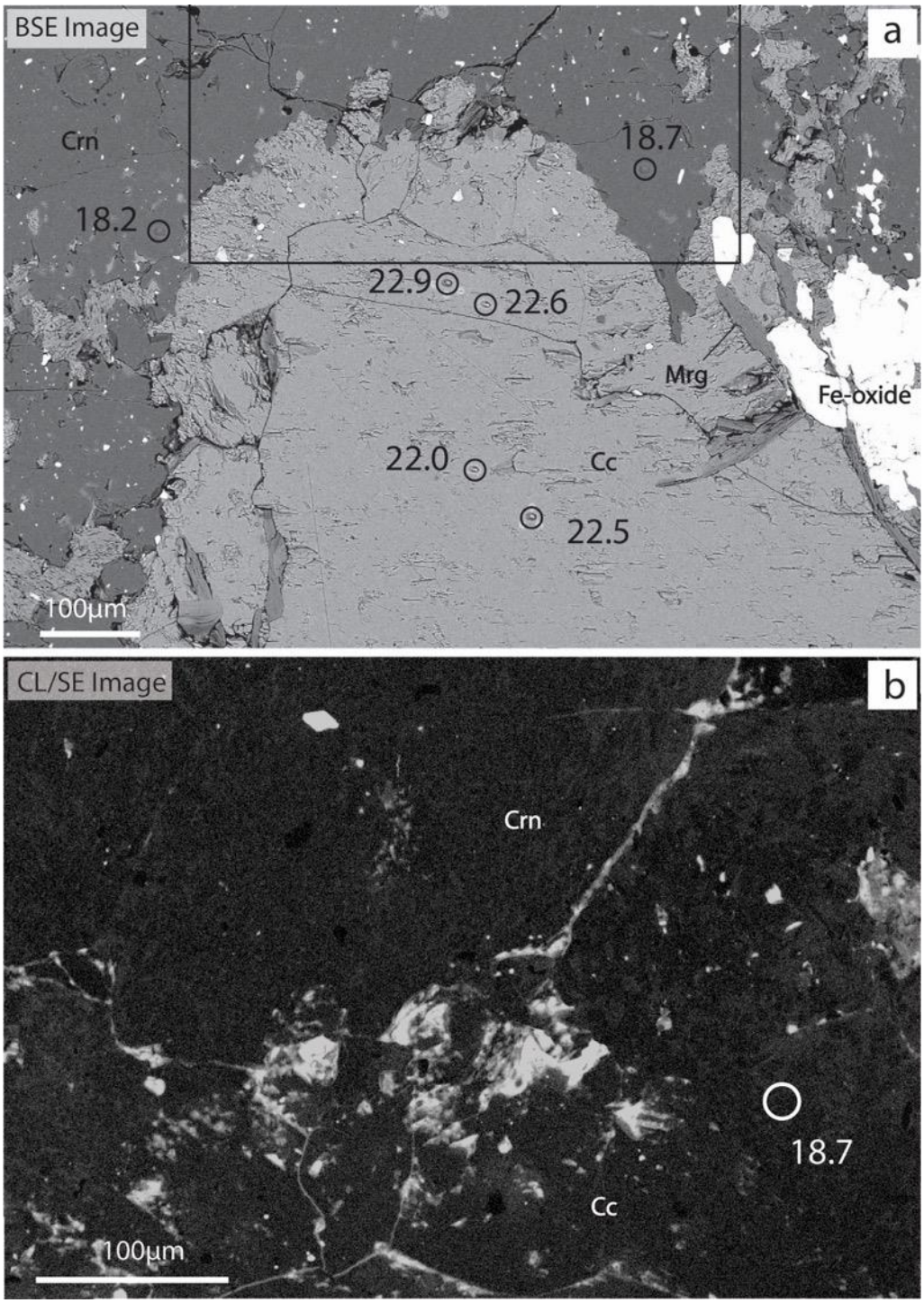

Figure S3.3. Representative CL/SE and BSE image of sample 2 (NL-4-351) showing SIMS data for $\delta_{18}O$ in calcite and corundum (circles and accompanying numbers). The partial black box in panel a) denotes the location of magnified CL/SE image in panel b); part of the image in b) extends beyond the field of view in a).

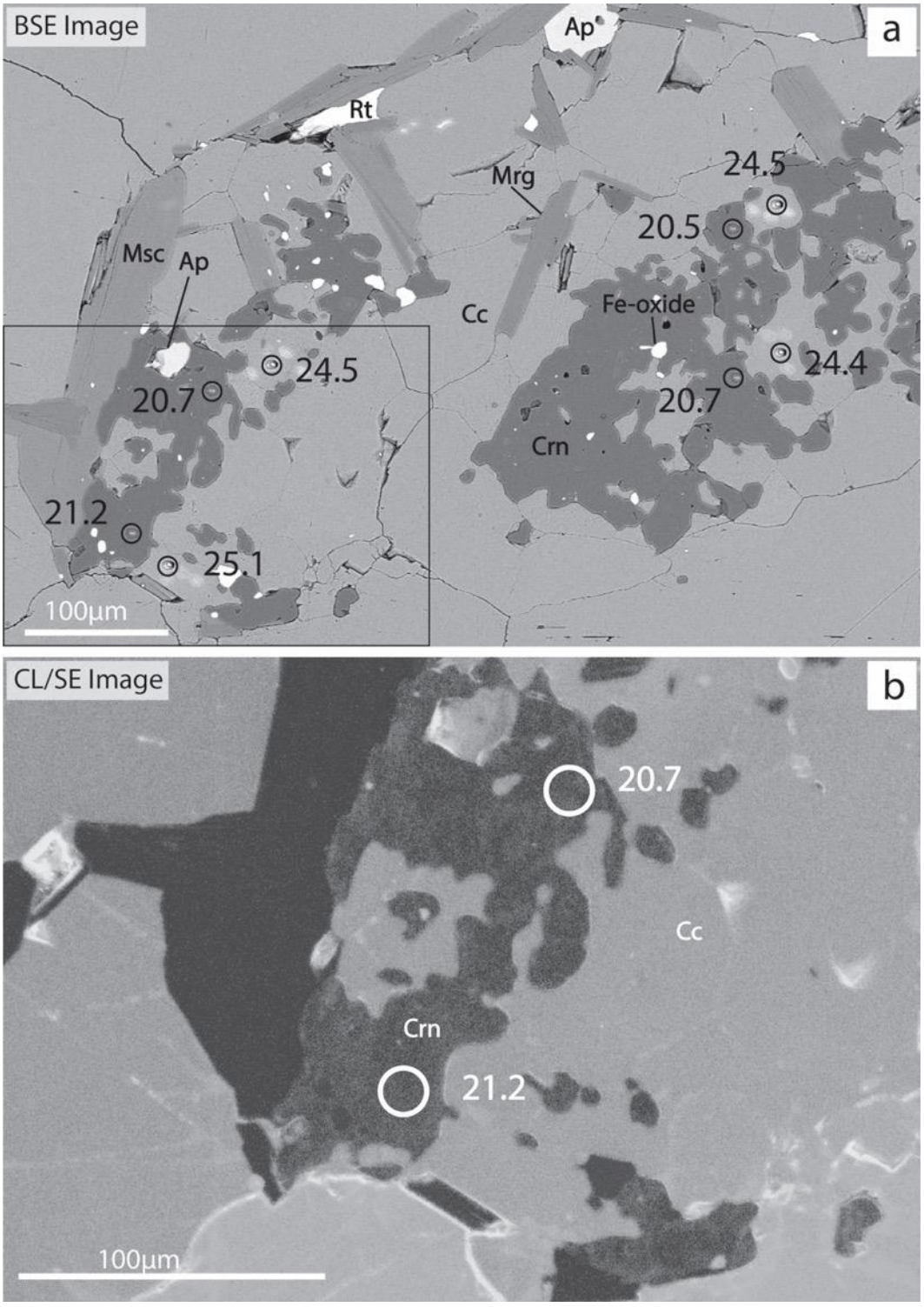

Figure S3.4. Representative CL/SE and BSE images of sample 3 (NL-7-358), including SIMS data for $\delta_{18}O$ in calcite and corundum (circles and accompanying numbers). Panel B highlights corundum CL and $\delta_{18}O$, showing limited growth texture. Ap = apatite, Crn = corundum, Cc = calcite, Rt = rutile, Mrg = margarite, and Msc = muscovite.

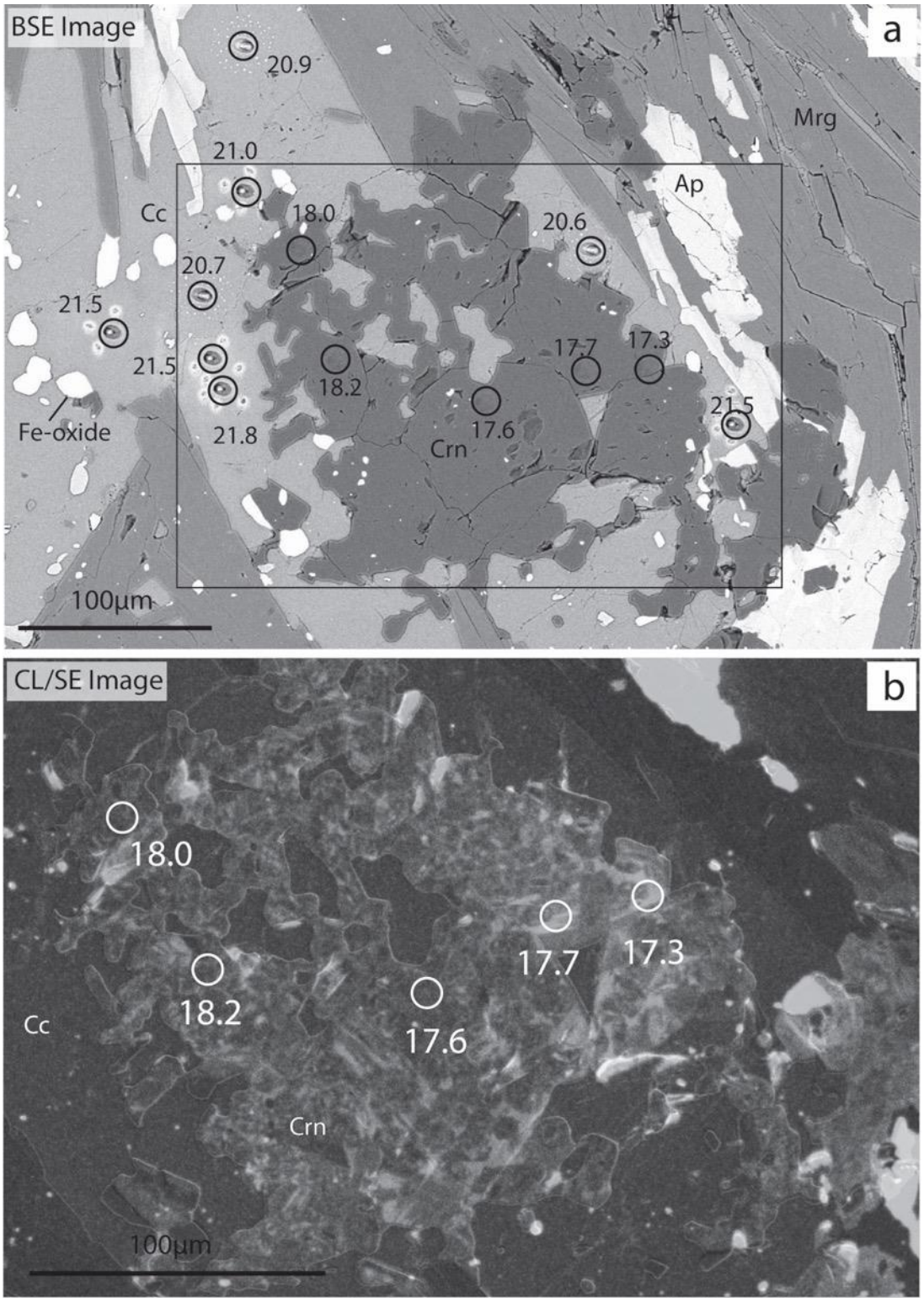

Figure S3.5. Representative CL/SE and BSE images of sample 4 (NL-3-40Aa) showing SIMS data for $\delta_{18}O$ in calcite and corundum (circles and accompanying numbers). Crn = corundum, Cc = calcite, Mrg = margarite, and Ap = apatite.

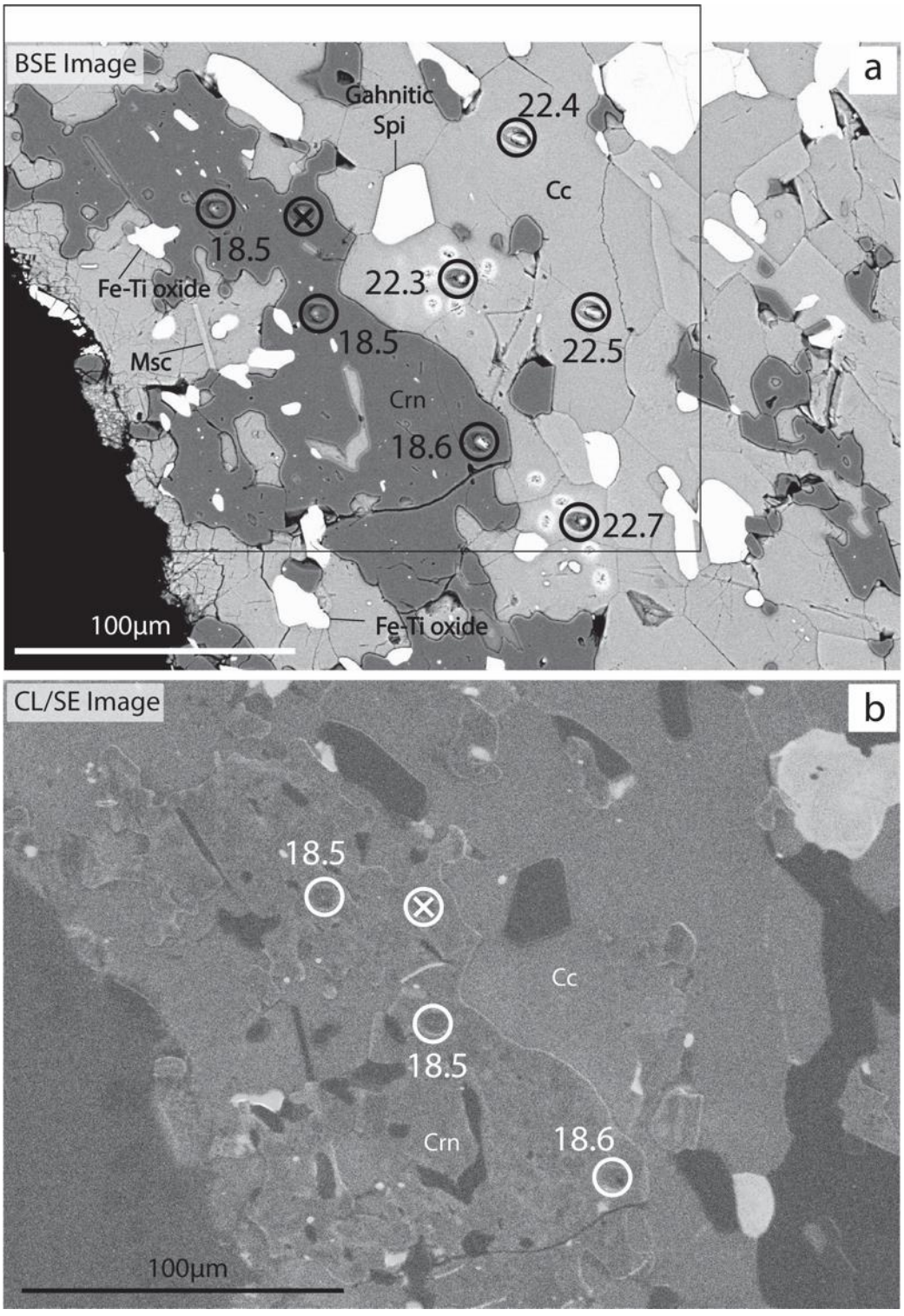

Figure S3.6. Representative CL/SE and BSE images of sample 6 (NL-8-359) showing SIMS data for $\delta_{18}O$ in calcite and corundum (circles and accompanying numbers). Circle with "x" through it marks location of bad analysis. Crn = corundum, Cc = calcite, Msc = muscovite, Rt = rutile, and Gahnitic Spi = spinel with Zn.

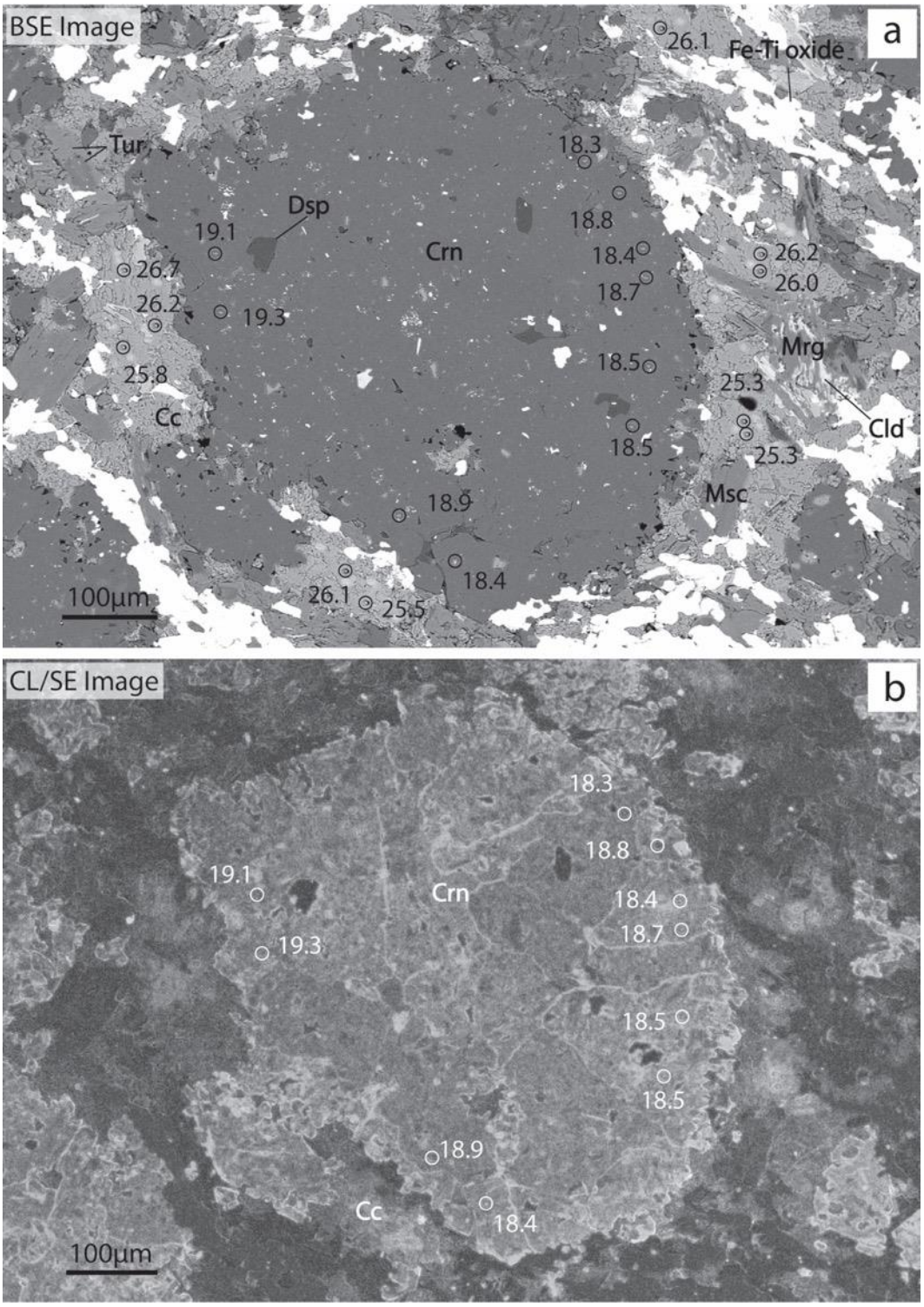

Figure S3.7. Representative CL/SE and BSE images of sample 7 (NOA-381) showing SIMS data for $\delta_{18}O$ in calcite and corundum (circles and accompanying numbers). Crn = corundum, Cc = calcite, Mrg = margarite, Cld = chloritoid, Tur = tourmaline, Msc = muscovite, and Dsp = diaspore.

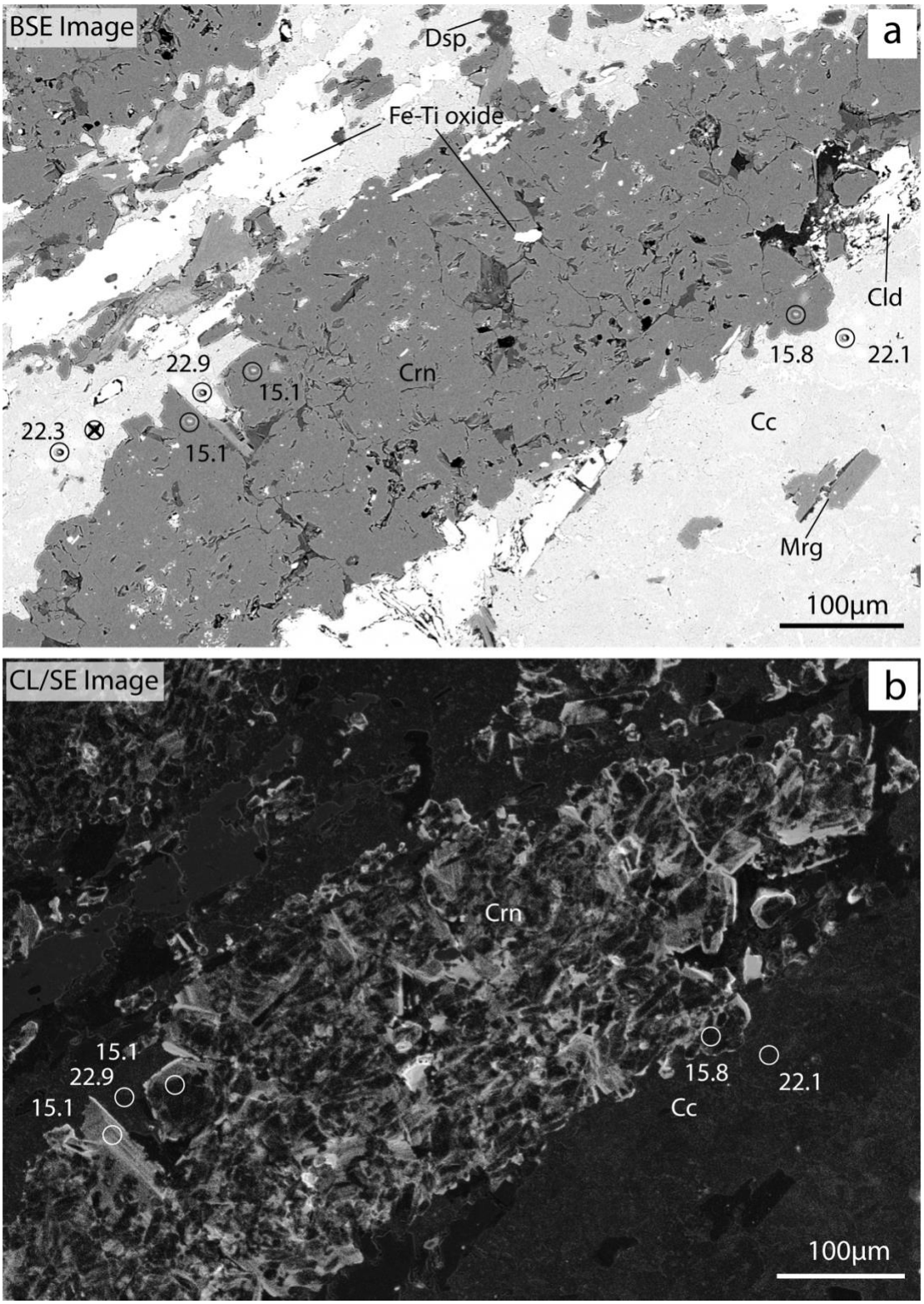

Figure S3.8. Representative CL/SE and BSE images of sample 8 (NZ-3-434) showing SIMS data for $\delta_{18}O$ in calcite and corundum (circles and accompanying numbers). Circle with black "x" indicates bad data point. Crn = corundum, Cc = calcite, Cld = chloritoid, and Dsp = diaspore.

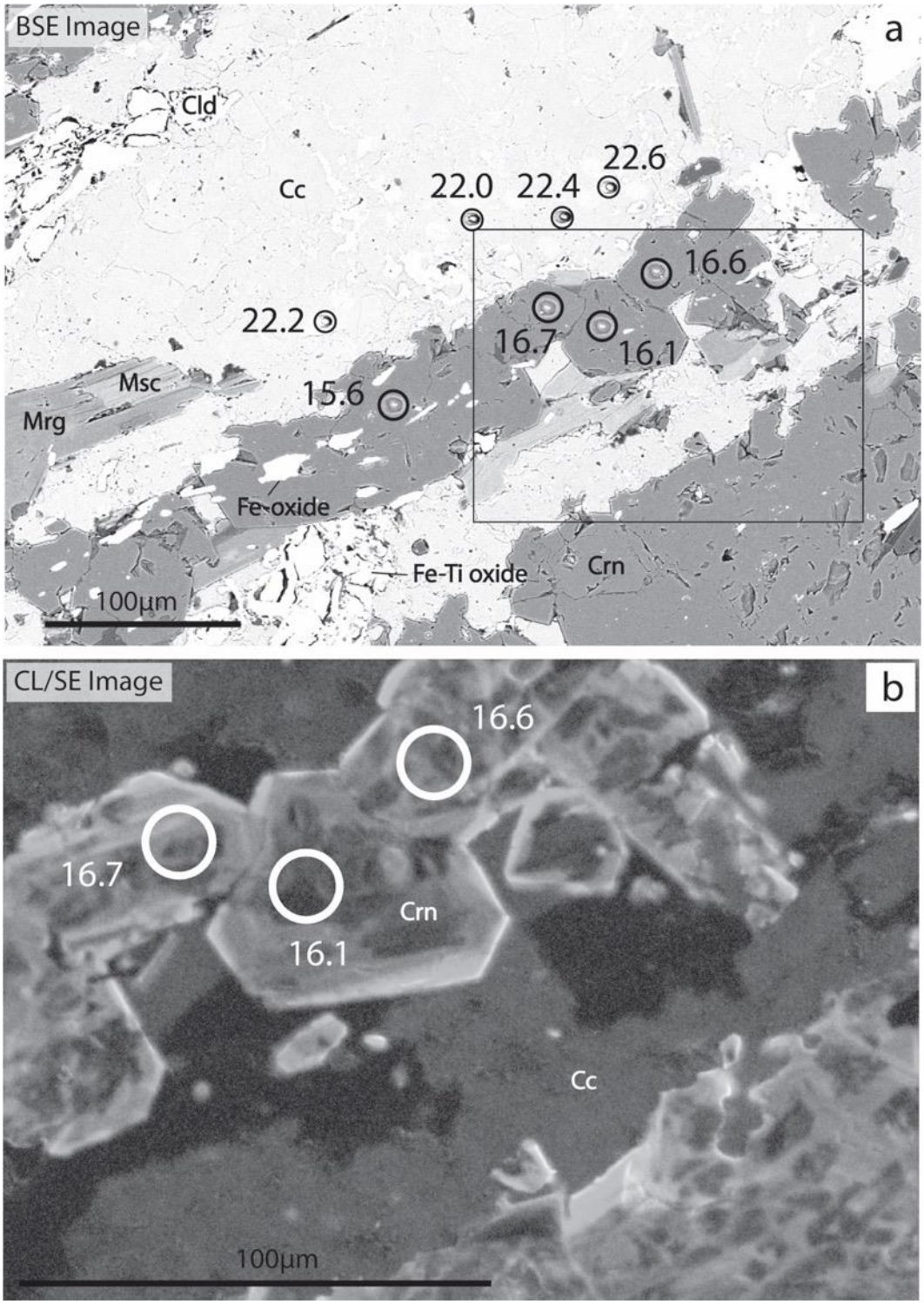

Figure S3.9. Representative CL/SE and BSE images of sample 8 (NZ-3-434) showing SIMS data for $\delta_{18}O$ in calcite and corundum (circles and accompanying numbers). Crn = corundum, Cc = calcite, Fe-oxide = iron oxide, Msc = muscovite, Mrg = margarite, and Cld = chloritoid.

Table S3.2. Tabulation of SIMS data for touching calcite-corundum mineral pairs used in A-factor calibration, with analytical 2SD values for calcite and corundum from SIMS precisions; fractionation 2SD propagated (prop.) is calculated from the square root of calcite and corundum analytical 2SD added in quadrature. The analytical 2SD values reported in "Averages" for measurements of calcite, corundum, and fractionation, are the maximum 2SD of all averaged measurements for a single sample. The 2SE for Δ(Cc-Crn) values is not equivalent to the analytical precision. It was determined from the 2SD of each sample's spot-to-spot fractionation values divided by the square root of the number of measurements from that sample. SIMS calcite data have been corrected for carbonate cation composition $\delta^{18}O$ bias.

Sample 1 Averages:

Calcite $\delta^{18}O$ and 2SD = 25.3 ± 0.20‰

Corundum $\delta^{18}O$ and 2SD = 21.9 ± 0.31‰

Δ(Cc-Crn) and 2SD prop. = 3.4 ± 0.37‰

(2SE of Δ(Cc-Crn) = 0.22‰)

Pair No.	Sample No.	Calcite Sample No.	$\delta^{18}O_{Cc}$ VSMOW	2SD	Corundum Sample No.	$\delta^{18}O_{Crn}$ VSMOW	2SD	Δ (Cc-Crn)	2SD Prop.
76	1	NM-1-368 Area1 g1 s1	25.2	0.20	NM-1-368 Area1 g1 s3	21.9	0.31	3.23	0.37
77	1	NM-1-368 Area1 g1 s2	25.1	0.20	NM-1-368 Area1 g1 s1	22.1	0.31	3.07	0.37
78	1	NM-1-368 Area1 g2 s1	25.2	0.20	NM-1-368 Area1 g1 s2	21.3	0.31	3.92	0.37
79	1	NM-1-368 Area1 g3 s1	25.9	0.20	NM-1-368 Area1 g1 s4	22.0	0.31	3.83	0.37
80	1	NM-1-368 Area2 g1 s1	25.0	0.20	NM-1-368 Area2 g1 s1	21.8	0.31	3.16	0.37
81	1	NM-1-368 Area2 g1 s2	25.2	0.20	NM-1-368 Area2 g2 s2	21.7	0.31	3.50	0.37
82	1	NM-1-368 Area2 g3 s1	25.2	0.20	NM-1-368 Area2 g2 s1	21.7	0.31	3.48	0.37
83	1	NM-1-368 Area3 g1 s1	25.4	0.20	NM-1-368 Area3 g1 s1	22.4	0.31	3.00	0.37
84	1	NM-1-368 Area3 g1 s2	25.4	0.20	NM-1-368 Area3 g1 s2	22.4	0.31	3.02	0.37
85	1	NM-1-368 Area3 g1 s3	25.3	0.20	NM-1-368 Area3 g2 s1	21.7	0.31	3.56	0.37

Sample 2 Averages:

Calcite $\delta_{18}O$ and 2SD = 22.0 ± 0.30‰
Corundum $\delta_{18}O$ and 2SD = 18.9 ± 0.51‰
Δ(Cc-Crn) and 2SD prop. = 3.1 ± 0.56‰
(2SE of Δ(Cc-Crn) = 0.56‰)

Pair No.	Sample No.	Calcite Sample No.	$\delta_{18}O_{Cc}$ VSMOW	2SD	Corundum Sample No.	$\delta_{18}O_{Crn}$ VSMOW	2SD	Δ (Cc-Crn)	2SD Prop.
46	2	NL-4-351 Area6 g1s2	21.8	0.30	NL-4-351 Area6 g1s1	19.6	0.51	2.19	0.59
47	2	NL-4-351 Area6 g3s2	21.8	0.30	NL-4-351 Area6 g1s3	19.4	0.51	2.43	0.59
48	2	NL-4-351 Area6 g3s2	21.8	0.30	NL-4-351 Area6 g1s3	19.4	0.51	2.43	0.59
49	2	NL-4-351 Area6E g1s5	21.7	0.30	NL-4-351 Area6E g2s1	18.8	0.51	2.86	0.59
50	2	NL-4-351 Area6E g1s5	21.7	0.30	NL-4-351 Area6E g1s2	18.5	0.51	3.13	0.59
51	2	NL-4-351 Area6E g1s5	21.7	0.30	NL-4-351 Area6E g3s1	18.5	0.51	3.13	0.59
52	2	NL-4-351 Area6S g1s3	22.6	0.30	NL-4-351 Area6S g1s1	18.2	0.38	4.43	0.49
53	2	NL-4-351 Area6S g1s3	22.6	0.30	NL-4-351 Area6S g1s3	18.7	0.38	3.99	0.49

Sample 3 Averages:

Calcite $\delta_{18}O$ and 2SD = 24.5 ± 0.26‰
Corundum $\delta_{18}O$ and 2SD = 20.7 ± 0.13‰
Δ(Cc-Crn) and 2SD prop. = 3.8 ± 0.30‰
(2SE of Δ(Cc-Crn) = 0.10‰)

Pair No.	Sample No.	Calcite Sample No.	$\delta_{18}O_{Cc}$ VSMOW	2SD	Corundum Sample No.	$\delta_{18}O_{Crn}$ VSMOW	2SD	Δ (Cc-Crn)	2SD Prop.
54	3	NL-7-358 Area1 g1 s1	24.7	0.26	NL-7-358 Area1 g1 s1	20.9	0.13	3.80	0.30
55	3	NL-7-358 Area1 g2 s1	24.6	0.26	NL-7-358 Area1 g2 s1	20.6	0.13	3.93	0.30
56	3	NL-7-358 Area2 g1 s1	24.2	0.26	NL-7-358 Area2 g1 s1	20.6	0.13	3.52	0.30
57	3	NL-7-358 Area2 g1 s2	24.2	0.26	NL-7-358 Area2 g3 s1	20.3	0.13	3.89	0.30
58	3	NL-7-358 Area2 g2 s1	24.5	0.26	NL-7-358 Area2 g2 s1	20.9	0.13	3.55	0.30
59	3	NL-7-358 Area2 g3 s1	24.1	0.26	NL-7-358 Area2 g2 s2	20.4	0.13	3.70	0.30
60	3	NL-7-358 Area3 g1 s1	24.5	0.26	NL-7-358 Area3 g1 s1	20.5	0.13	3.99	0.30
61	3	NL-7-358 Area3 g2 s1	24.4	0.26	NL-7-358 Area3 g1 s2	20.7	0.13	3.70	0.30
62	3	NL-7-358 Area3 g3 s1	24.5	0.26	NL-7-358 Area3 g2 s1	20.7	0.13	3.71	0.30
63	3	NL-7-358 Area3 g4 s1	25.1	0.26	NL-7-358 Area3 g2 s2	21.2	0.13	3.92	0.30

Sample 4 Averages:

Calcite $\delta_{18}O$ = 20.6 ± 0.26‰

Corundum $\delta_{18}O$ = 17.7 ± 0.32‰

Δ(Cc-Crn) and 2SD prop. = 2.93 ± 0.41‰

(2SE of Δ(Cc-Crn) = 0.21‰)

Pair No.	Sample No.	Calcite Sample No.	$\delta_{18}O_{Cc}$ VSMOW	2SD	Corundum Sample No.	$\delta_{18}O_{Crn}$ VSMOW	2SD	Δ (Cc-Crn)	2SD Prop.
1	4	NL-3-40Aa Area1 g1s2	20.5	0.26	NL-3-40Aa Area1 g1s3	17.7	0.32	2.76	0.41
2	4	NL-3-40Aa Area1 g2s5	20.8	0.26	NL-3-40Aa Area1 g1s5	18.0	0.32	2.76	0.41
3	4	NL-3-40Aa Area1 g2s6	20.7	0.26	NL-3-40Aa Area1 g1s4	18.2	0.32	2.48	0.41
4	4	NL-3-40Aa Area1 g2s6	20.7	0.26	NL-3-40Aa Area1 g1s4	18.2	0.32	2.48	0.41
5	4	NL-3-40Aa Area1 g3s2	20.8	0.26	NL-3-40Aa Area1 g2s2	17.7	0.32	3.08	0.41
6	4	NL-3-40Aa Area1 g3s3	20.4	0.26	NL-3-40Aa Area1 g2s1	17.5	0.32	2.86	0.41
7	4	NL-3-40Aa Area2 g1s2	20.9	0.26	NL-3-40Aa Area2 g1s1	17.5	0.31	3.33	0.41
8	4	NL-3-40Aa Area2 g1s2	20.9	0.26	NL-3-40Aa Area2 g1s3	17.7	0.31	3.18	0.41
9	4	NL-3-40Aa Area2 g1s2	20.9	0.26	NL-3-40Aa Area2 g1s2	17.2	0.31	3.27	0.41
10	4	NL-3-40Aa Area2 g3s2	20.0	0.26	NL-3-40Aa Area2 g2s1	17.3	0.31	2.62	0.41
11	4	NL-3-40Aa Area2 g3s2	20.0	0.26	NL-3-40Aa Area2 g2s4	17.7	0.31	2.25	0.41
12	4	NL-3-40Aa Area2 g5s3	20.3	0.26	NL-3-40Aa Area2 g2s2	18.2	0.31	2.07	0.41
13	4	NL-3-40Aa Area3 g1s2	21.1	0.26	NL-3-40Aa Area3 g3s3	17.3	0.31	3.84	0.42
14	4	NL-3-40Aa Area3 g2s1	21.0	0.26	NL-3-40Aa Area3 g2s1	17.9	0.32	3.02	0.42
15	4	NL-3-40Aa Area3 g3s1	20.1	0.26	NL-3-40Aa Area3 g1s1	17.7	0.32	2.40	0.41
16	4	NL-3-40Aa Area3 g4s1	20.8	0.26	NL-3-40Aa Area3 g3s2	18.0	0.31	2.85	0.41
17	4	NL-3-40Aa Area3 g5s1	21.2	0.26	NL-3-40Aa Area3 g3s1	17.9	0.31	3.33	0.41
18	4	NL-3-40Aa Area5 g1s2	20.8	0.26	NL-3-40Aa Area5 g1s1	16.9	0.28	3.84	0.39
19	4	NL-3-40Aa Area5 g2s2	20.7	0.26	NL-3-40Aa Area5 g4s1	18.0	0.28	2.68	0.39
20	4	NL-3-40Aa Area5 g4s1	20.4	0.26	NL-3-40Aa Area5 g3s1	17.2	0.28	3.15	0.39
21	4	NL-3-40Aa Area5 g5s2	21.0	0.26	NL-3-40Aa Area5 g2s1	17.7	0.28	3.27	0.39

Sample 5 Averages:

Calcite $\delta_{18}O$ and 2SD = 21.02 ± 0.21‰

Corundum $\delta_{18}O$ and 2SD = 17.7 ± 0.39‰

Δ(Cc-Crn) and 2SD prop. = 3.28 ± 0.38‰

(2SE of Δ(Cc-Crn) = 0.26‰)

Pair No.	Sample No.	Calcite Sample No.	$\delta_{18}O_{Cc}$ VSMOW	2SD	Corundum Sample No.	$\delta_{18}O_{Crn}$ VSMOW	2SD	Δ (Cc-Crn)	2SD Prop.
22	5	NL-3-40Ba Area1 g1 s5	20.1	0.17	NL-3-40Ba Area1 g1 s3	18.3	0.33	1.73	0.38
23	5	NL-3-40Ba Area1 g1 s6	20.5	0.17	NL-3-40Ba Area1 g1 s3	18.3	0.33	2.13	0.38
24	5	NL-3-40Ba Area1 g2 s2	20.7	0.17	NL-3-40Ba Area1 g1 s2	18.2	0.33	2.52	0.38
25	5	NL-3-40Ba Area1 g3 s2	20.2	0.17	NL-3-40Ba Area1 g1 s2	18.2	0.33	2.00	0.38
26	5	NL-3-40Ba Area2 g1 s3	21.2	0.17	NL-3-40Ba Area2 g2 s1	17.8	0.33	3.35	0.38
27	5	NL-3-40Ba Area2 g2 s6	21.1	0.17	NL-3-40Ba Area2 g3 s2	17.4	0.33	3.69	0.38
28	5	NL-3-40Ba Area2 g2 s6	21.1	0.17	NL-3-40Ba Area2 g3 s6	16.8	0.39	4.30	0.38
29	5	NL-3-40Ba Area2 g2 s7	21.4	0.17	NL-3-40Ba Area2 g3 s4	17.6	0.39	3.70	0.38
30	5	NL-3-40Ba Area2 g3 s3	20.8	0.17	NL-3-40Ba Area2 g1 s5	18.1	0.33	2.68	0.43
31	5	NL-3-40Ba Area2 g4 s2	21.1	0.17	NL-3-40Ba Area2 g1 s2	17.5	0.33	3.64	0.43
32	5	NL-3-40Ba Area2 g5 s1	21.7	0.17	NL-3-40Ba Area2 g2 s1	17.8	0.33	3.88	0.38
33	5	NL-3-40Ba Area3 g1 s4	21.2	0.21	NL-3-40Ba Area3 g1 s4	17.5	0.26	3.64	0.33
34	5	NL-3-40Ba Area3 g1 s5	21.3	0.21	NL-3-40Ba Area3 g1 s3	17.8	0.26	3.52	0.33
35	5	NL-3-40Ba Area3 g1 s5	21.3	0.21	NL-3-40Ba Area3 g1 s5	17.6	0.26	3.75	0.33
36	5	NL-3-40Ba Area3 g2 s2	20.9	0.21	NL-3-40Ba Area3 g1 s2	17.6	0.26	3.24	0.33
37	5	NL-3-40Ba Area4 g1 s3	21.0	0.21	NL-3-40Ba Area4 g2 s2	18.0	0.39	3.02	0.44
38	5	NL-3-40Ba Area4 g1 s4	21.0	0.21	NL-3-40Ba Area4 g1 s2	17.4	0.39	3.64	0.44
39	5	NL-3-40Ba Area4 g3 s2	21.4	0.21	NL-3-40Ba Area4 g2 s3	18.0	0.39	3.40	0.44
40	5	NL-3-40Ba Area4 g4 s4	21.1	0.21	NL-3-40Ba Area4 g2 s1	18.0	0.39	3.09	0.44
41	5	NL-3-40Ba Area4 g4 s4	21.1	0.21	NL-3-40Ba Area4 g3 s2	17.8	0.26	3.27	0.33
42	5	NL-3-40Ba Area4 g4 s5	21.1	0.21	NL-3-40Ba Area4 g3 s1	17.0	0.26	4.11	0.33
43	5	NL-3-40Ba Area4 g5 s4	21.1	0.21	NL-3-40Ba Area4 g4 s2	17.8	0.26	3.34	0.33
44	5	NL-3-40Ba Area4 g5 s4	21.1	0.21	NL-3-40Ba Area4 g4 s1	17.4	0.26	3.67	0.33
45	5	NL-3-40Ba Area4 g5 s4	21.1	0.21	NL-3-40Ba Area4 g5 s1	17.8	0.26	3.36	0.33

Sample 6 Averages:

Calcite $\delta_{18}O$ and 2SD = 22.3 ± 0.45‰

Corundum $\delta_{18}O$ and 2SD = 18.7 ± 0.43‰

Δ(Cc-Crn) and 2SD prop. = 3.7 ± 0.43‰

(2SE of Δ(Cc-Crn) = 0.15‰)

Pair No.	Sample No.	Calcite Sample No.	$\delta_{18}O_{Cc}$ VSMOW	2SD	Corundum Sample No.	$\delta_{18}O_{Crn}$ VSMOW	2SD	Δ (Cc-Crn)	2SD Prop.
64	6	NL-8-359 Area1 g1s2	22.4	0.23	NL-8-359 Area1 g1s3	18.5	0.28	3.85	0.36
65	6	NL-8-359 Area1 g1s3	22.4	0.23	NL-8-359 Area1 g1s4	18.6	0.28	3.82	0.36
66	6	NL-8-359 Area5 g4s2	22.2	0.23	NL-8-359 Area5 g1s4	18.5	0.21	3.73	0.31
67	6	NL-8-359 Area5 g4s2	22.2	0.23	NL-8-359 Area5 g1s5	18.2	0.21	3.93	0.31
68	6	NL-8-359 Area5 g7s1	22.2	0.23	NL-8-359 Area5 g1s2	18.7	0.28	3.41	0.36
69	6	NL-8-359 Area5 g8s1	22.2	0.23	NL-8-359 Area5 g1s6	18.8	0.21	3.37	0.31
70	6	NL-8-359 Area6 g4s1	22.3	0.45	NL-8-359 Area6 g5s1	18.6	0.43	3.74	0.62
71	6	NL-8-359 Area6 g4s1	22.3	0.45	NL-8-359 Area6 g1s2	19.2	0.43	3.06	0.62
72	6	NL-8-359 Area6N g1s3	22.3	0.23	NL-8-359 Area6N g3s2	18.4	0.43	3.91	0.49
73	6	NL-8-359 Area7 g1s2	22.5	0.45	NL-8-359 Area7 g6s1	18.7	0.21	3.78	0.49
74	6	NL-8-359 Area7 g4s4	22.7	0.45	NL-8-359 Area7 g7s1	19.0	0.21	3.64	0.49
75	6	NL-8-359 Area7 g6s5	22.5	0.45	NL-8-359 Area7 g5s1	18.7	0.21	3.77	0.49

Sample 7 Averages:

Calcite $\delta_{18}O$ and 2SD = 26.0 ± 0.30‰

Corundum $\delta_{18}O$ and 2SD = 18.8 ± 0.31‰

Δ(Cc-Crn) and 2SD prop. = 7.2 ± 0.37‰

(2SE of Δ(Cc-Crn) = 0.17‰)

Pair No.	Sample No.	Calcite Sample No.	$\delta_{18}O_{Cc}$ VSMOW	2SD	Corundum Sample No.	$\delta_{18}O_{Crn}$ VSMOW	2SD	Δ (Cc-Crn)	2SD Prop.
86	7	NOA-381 Area4 g3 s4	26.0	0.30	NOA-381 Area4 g1 s1	18.8	0.17	7.17	0.35
87	7	NOA-381 Area4 g3 s4	26.0	0.30	NOA-381 Area4 g1 s2	18.7	0.17	7.21	0.35
88	7	NOA-381 Area4 g3 s4	26.0	0.30	NOA-381 Area5 g1 s1	19.2	0.16	6.80	0.34
89	7	NOA-381 Area4 g3 s4	26.0	0.30	NOA-381 Area2 g1 s4	18.8	0.11	7.17	0.32
90	7	NOA-381 Area4 g3 s4	26.0	0.30	NOA-381 Area2 g1 s3	18.8	0.11	7.12	0.32
91	7	NOA-381 Area6 g1 s1	26.7	0.23	NOA-381 Area6 g1 s2	19.1	0.31	7.58	0.39
92	7	NOA-381 Area6 g1 s10	26.1	0.23	NOA-381 Area6 g1 s9	18.3	0.31	7.77	0.39
93	7	NOA-381 Area6 g1 s10	26.1	0.23	NOA-381 Area6 g1 s10	18.8	0.31	7.30	0.39
94	7	NOA-381 Area6 g1 s2	26.2	0.23	NOA-381 Area6 g1 s1	19.3	0.31	6.84	0.39
95	7	NOA-381 Area6 g1 s4	26.1	0.23	NOA-381 Area6 g1 s8	18.9	0.31	7.18	0.39
96	7	NOA-381 Area6 g1 s5	25.5	0.23	NOA-381 Area6 g1 s7	18.4	0.31	7.10	0.39
97	7	NOA-381 Area6 g1 s6	25.3	0.23	NOA-381 Area6 g1 s6	18.5	0.31	6.79	0.39
98	7	NOA-381 Area6 g1 s7	25.3	0.23	NOA-381 Area6 g1 s5	18.5	0.31	6.85	0.39
99	7	NOA-381 Area6 g1 s8	26.0	0.23	NOA-381 Area6 g1 s4	18.7	0.31	7.27	0.39
100	7	NOA-381 Area6 g1 s9	26.2	0.23	NOA-381 Area6 g1 s3	18.4	0.31	7.80	0.39

Sample 8 Averages:

Calcite $\delta_{18}O$ and 2SD = 22.3 ± 0.21‰
Corundum $\delta_{18}O$ and 2SD = 15.9 ± 0.26‰
Δ(Cc-Crn) and 2SD prop. = 5.9 ± 0.33‰
(2SE of Δ(Cc-Crn) = 0.40‰)

Pair No.	Sample No.	Calcite Sample No.	$\delta_{18}O_{Cc}$ VSMOW	2SD	Corundum Sample No.	$\delta_{18}O_{Crn}$ VSMOW	2SD	Δ (Cc-Crn)	2SD Prop.
101	8	NZ-3-434 Area1 g1 s1	22.1	0.21	NZ-3-434 Area1 g1 s2	16.2	0.26	5.85	0.33
102	8	NZ-3-434 Area1 g2 s1	22.4	0.21	NZ-3-434 Area1 g1 s1	16.2	0.26	6.13	0.33
103	8	NZ-3-434 Area1 g3 s1	22.2	0.21	NZ-3-434 Area1 g1 s3	15.1	0.26	7.07	0.33
104	8	NZ-3-434 Area2 g1 s1	22.2	0.21	NZ-3-434 Area2 g1 s3	15.8	0.26	6.47	0.33
105	8	NZ-3-434 Area2 g3 s2	22.3	0.21	NZ-3-434 Area2 g1 s1	15.1	0.26	7.25	0.33
106	8	NZ-3-434 Area4 g1 s1	22.2	0.21	NZ-3-434 Area4 g1 s4	15.6	0.26	6.62	0.33
107	8	NZ-3-434 Area4 g2 s1	22.0	0.21	NZ-3-434 Area4 g1 s3	16.7	0.26	5.31	0.33
108	8	NZ-3-434 Area4 g3 s1	22.4	0.21	NZ-3-434 Area4 g1 s1	16.1	0.26	6.26	0.33
109	8	NZ-3-434 Area4 g4 s1	22.6	0.21	NZ-3-434 Area4 g1 s2	16.6	0.26	6.01	0.33

Average of all Δ(Cc-Crn) 2SE: ± 0.26‰
Max: ± 0.56‰
Min: ± 0.10‰

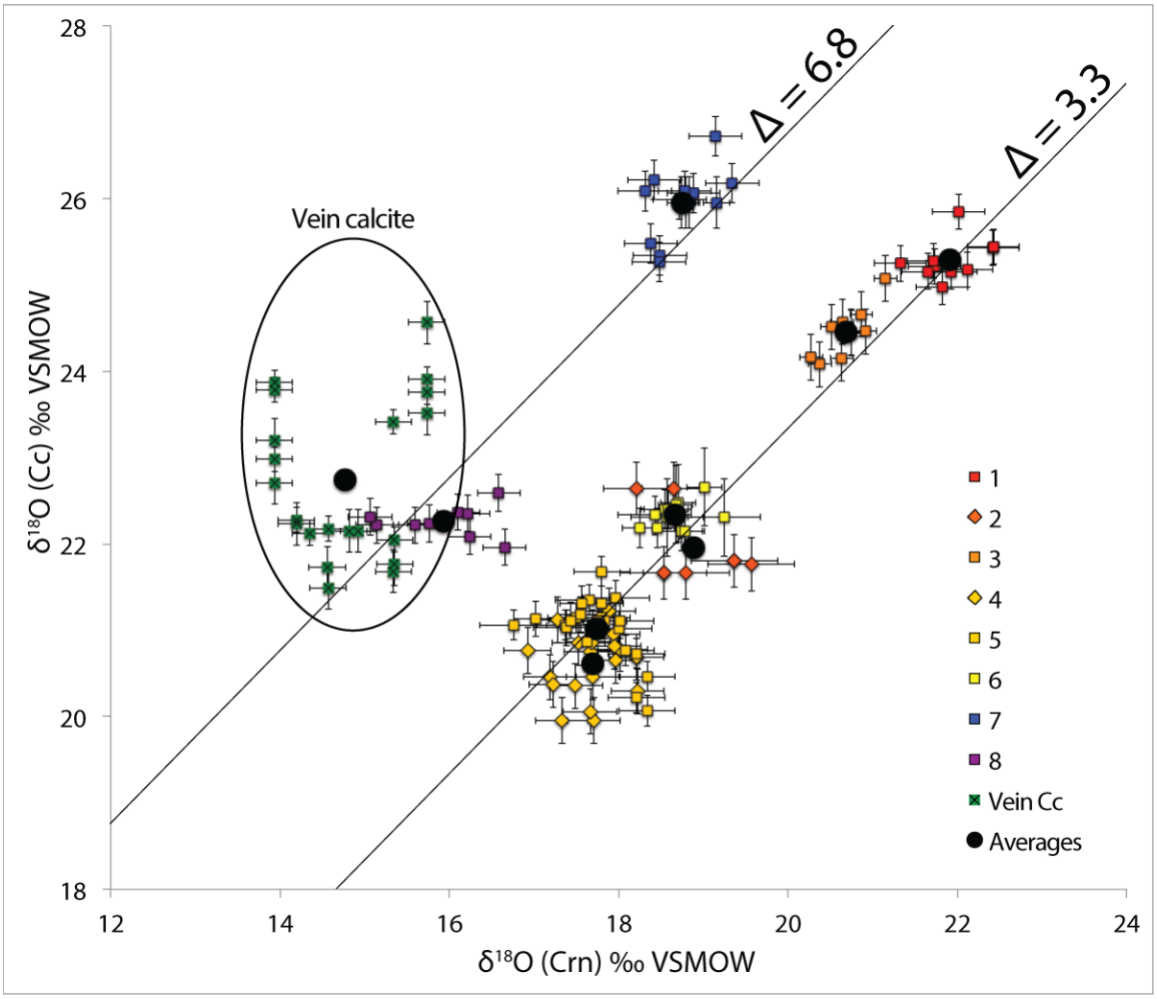

Figure S3.10. Plot of $\delta_{18}O$(Cc) vs. $\delta_{18}O$(Crn) for calcite coexisting with corundum. All pairs are close mineral pairs that are interpreted to be equilibrated, except green symbols that are from texturally late vein calcite (BSE, CL images in Figure 7; sample NOA-2-3a).

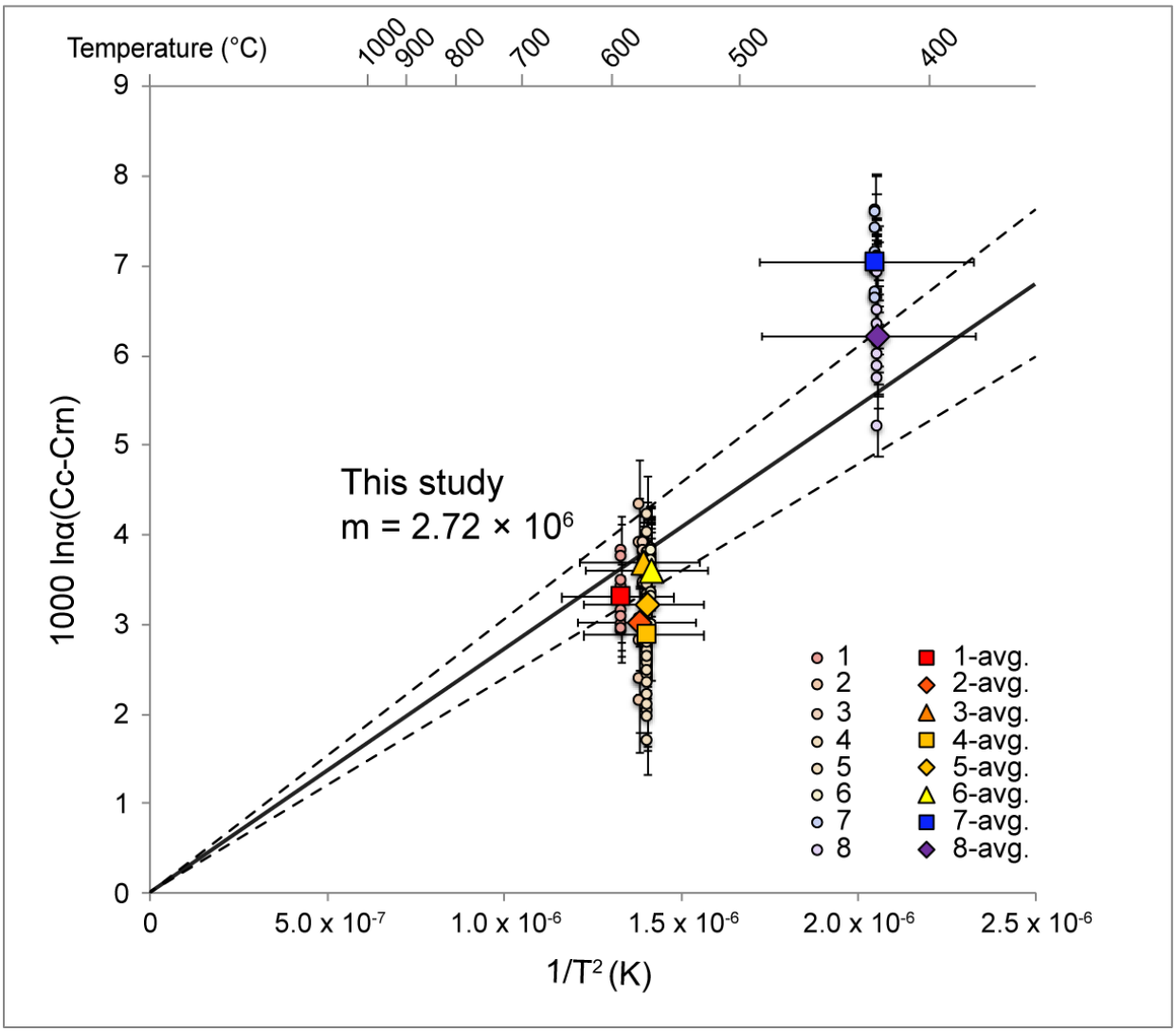

Figure S3.11. Plot showing 1000lnα(Cc-Crn) vs. $1/T^2$ (K) of individual calcite-corundum pairs for each sample with y-axis error bars from analytical 2SD and x-axis error bars from the isograd temperature uncertainty (±50 °C). For reference, temperature in ^{o}C is included on the upper x-axis. Based on this study's data, the line going through to the origin, whose slope is the A-factor, shows value of 2.72.

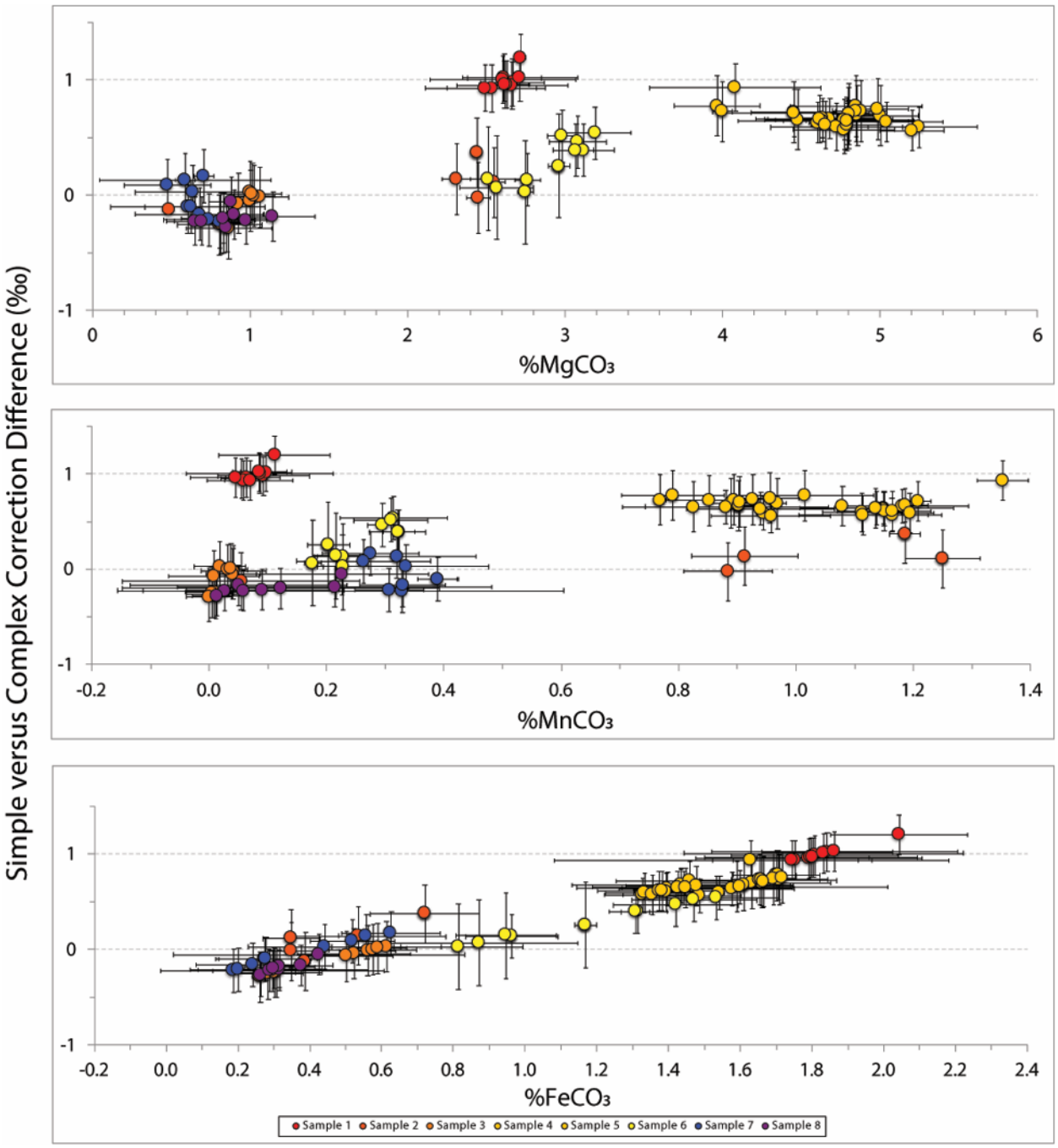

Figure S3.12. Plots of the $\delta_{18}O$ (Cc) VSMOW difference (‰) between simple and minor element carbonate bias correction vs. mol % $MgCO_3$, $MnCO_3$, and $FeCO_3$. Mol % concentrations are from EPMA measurements. The extent of $\delta_{18}O$ difference between measurements corrected by the simple vs. carbonate composition bias methodology varies depending on calcite composition.

Appendix S4. SIMS Carbonate Composition Bias Correction

Matrix Effects on Instrumental Mass Fractionation (IMF): Correcting for Carbonate Composition SIMS bias

In some minerals with variable solid solution, major or minor element differences can cause a matrix effect and raw $\delta^{18}O$ values by SIMS can be systematically offset from their true value. These effects have been observed in many minerals including dolomite-ankerite, feldspars, pyroxenes, olivine, and garnet (Valley and Kita, 2009; Page et al., 2010; Śliwiński et al., 2016). This has also been observed in calcite, where minor compositional differences in Mg, Fe, and Mn between the standard and sample can bias the measured $\delta^{18}O$ value. Bias can be corrected by analyzing calcite standards that span the range of sample minor element compositions and correcting the sample raw $\delta^{18}O$ value. The full procedure for these corrections can be found in Turnier (2017; Appendix A5) and is summarized here:

1. After tuning the instrument for each SIMS session, each carbonate standard was analyzed. To properly correct for bias, it is necessary to obtain a calibration relationship based on the compositionally-distinct standards. For example, as the Mn, Fe, or Mg minor element compositions change the bias will change. Using the standards and their range in composition (plotted in Fig. 6), interpolation between standard compositions is used to correct the sample $\delta^{18}O$ value.

Table S4.1. Carbonate standards with compositions (in mol %) determined by EPMA and stable isotope ratios determined by reaction with concentrated phosphoric acid and gas-source mass spectrometry at UW-Madison.

STD No.	$\%MgCO_3$	2SD	$\%FeCO_3$	2SD	$\%MnCO_3$	2SD	$\%SrCO_3$	2SD	$\%CaCO_3$	2SD	$\delta^{18}O$	2SD
UWC-1	0.00	-	0.00	-	0.00	-	0.00	-	100.00	-	23.36	-
UWC-3	2.27	0.17	0.74	0.11	0.23	0.07	0.25	0.21	96.52	0.29	12.49	0.03
UWC-4	0.25	0.08	0.96	0.20	3.71	0.41	0.02	0.02	95.06	0.64	5.69	0.05
UWC-5	0.51	0.31	2.33	0.95	0.39	0.30	0.10	0.07	96.67	1.29	11.55	0.01
UW6220	49.66	0.95	0.10	0.18	-	-	-	-	50.23	0.99	22.60	0.02
UW6250	49.81	1.00	0.08	0.23	-	-	-	-	50.10	1.00	21.40	0.11

2. When analyzing the calcite standards at the beginning of the session, UWC-3 analyses should bracket analyses of standards. This serves as a monitor of possible instrument drift.
3. After standards and sample are analyzed, use electron probe microanalysis (EPMA) to determine the local carbonate composition of samples around each SIMS pit.
4. Using the minor element composition of the standards and the samples, bias can be corrected by using a series of equations that relate the standard bias to its composition in terms of Ca-Fe, Ca-Mg, and Ca-Mn (Turnier, 2017; Appendix A5). Each of these standards has a bias* with respect to pure calcite (UWC-1), so upon normalizing these bias* values to UWC-1 the bias from each minor element can be accounted for by interpolation between the standard bias* corrections and compositions to the sample's bias and composition.

References

Page, F.Z., Kita, N.T., and Valley, J.W. (2010) Ion microprobe analysis of oxygen isotopes in garnets of complex chemistry. Chem. Geol., 270: 9-19. doi.org/10.1016/j.chemgeo.2009.11.001

Śliwiński M. G., Kitajima K., Kozdon R., Spicuzza M. J., Fournelle J. H., Denny A. and Valley J. W. (2016) Secondary Ion Mass Spectrometry Bias on Isotope Ratios in Dolomite–Ankerite, Part I: $\delta_{18}O$ Matrix Effects. *Geostand. Geoanalytical Res.* **40**, 157–172.

Turnier R. B. (2017) Calibration of Oxygen Isotope Fractionation and Corundum-Calcite Thermometry in Emery at Naxos, Greece: *In Situ* Versus Bulk Analysis. MS Thesis, Univ. Wisconsin-Madison.

Valley J. W. and Kita N. T. (2009) In Situ Oxygen Isotope Geochemistry by Ion Microprobe. *Mineral. Assoc. Can. Short Course* **41**, 19–63.

1 Table 1.

Sample No. (Fig. 1)	Sample Name	Minerals	Isograd T (°C)	$\delta^{18}O_{Cc}$ Avg. ±2SD (‰) VSMOW	$\delta^{18}O_{Crn}$ Avg. ±2SD (‰) VSMOW	$\Delta_{Cc\text{-}Crn}$	Within-Sample 2SD $\Delta_{Cc\text{-}Crn}$ Variability (‰)	Latitude	Longitude
1	NM-1-368	Cc, Crn, mica, oxides, An	593	25.3 ±0.20 (n=10)	21.9 ±0.31 (n=10)	3.38	0.67	37°6'42.00"N	25°32'24.48"E
2	NL-4-351	Cc, Crn, mica, oxides, Czo/Ep	577	22.0 ±0 .30 (n=8)	18.9 ±0.51 (n=8)	3.08	1.57	37°7'56.16"N	25°33'49.05"E
3	NL-7-358	Cc, Crn, mica, oxides, Tur	574	24.5 ±0.26 (n=10)	20.7 ±0.13 (n=10)	3.77	0.33	37°8'3.91"N	25°34'2.73"E
4	NL-3-40Aa	Cc, Crn, mica, oxides, Ap	570	20.6 ±0.26 (n=21)	17.7 ±0.32 (n=21)	2.93	0.95	37°7'28.98"N	25°33'55.20"E
5	NL-3-40Ba	Cc, Crn, mica, oxides	570	21.0 ±0.21 (n=24)	17.7 ±0.39 (n=24)	3.28	1.30	37°7'28.98"N	25°33'55.20"E
6	NL-8-359	Cc, Crn, mica, oxides, Czo/Ep	568	22.3 ±0.45 (n=12)	18.7 ±0.45 (n=12)	3.67	0.52	37°7'39.94"N	25°33'53.75"E
7	NOA-381	Cc, Crn, mica, oxides, Dsp	425	26.0 ±0.45 (n=15)	18.75 ±0.31 (n=15)	7.20	0.64	36°56'44.20"N	25°25'34.69"E
8	NZ-3-434	Cc, Crn, mica, oxides, Czo/Ep	424	22.3 ±0.21 (n=9)	15.9 ±0.26 (n=10)	6.33	1.21	36°58'42.99"N	25°28'26.04"E
Overall average 2SD of $\Delta^{18}O$(Cc-Crn) variability for all samples: 0.9‰									

2

3 Table 2.

Sample #:	**1**	**2**	**3**	**4**	**5**	**6**	**7**	**8**
Phase	**Modal (%)**	**Modal (%)**	**Modal (%)**	**Modal (%)**	**Modal (%)**	**Modal (%)**	**Modal (%)**	**Modal (%)**
Cc	68	28	78	52	67	66	26	32
Crn	12	50	9	15	12	14	46	42
mica	5	14	4	23	15	10	10	6
oxides	2	5	1	6	5	5	6	11
Tur	–	–	8	–	–	–	–	–
An	13	–	–	–	–	–	–	–
Czo	–	3	–	–	–	4	–	9
Ap	–	–	–	3	–	–	–	–
Dsp	–	–	–	–	–	–	12	–

4

5 Table 3.

Pv	-3.64												
Mt	-3.13	0.51											
Ru	-1.53	2.11	1.60										
Fo	-0.51	3.13	2.62	1.02									
Ttn	-0.50	3.14	2.63	1.03	0.01								
Gr	0.13	3.77	3.26	1.66	0.64	0.63							
Di	0.41	4.05	3.54	1.94	0.92	0.91	0.28						
Alm	0.45	4.09	3.58	1.98	0.96	0.95	0.32	0.04					
Zrc	0.52	4.16	3.65	2.05	1.03	1.02	0.39	0.11	0.07				
Ap	0.65	4.29	3.78	2.18	1.16	1.15	0.52	0.24	0.20	0.13			
An	1.17	4.81	4.30	2.70	1.68	1.67	1.04	0.76	0.72	0.65	0.52		
Ab	2.22	5.86	5.35	3.75	2.73	2.72	2.09	1.81	1.77	1.70	1.57	1.05	
Cc	2.78	6.42	5.91	4.31	3.29	3.28	2.65	2.37	2.33	2.26	2.13	1.61	0.56
	Crn	**Pv**	**Mt**	**Ru**	**Fo**	**Ttn**	**Gr**	**Di**	**Alm**	**Zrc**	**Ap**	**An**	**Ab**

$$\Delta_{Y\text{-}X} \approx 1000 \ln \alpha_{Y\text{-}X} = A_{Y\text{-}X} \times 10^6 \, T^{-2}$$

Where Y = Y-axis and X = X-axis mineral

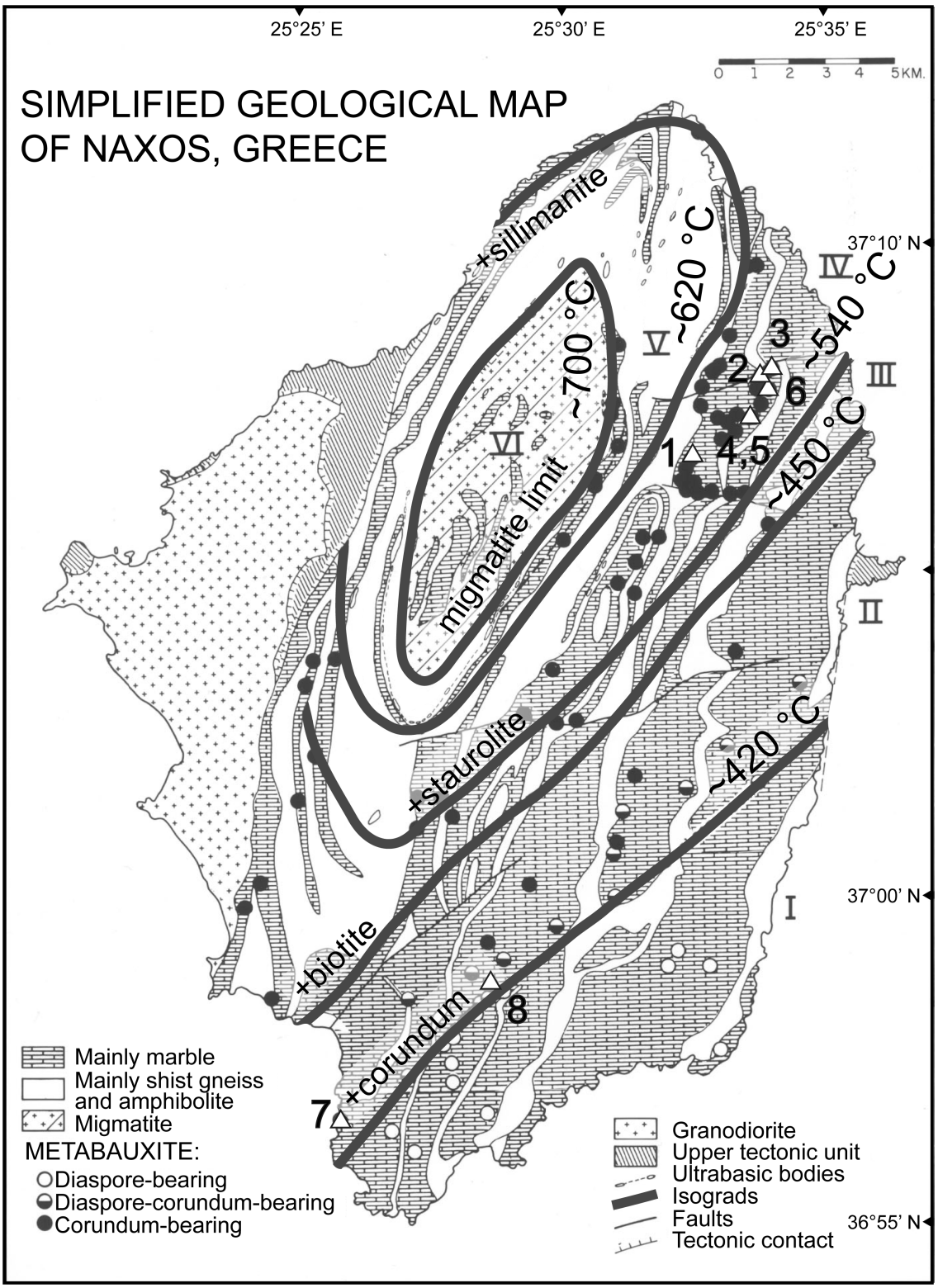
25°25' E
25°30' E
25°35' E
0 1 2 3 4 5KM.
SIMPLIFIED GEOLOGICAL MAP
OF NAXOS, GREECE
37°10' N
37°00' N
36°55' N
+sillimanite
~620 °C
~700 °C
~540 °C
~450 °C
~420 °C
migmatite limit
+staurolite
+biotite
+corundum
IV
V
VI
III
II
I
1
2
3
4,5
6
7
8
Mainly marble
Mainly shist gneiss and amphibolite
Migmatite
METABAUXITE:
Diaspore-bearing
Diaspore-corundum-bearing
Corundum-bearing
Granodiorite
Upper tectonic unit
Ultrabasic bodies
Isograds
Faults
Tectonic contact

Fig. 1.

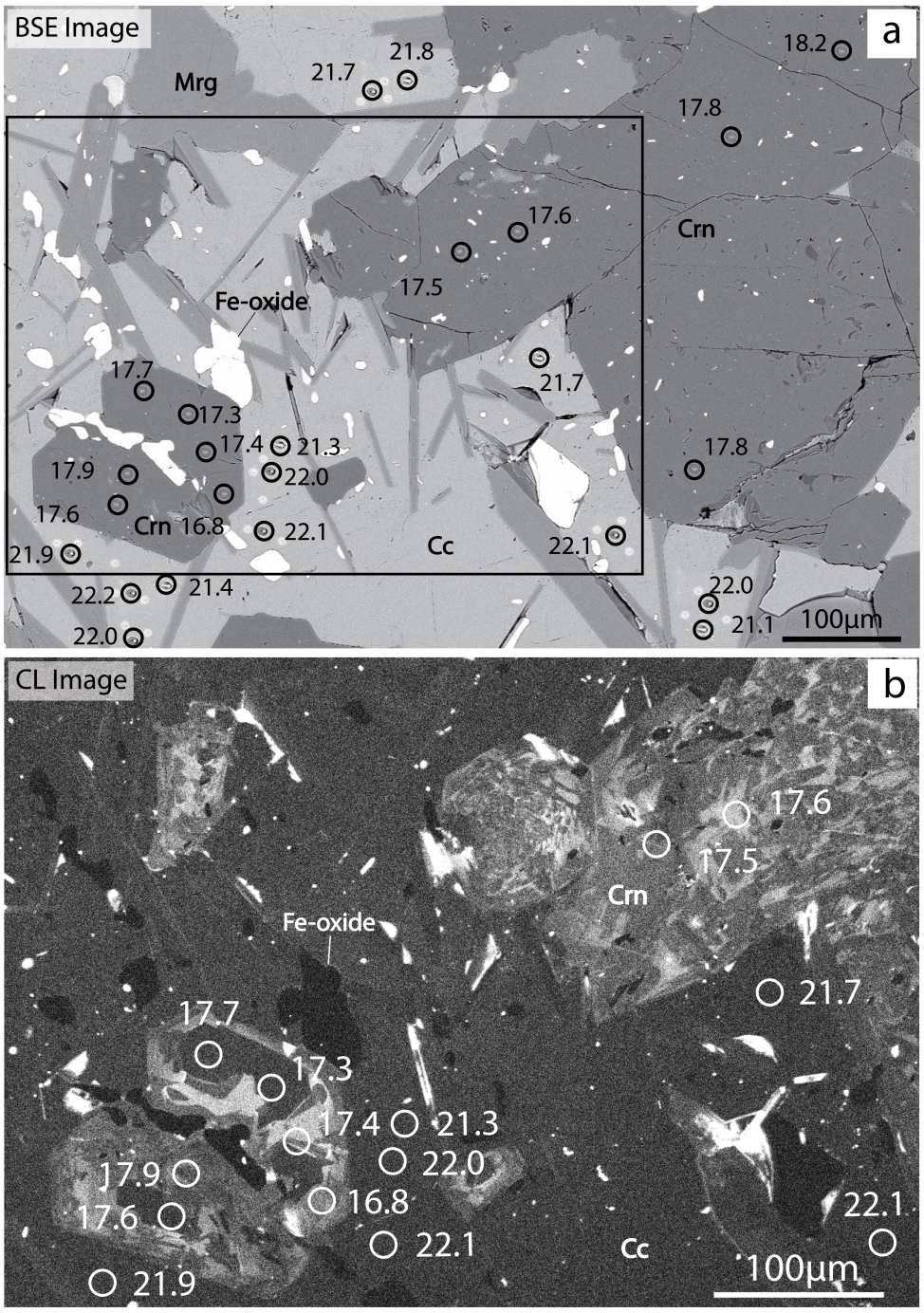
BSE Image
a
Mrg
21.8
21.7
18.2
17.8
17.6
Crn
17.5
Fe-oxide
21.7
17.7
17.3
17.4
21.3
17.8
17.9
22.0
17.6
Crn
16.8
22.1
Cc
22.1
21.9
22.2
21.4
22.0
22.0
21.1
100µm
CL Image
b
17.6
17.5
Crn
Fe-oxide
21.7
17.7
17.3
17.4
21.3
22.0
17.9
16.8
22.1
17.6
22.1
Cc
21.9
100µm

Fig. 2.

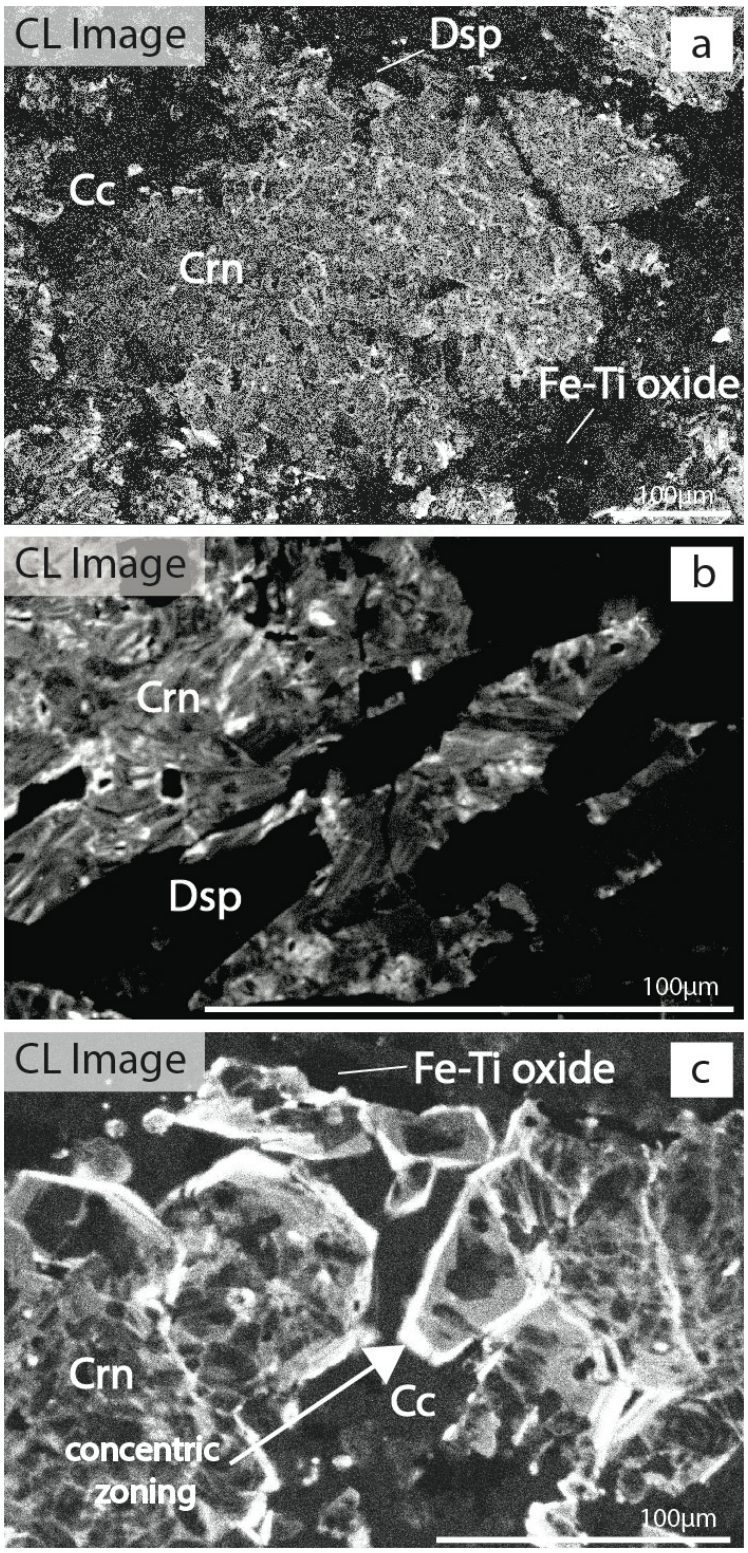
CL Image
Dsp
a
Cc
Crn
Fe-Ti oxide
100µm
CL Image
b
Crn
Dsp
100µm
CL Image
Fe-Ti oxide
c
Crn
Cc
concentric
zoning
100µm

Fig. 3.

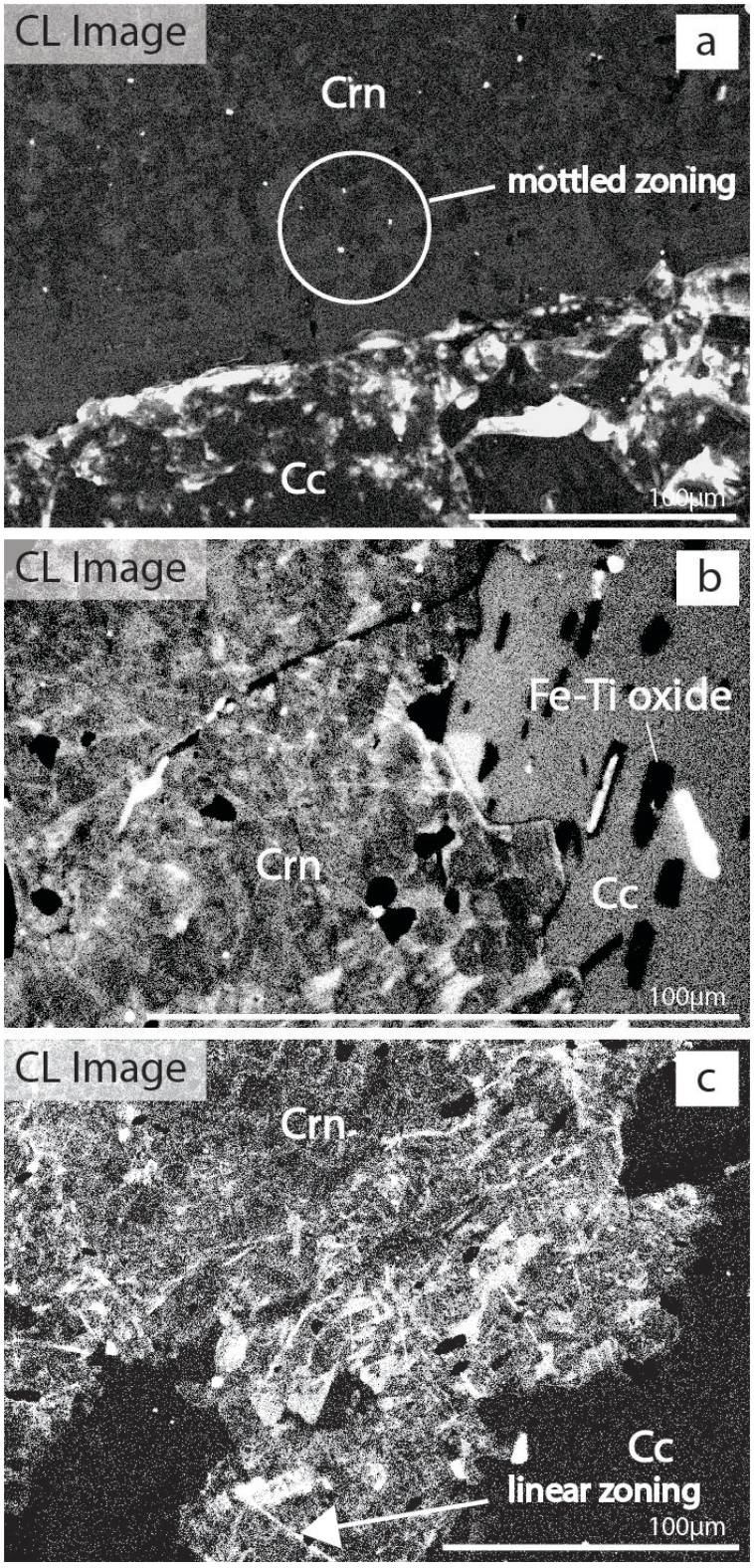
CL Image
a
Crn
mottled zoning
Cc
100µm
CL Image
b
Fe-Ti oxide
Crn
Cc
100µm
CL Image
c
Crn
Cc
linear zoning
100µm

Fig. 4.

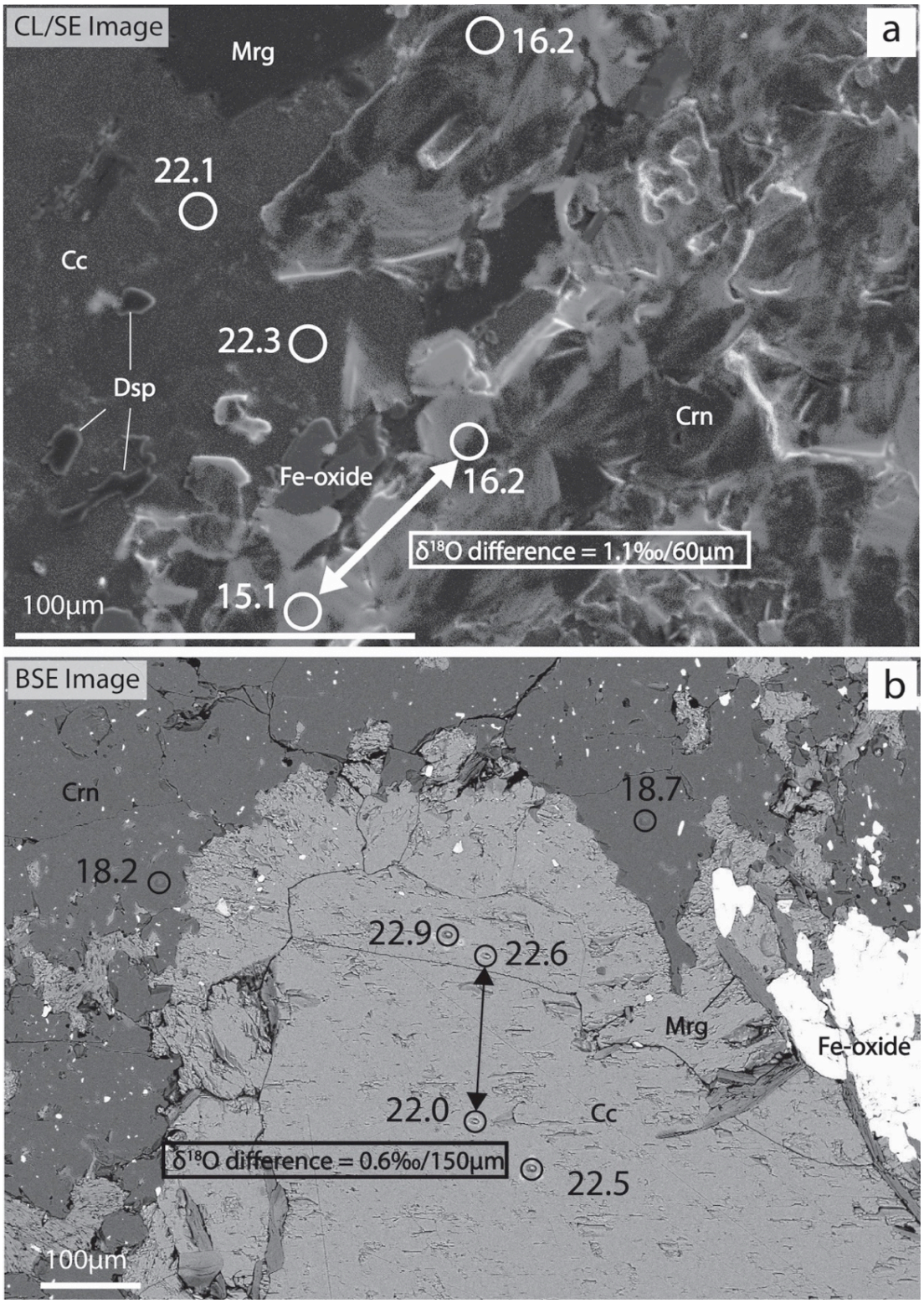
CL/SE Image
a
Mrg
16.2
22.1
Cc
22.3
Dsp
Crn
Fe-oxide
16.2
δ18O difference = 1.1‰/60µm
100µm
15.1
BSE Image
b
Crn
18.7
18.2
22.9
22.6
Mrg
Fe-oxide
22.0
Cc
δ18O difference = 0.6‰/150µm
22.5
100µm

Fig. 5.

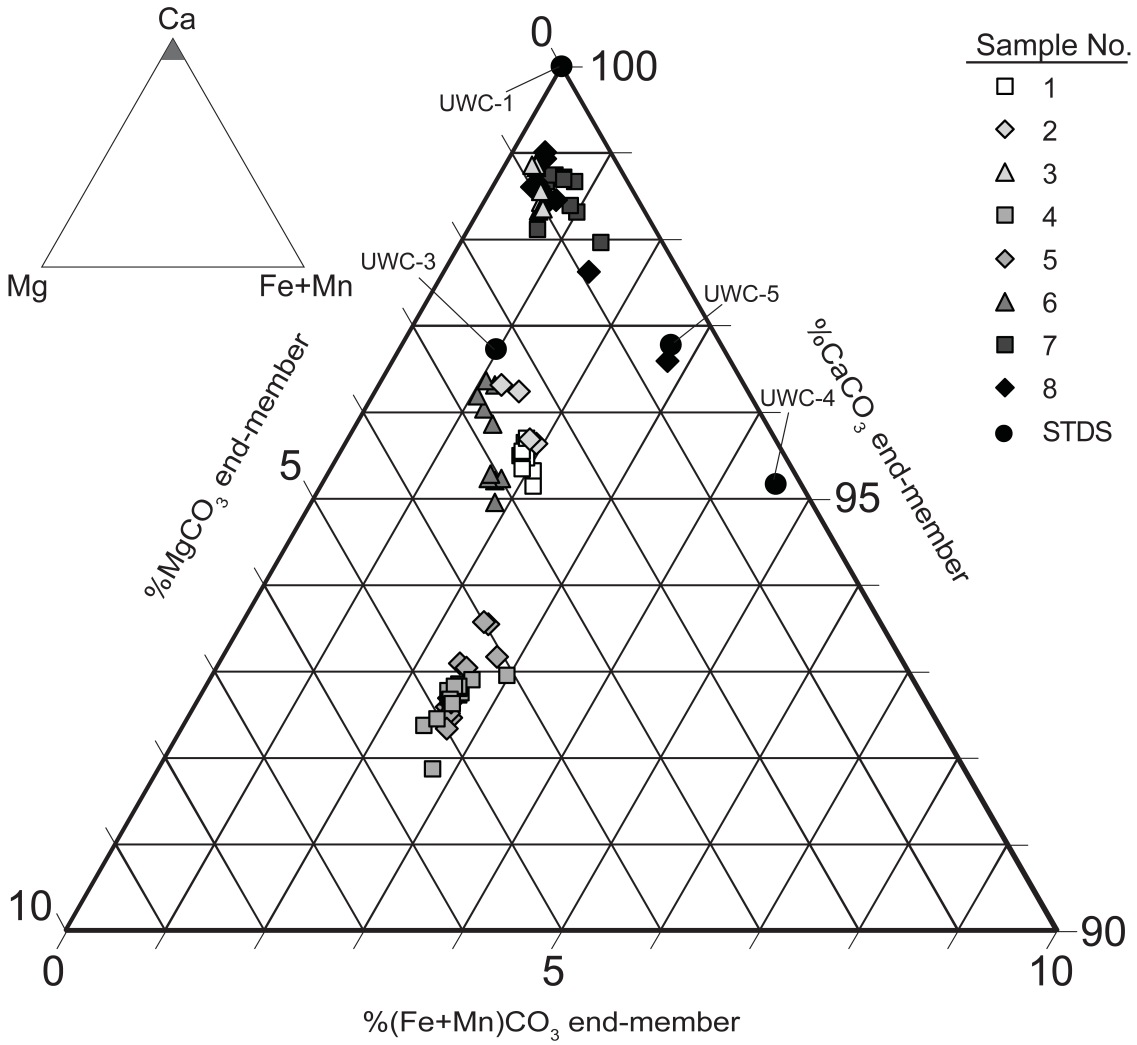
Ca
Mg
Fe+Mn
0
100
UWC-1
UWC-3
UWC-5
UWC-4
%MgCO3 end-member
%CaCO3 end-member
%(Fe+Mn)CO3 end-member
5
95
10
0
5
10
90
Sample No.
1
2
3
4
5
6
7
8
STDS

16
17 Fig. 6.

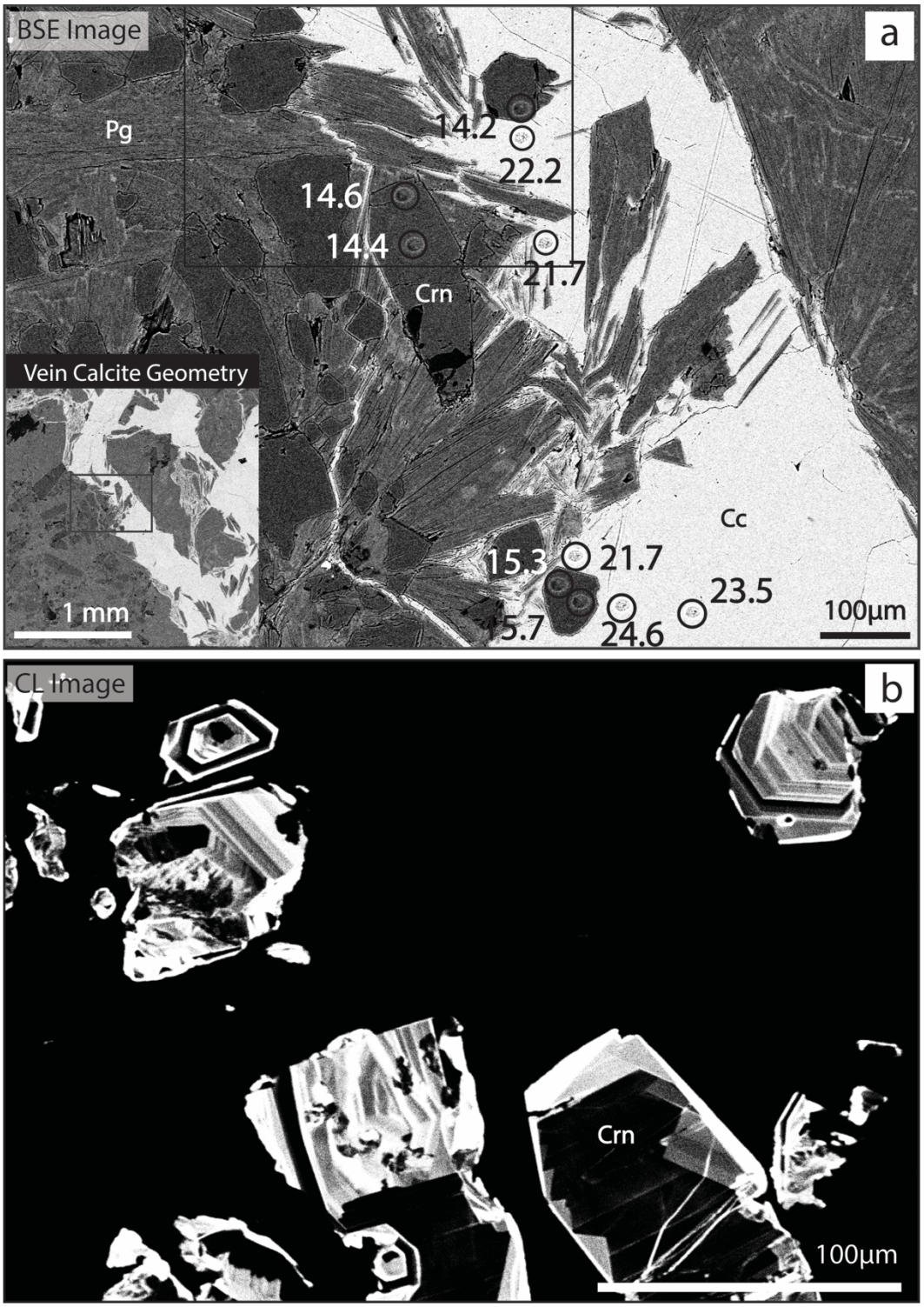
BSE Image
a
Pg
14.2
22.2
14.6
14.4
21.7
Crn
Vein Calcite Geometry
1 mm
Cc
15.3
21.7
23.5
5.7
24.6
100µm
CL Image
b
Crn
100µm

Fig. 7.

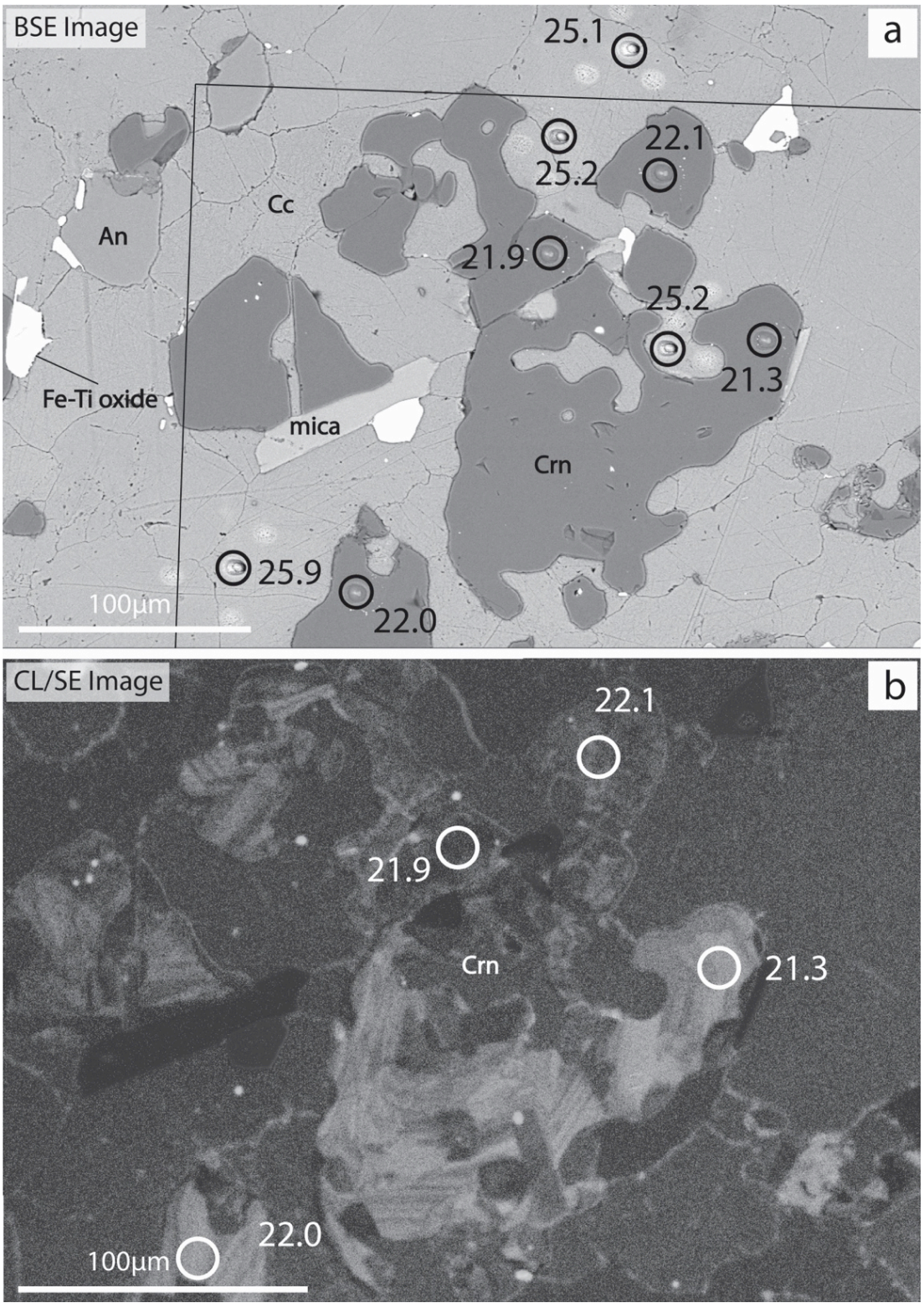
BSE Image
a
25.1
22.1
25.2
Cc
An
21.9
25.2
21.3
Fe-Ti oxide
mica
Crn
25.9
22.0
100µm
CL/SE Image
b
22.1
21.9
Crn
21.3
22.0
100µm

Fig. 8.

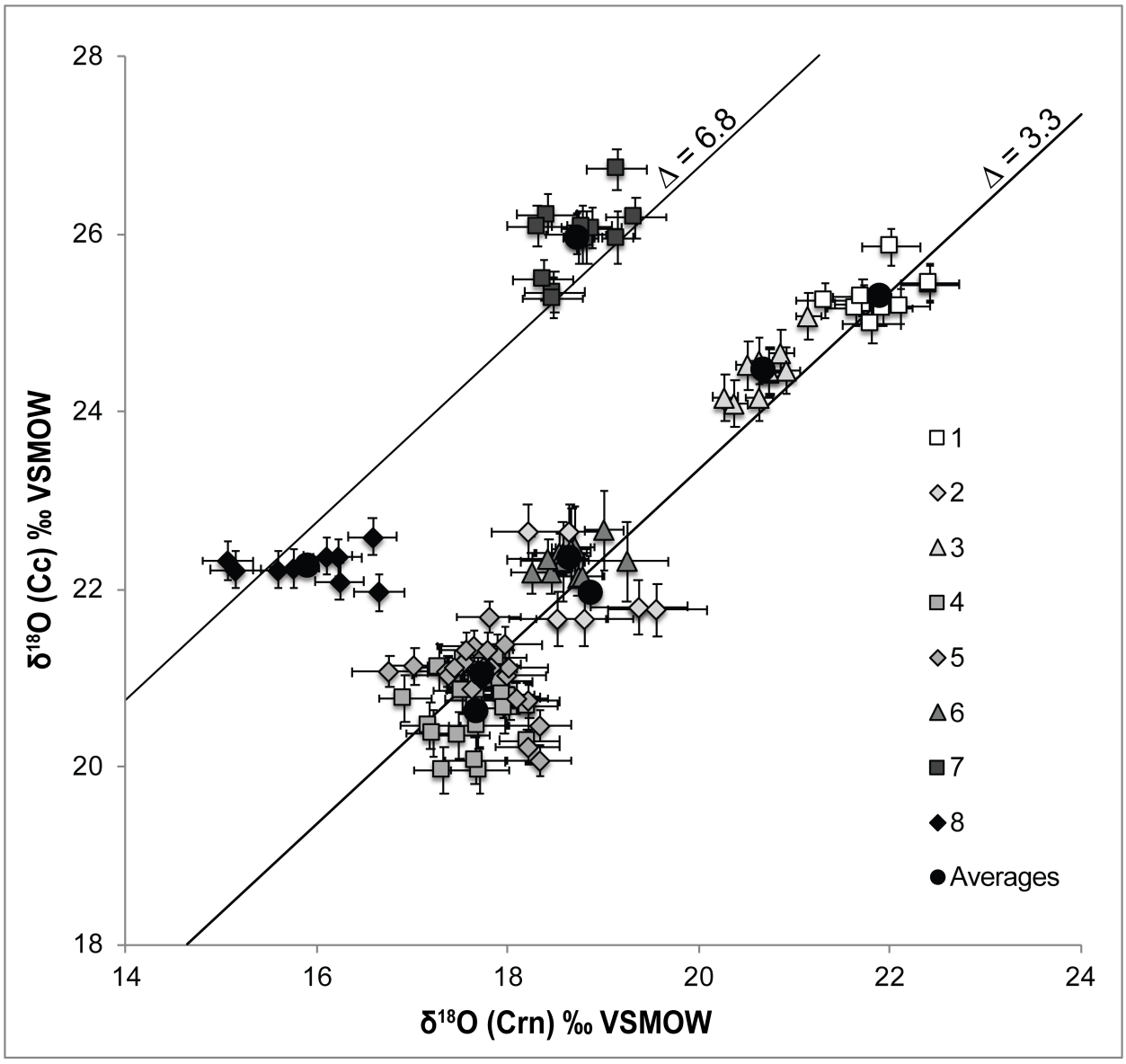
28
26
24
22
20
18
14
16
18
20
22
24
δ18O (Cc) ‰ VSMOW
δ18O (Crn) ‰ VSMOW
Δ = 6.8
Δ = 3.3
1
2
3
4
5
6
7
8
Averages

Fig. 9.

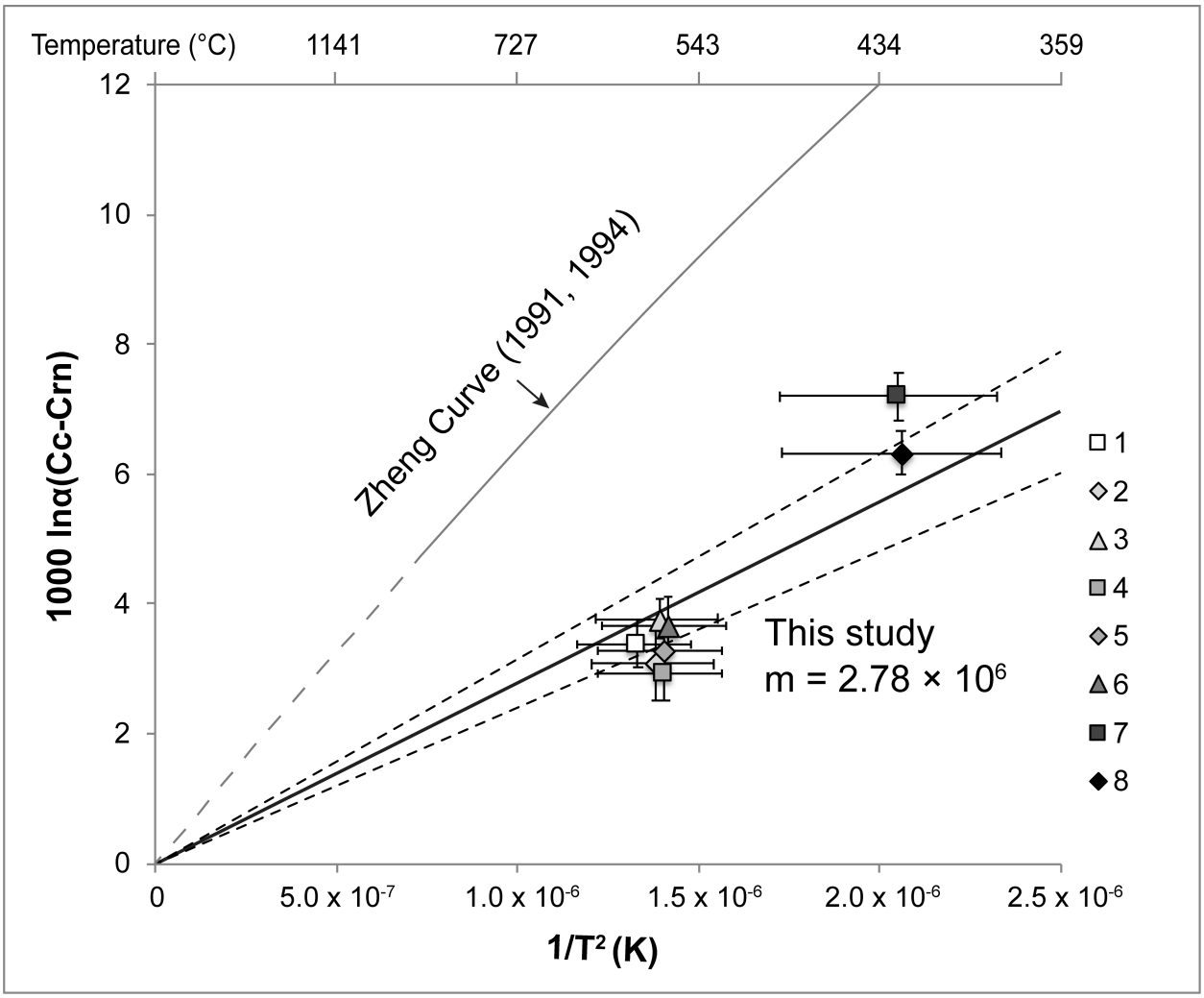
Temperature (°C)
1141
727
543
434
359
12
10
8
6
4
2
0
1000 Inα(Cc-Crn)
Zheng Curve (1991, 1994)
This study
m = 2.78 × 10⁶
1
2
3
4
5
6
7
8
0
5.0 x 10-7
1.0 x 10-6
1.5 x 10-6
2.0 x 10-6
2.5 x 10-6
1/T² (K)

Fig. 10.

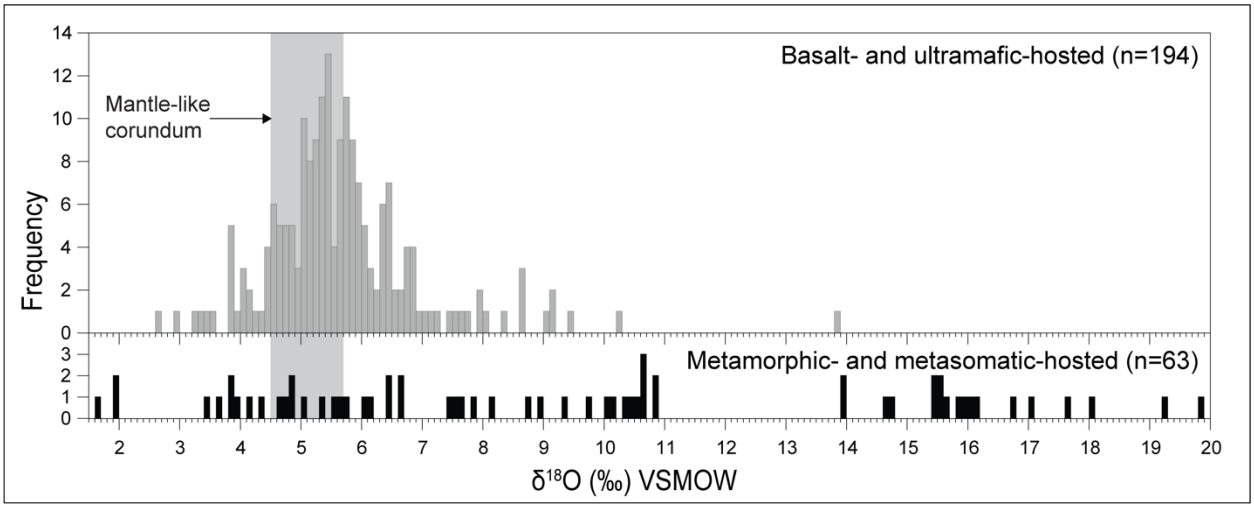
Basalt- and ultramafic-hosted (n=194)
Mantle-like
corundum
Frequency
Metamorphic- and metasomatic-hosted (n=63)
δ18O (‰) VSMOW

Fig. 11.